

Electronic Thesis and Dissertation Repository

7-23-2014 12:00 AM

A CFD assisted control system design for supercritical water cooled reactor

Rohit V. Maitri
The University of Western Ontario

Supervisor
Prof. Chao Zhang
The University of Western Ontario Joint Supervisor
Prof. Jin Jiang
The University of Western Ontario

Graduate Program in Mechanical and Materials Engineering
A thesis submitted in partial fulfillment of the requirements for the degree in Master of Engineering Science
© Rohit V. Maitri 2014

Follow this and additional works at: <https://ir.lib.uwo.ca/etd>



Part of the [Controls and Control Theory Commons](#), and the [Heat Transfer, Combustion Commons](#)

Recommended Citation

Maitri, Rohit V., "A CFD assisted control system design for supercritical water cooled reactor" (2014).
Electronic Thesis and Dissertation Repository. 2169.
<https://ir.lib.uwo.ca/etd/2169>

This Dissertation/Thesis is brought to you for free and open access by Scholarship@Western. It has been accepted for inclusion in Electronic Thesis and Dissertation Repository by an authorized administrator of Scholarship@Western. For more information, please contact wlsadmin@uwo.ca.

A CFD ASSISTED CONTROL SYSTEM DESIGN FOR SUPERCRITICAL
WATER COOLED REACTOR

(Thesis format: Integrated Article)

by

Rohit Maitri

Graduate Program in Mechanical and Materials Engineering

A thesis submitted in partial fulfilment
of the requirements for the degree of
Masters of Engineering Science

The School of Graduate and Postdoctoral Studies
The University of Western Ontario
London, Ontario, Canada

© Rohit Vishwanath Maitri, 2014

Abstract

In this study, the methodology to construct a control system based on computational fluid dynamics (CFD) simulations is developed for supercritical water cooled reactor (SCWR). The CFD model using Reynolds Stress Model (RSM) and $k - \omega SST$ model is validated with the experimental cases of steady state and vertically up flowing supercritical water in circular tubes for normal heat transfer and deteriorated heat transfer (DHT) cases. This model is extended to simulate the transient thermal-hydraulic behaviour of supercritical fluid flow and heat transfer, and the results are also compared with the 1-D numerical model, THRUST. The DHT phenomenon is investigated using the turbulence kinetic energy (TKE) and velocity distribution and their effect on the heat transfer. A correlation is reported between the TKE and velocity profiles and heat transfer phenomenon at supercritical condition. The non-dimensional buoyancy and acceleration parameters are also used to predict the occurrence of DHT in the supercritical water flow in circular tubes.

In the process of developing a control system for Canadian version of SCWR, system identification method is used to develop the linear dynamic models based on non-linear CFD simulations. Considering the strong cross-coupling between the inputs and outputs of the SCWR, multiple input and multiple output (MIMO) system is decoupled and is converted to several single input and single output (SISO) systems using pre-compensator. Based on the decoupled SISO systems, loop compensator is developed for the control and stability of the reactor.

Keywords: Supercritical water cooled reactor (SCWR), Computational fluid dynamic (CFD), THRUST, Deteriorated heat transfer, Buoyancy parameter, Acceleration parameter, Control system, System identification, Decoupling, Linear dynamic model.

Co-Authorship Statement

Chapters 3, 4 and 5 of this thesis will be submitted for publications.

All papers are drafted by Rohit Maitri and modified under the supervision of Prof. Chao Zhang and Prof. Jin Jiang and in consultation with Dr. Dutta. The 1-D model THRUST development work in chapters 3 and 4 has been carried out by Dr. Goutam Dutta from Prof. Jin Jiang's research group.

Acknowledgement

I would like to express my sincere gratitude to Prof. Chao Zhang and Prof. Jin Jiang for their valuable guidance and support throughout my research work.

I would like thank to Dr. Goutam Dutta, a post-doctoral fellow in the Department of Electrical and Computer Engineering at Western University and Associate Professor in the Department of Mechanical Engineering IIITDM, Jabalpur, India, who provided valuable inputs to my research work.

I would like to thank my lab-mates of the CFD laboratory at Western University who helped me through long discussions on technical details of my research.

I would also like to thank my parents and my sister for their support and love during the stressful period of this course.

Contents

Abstract	iii
Co-Authorship Statement	iv
Acknowledgement	v
Nomenclature	ix
Glossary	xi
List of Figures	xii
List of Tables	xiv
1 Introduction	1
1.1 Overview	1
1.2 Supercritical Fluids	2
1.3 Supercritical Water Cooled Reactor (SCWR)	4
1.4 Methodology	6
1.5 Outline of the thesis	8
References	9
2 Literature Review	10
2.1 Flow Dynamics and Heat transfer studies of supercritical fluid flow	10
2.1.1 Theoretical Background	10
2.1.2 Experimental Studies	11
2.1.3 Computational Studies	15
2.2 Control System Studies	17
2.3 Motivation	18
References	20

3	Validation of Numerical Models and Transient Simulations	25
	Abstract	25
3.1	Introduction	31
3.2	Mathematical details of the numerical models	33
3.2.1	GE of TH model	33
	Steady state solution methodology	35
	Heat transfer coefficient and friction factor	35
	Methodology to determine the local wall temperature	36
	Determination of critical heat flux for DHT	37
3.2.2	Mathematical formulation of the CFD model	38
3.3	Results and Discussions	40
3.3.1	Validation of the numerical models at steady state condition	40
3.3.2	Comparison of the numerical models at transient condition	47
3.4	Conclusions	53
	References	55
4	Numerical Analysis of DHT	59
	Abstract	59
4.1	Introduction	65
4.2	Mathematical details of the numerical models	68
4.2.1	Mathematical formulation of CFD model	68
4.2.2	Mathematical formulations of the THRUST	70
	Solution methodology	70
	Heat transfer coefficient and friction factor	71
4.2.3	Parameters to analyze DHT	71
4.3	Results and Discussions	73
4.3.1	Flow structure of supercritical water under various heat transfer conditions using CFD	74
4.3.2	Analysis of DHT based on the acceleration parameters using THRUST	78

4.3.3	Prediction of DHT based on the buoyancy parameters and pressure drop components using THRUST	80
	No DHT in the experiment	82
	DHT in the experiment observed at a low mass flux condition	82
	DHT in the experiment at a high mass flux condition	82
4.4	Conclusions	86
	References	89
5	A CFD Assisted Control System Design Methodology	94
	Abstract	94
5.1	Introduction	96
5.2	CFD method for CANDU SCWR simulations	97
5.3	Development of a linear dynamic model	99
5.4	Designing of a control system	103
5.4.1	Design of a pre-compensator	106
5.4.2	Design of a loop compensator	107
	Outlet Mass Flow Rate Control	109
	Outlet Temperature Control	109
5.5	Conclusions	110
	References	111
6	Conclusions and Future Work	112
6.1	Conclusions	113
6.2	Future work	115
	Curriculum Vitae	117

Nomenclature

symbols

C_p	Specific heat capacity
E	Eckert Number, $(T_{pc} - T_b)/(T_w - T_b)$
g	Gravitational acceleration
k	Turbulence kinetic energy
P	Pressure
Pr	Prandtl number
T	Temperature

Subscripts

b, ∞	Bulk
cr	Value at critical point
pc	Pseudo-critical
w	Wall

Greek Letters

ϵ	Energy dissipation
λ	Thermal conductivity
μ	Dynamic viscosity
ρ	Density of a fluid
ω	Specific energy dissipation

Acronyms

BWR	Boiling Water Reactor
CFD	Computational Fluid Dynamics
DNS	Direct numerical Simulations
GIF	Generation IV Forum
HTD	Heat Transfer Deterioration
LES	Large Eddy Simulation
MIMO	Multiple Input and Multiple Output
PCL	Pseudo-critical Line
PCP	Pseudo-critical Point
PCR	Pseudo-critical Region
PDE	Partial Differential Equations
PWR	Pressurized Water Reactor
RANS	Reynolds Averaged Navier-Stokes
R & D	Research and Development
RSM	Reynolds Stress Model
SCFPP	Supercritical Fossil Power Plant
SCFR	Supercritical Fast Reactor
SCWR	Supercritical Water Cooled Reactor
SISO	Single Input and Single Output
SST	Shear Stress Transport
TKE	Turbulence Kinetic Energy

Glossary

- **Critical point** - is the point where the distinction between the liquid and gas phases disappears, i.e. both phases have the same temperature, pressure and volume. This point is characterized by the T_{cr} , P_{cr} , V_{cr} which have unique values for each pure substance.
- **Supercritical fluid** is a fluid at pressures and temperature that are higher than the critical pressure and critical temperature.
- **Pseudo-critical point (PCP)** is a point at a pressure and temperature above the critical values corresponding to the maximum value of the specific heat for this particular pressure.
- **Normal heat transfer** can be characterized in general with wall heat transfer coefficients similar to those of subcritical convective heat transfer far from the critical or pseudo-critical regions, when are calculated according to the conventional single-phase Dittus-Boelter type correlations.
- **Deteriorated heat transfer** is characterized by lower values of the wall heat transfer coefficient compared to those at normal heat transfer; and hence has higher values of wall temperature within some part of a test section or within entire test section.
- **Improved heat transfer** is characterized by higher values of the wall; heat transfer coefficient compared to those at the normal heat transfer; and hence lower values of wall temperature within some part of a test section or within the entire test section.
- **Near-critical point** is actually a narrow region around the critical point where all the thermo-physical properties of a pure fluid exhibit rapid variations.
- **Pseudo-film boiling** is a physical phenomenon similar to subcritical pressure film boiling, which may appear at supercritical pressures. At pseudo-film boiling, a low density fluid at temperatures above the pseudo-critical temperature prevents a high-density fluid from contacting (“rewetting”) a heated surface. Pseudo-film boiling leads to the deteriorated heat transfer region.

List of Figures

1.1	Overview of development of nuclear reactors ¹	2
1.2	Phase diagram of water ⁵	4
1.3	Variation of properties of water near pseudo-critical point ⁴	5
1.4	Layout of Supercritical Water Cooled Reactor (SCWR)	6
1.5	Methodology for control system design of SCWR	7
3.1	Comparison of the heat transfer coefficient by THRUST with the experimental data ²⁶ for Case 1	41
3.2	Comparison of the wall temperatures with the experimental data ²⁶ for Case 1	41
3.3	Comparison of the wall temperatures with the experimental data ²⁹ for Case 2	42
3.4	Comparison of the wall temperatures with the experimental data ²⁶ for Case 3	43
3.5	Comparison of the wall temperatures with the experimental data ²⁶ for Case 4	43
3.6	Comparison of the wall temperatures with the experimental data ²⁶ for Case 5	44
3.7	Comparison of the wall temperatures with the experimental data ²⁹ for Case 6	45
3.8	Comparison of the wall temperatures with the experimental data ²⁶ for Case 7	46
3.9	Step decrease in the inlet mass flow rate by 20% for Case 3	49
3.10	Step increase in the wall heat flux by 10% for Case 3	50
3.11	Sinusoidal variation of the inlet mass flow rate for Case 3	51
4.1	Results using CFD for Case 1	75
4.2	Results using CFD for Case 2a	76
4.3	Results using CFD for Case 3	79
4.4	Results using THRUST for Case 1	81
4.5	Results using THRUST for Case 2a	83
4.6	Results using THRUST for Case 2b	84

4.7	Results using THRUST for Case 3	85
5.1	CANDU SCWR Fuel ⁷ channel	98
5.2	Dynamic model for the CANDU SCWR	100
5.3	Transient response to the step decrease in the inlet mass flow rate by 10%	101
5.4	Transient response to the step increase in the heat flux rate by 10%	102
5.5	Linear dynamic model validation with the CFD results with the step change in the inlet mass flow rate	103
5.6	Linear dynamic model validation with the CFD results with the step change in the input heat flux	104
5.7	Block diagram of the control system for the CANDU SCWR	105
5.8	The distribution of $d_j(w)$ for different columns of original and pre-compensated plant	108

List of Tables

2.1	Parameters corresponding to Heat Transfer correlations	14
3.1	Parameters corresponding to HTC correlations	37
3.2	Geometrical and operating parameters of the experiments under consideration .	40
3.3	Relative errors between the numerical and experimental results for the wall temperature	46
3.4	Relative difference obtained by CFD and THRUST for the wall temperature (%)	52
4.1	Geometrical and operating parameters of experiments	74
4.2	Prediction of DHT on the basis of buoyancy parameters	80
5.1	Specifications of the CANDU-SCWR ^{6,7}	98

Chapter 1

Introduction

1.1 Overview

The global demand for energy keeps on increasing each year. Considering the environmental concerns and depletion of fossil fuels, the use of alternate energy sources is important for the future of mankind. Among these energy sources, the nuclear energy is one of the major alternatives and it is being investigated widely to make nuclear reactors reliable, safe and economically viable for electricity generation.

The first generation of nuclear reactors was developed in the 1950s and 60s as a prototype reactors. In the next decade, the second generation reactors began as a commercial power plants. With the number of modifications and evolutionary designs, Generation III reactors were developed in 1990s. Currently, the advances to Generation III reactors are under development and the new plants to be built till 2030 will be chosen from the Generation III+ reactor concepts. At every stage, the next generation reactors are designed with the aim of higher safety and better economics. The research community has continuously explored the innovative advances to existing reactors and hence R&D for Generation IV reactors which are planned to be in operation after 2030 has stimulated worldwide interest in the researchers. The timeline of the different nuclear designs is shown in Fig.1.1.

The Generation IV forum (GIF) has investigated different designs and finalised on the fol-

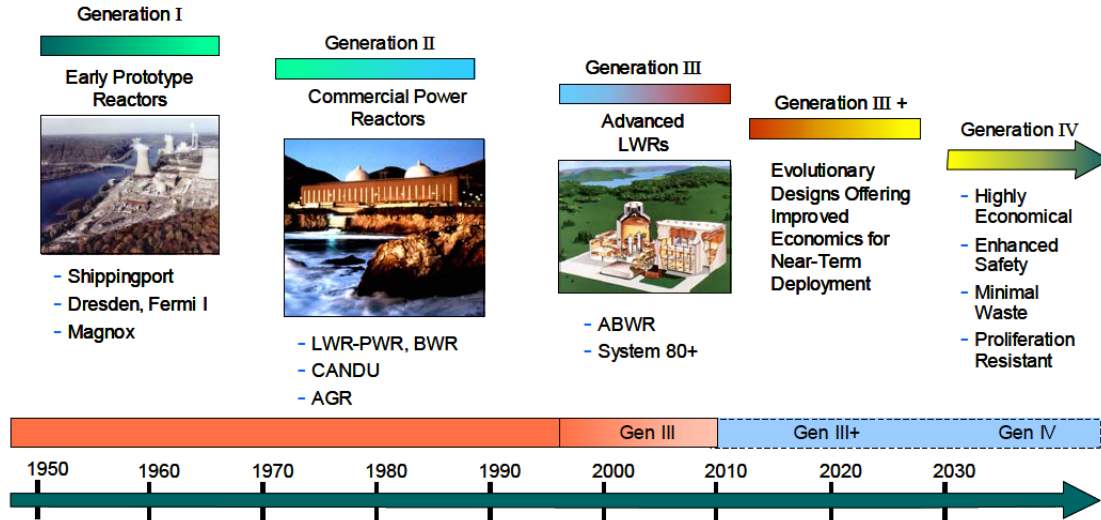


Figure 1.1: Overview of development of nuclear reactors¹

Following six reactor concepts as Generation IV reactors :

1. Gas-Cooled Fast Reactor (GFR)
2. Lead-Cooled Fast Reactor (LFR)
3. Molten Salt Reactor (MSR)
4. Sodium-Cooled Fast Reactor (SFR)
5. Supercritical-Water-Cooled Reactor (SCWR)
6. Very-High Temperature Reactor (VHTR)

Among the above-mentioned reactors, the SCWR is the only reactor which uses water as a coolant. The SCWR uses the water at supercritical pressures whereas all the previous water cooled reactors used water at subcritical pressures. The use of water at supercritical pressures in nuclear reactors is new and it will be investigated in this study.

1.2 Supercritical Fluids

*“The use of supercritical fluids in different processes is not new, and is not a human invention”.*² Supercritical fluid is a fluid at thermodynamic state where its temperature and pressure

is above its critical point. Supercritical fluids have been of interest for industry due to its various applications. Supercritical fluids have been used to increase the efficiency of fossil power plants, as a fuel in chemical and nuclear rockets, as a coolant for power transmission equipments, as a refrigerant in air-conditioning and refrigerating systems, as a coolant and fuel for supersonic transport, for transforming geothermal energy into electricity, for processes such as supercritical fluid extraction, supercritical fluid chromatography and polymer processing in chemical and pharmaceutical industries.²

It is important to note that the term “supercritical fluid” is not used to identify some specific class of fluids but it is used as an indication of the thermodynamic state of the fluid. At supercritical condition, the temperature and pressure of the fluid is greater than T_{cr} and P_{cr} , respectively. The unique feature of a fluid at supercritical condition is the absence of phase boundaries. As it can be observed from the phase diagram (Figure 1.2) that there does not exist any phase boundary (solid line) at supercritical condition and it is a single phase fluid. The critical temperature and pressure for water is 647 K and 22.1 MPa and for CO_2 is 304.21 K and 7.3825 MPa, respectively.^{3,4}

It is observed that, at a critical point, water has maximum specific heat.⁴ The point where the specific heat is maximum for a given supercritical pressure is characterized as pseudo-critical point (PCP) and the line joining these points is called as pseudo-critical line (PCL) (Fig. 1.2). When compressed water ($P > P_{cr}$) is heated to temperature higher than the critical temperature, a transition from liquid like substance to vapour like substance is observed.⁴ Although this transition is continuous, the thermo-physical properties of water vary significantly near PCL.⁴ Fig. 1.3 shows the variation of some of the thermophysical properties of supercritical water near PCP.

Near PCP, the density, thermal conductivity and dynamic viscosity decrease and become constant after that. The same trend is observed for kinematic viscosity except that it regains its values as we increase the temperature. The sharp peak is observed at PCP for Prandtl number, specific heat capacity and thermal expansion coefficient.

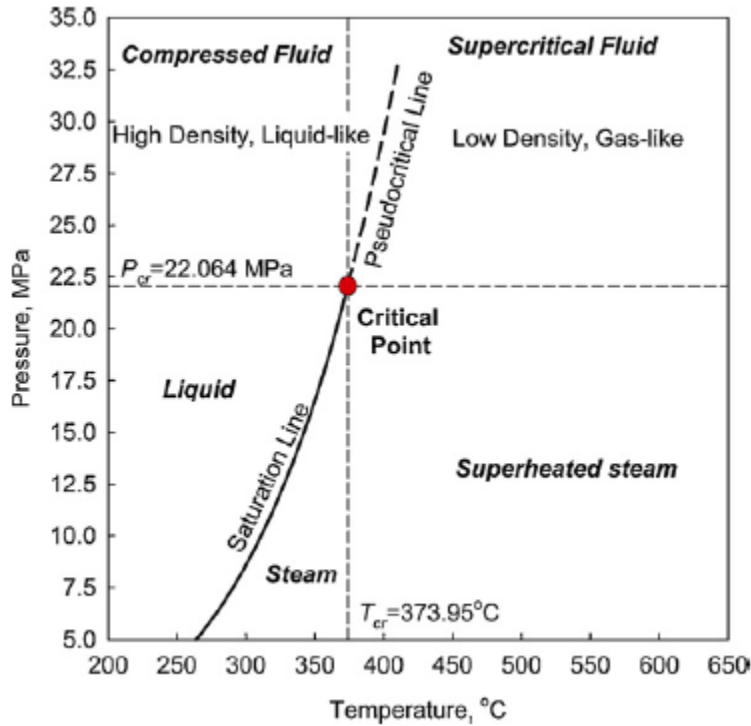


Figure 1.2: Phase diagram of water⁵

1.3 Supercritical Water Cooled Reactor (SCWR)

Although nuclear reactors with supercritical water have never been in operation, supercritical water has been used in the commercial fossil power plants already. The advantage of improved thermal efficiency of supercritical water in fossil power plants over subcritical water was decisive factor to operate Supercritical Fossil Power Plants (SCFPP). In steam power plants (where water at subcritical condition is used), water is converted to steam by heating and then it is passed to turbines for power generation. The major problem faced with these power plants is the ‘boiling crisis’ which is often referred as ‘dryout’ also. While phase change occurs during the heating of water, bubble formation is observed near metal surface which decreases the efficiency of heat transfer, thus causes localized overheating of heating surface.^{2,3} But in supercritical fluids, due to smooth transition from liquid like substance to vapour like substance,

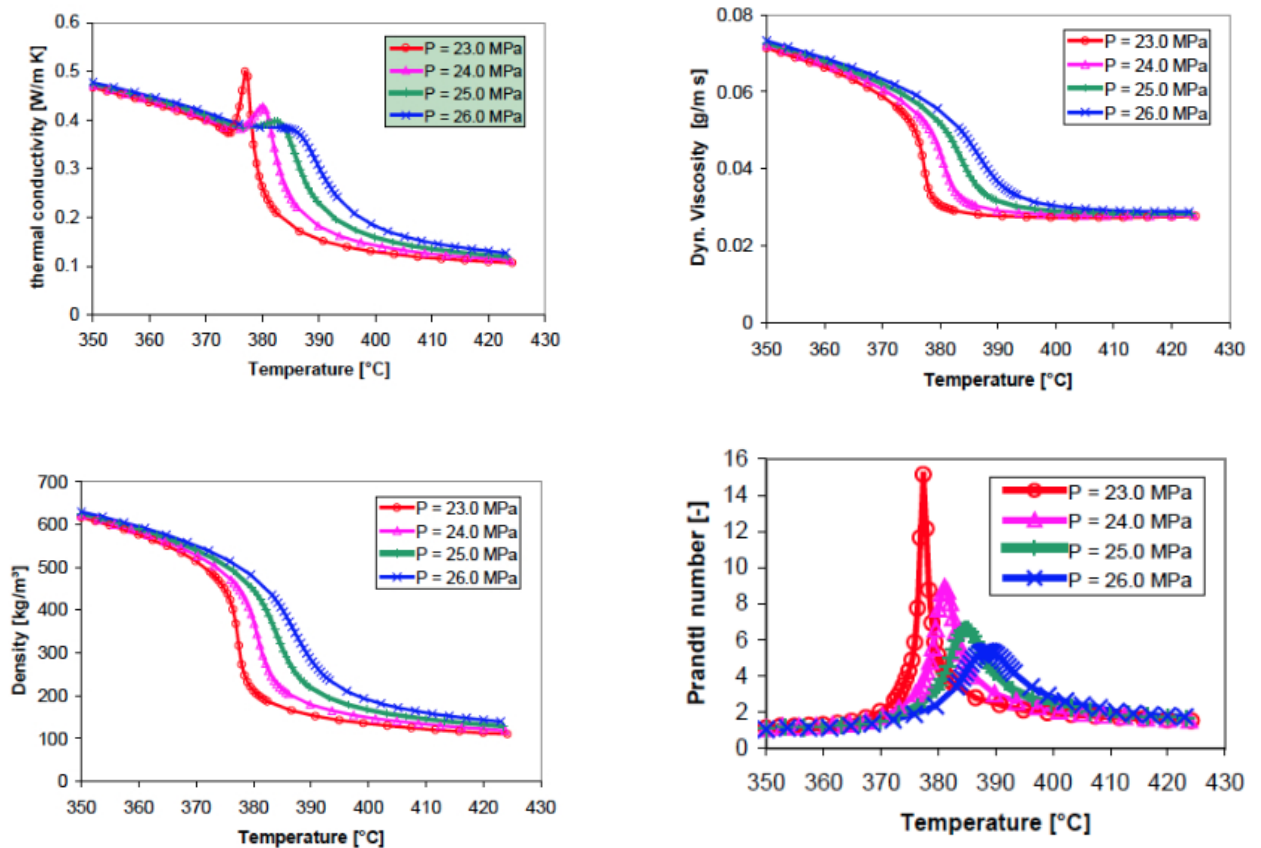


Figure 1.3: Variation of properties of water near pseudo-critical point⁴

there is no ‘dryout’ problem and hence the problem of overheating is avoided. Higher enthalpy of the supercritical water makes it an effective coolant as it needs lower mass flow rate per unit core thermal power. This results in the reduction in the size of pumps, piping, associated equipments and pumping power as well. As the supercritical condition ensures single phase flow dynamics, the needs for steam separators, recirculation pumps and steam generators are also eliminated.¹ Moreover, the most important advantage is the improved thermal efficiency of the SCWR (around 44%) compared to the existing LWRs (33-35%).

Higher efficiency, single phase flow, higher enthalpy, smooth transition at PCL are the advantages for use of supercritical water in power plants. Along with these advantages, challenges also exist.

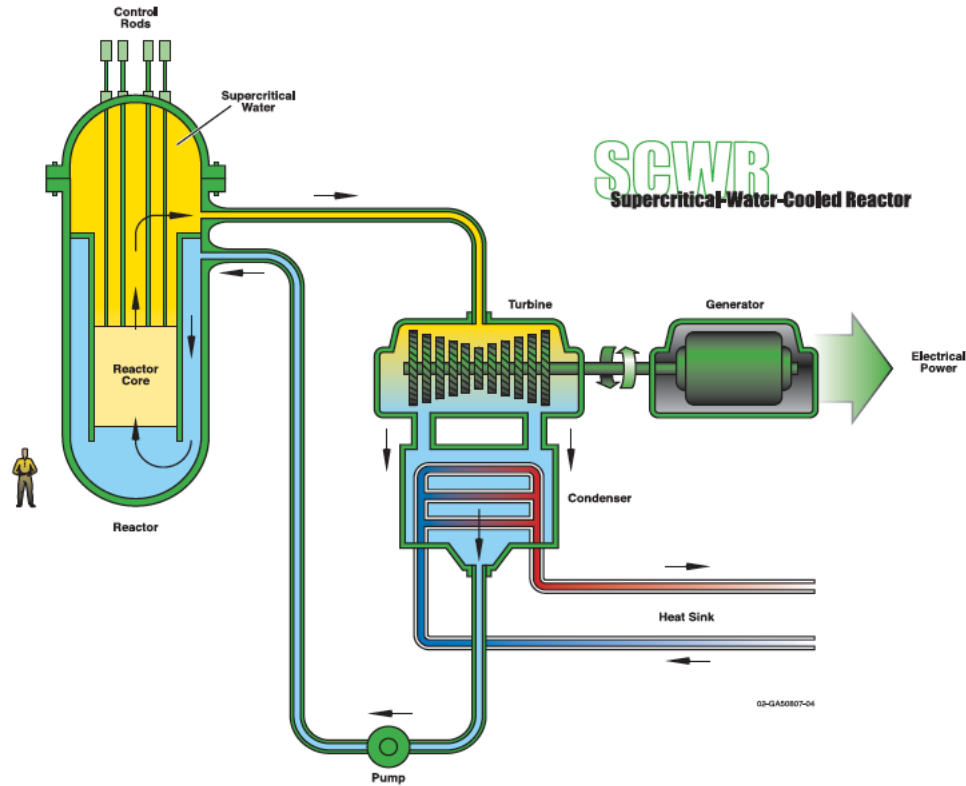


Figure 1.4: Layout of Supercritical Water Cooled Reactor (SCWR)

Although the supercritical fluid shows higher enthalpy (as an advantage), it also has sharp decrease in density (as a disadvantage). This density behaviour produces prominent buoyancy effects and sharp increase in thermal expansion coefficient results in large acceleration effects. These two effects combined with the large property changes near PCL cause decrease in the heat transfer coefficient. This phenomenon is referred as heat transfer deterioration (HTD) which results in an increase in the wall temperature.

1.4 Methodology

The nuclear reactors are generally operated at given operating conditions. Hence, the perturbation in the inputs affects the outputs and consequently the operating conditions. Hence, it is important to control the inputs to keep the reactor at designed operating conditions.

The governing equations for the fluid flow and heat transfer in a SCWR are non-linear partial differential equations (PDEs) and it is difficult to directly establish the dynamic relationship between the inputs and outputs, so, the white box method could not be used. Hence, for the non-linear systems like SCWRs, the black box method is useful for designing a control system. The black box method requires the input and output data for finding a dynamic relationships between them. For generating the input-output data, computational fluid dynamics (CFD) simulations are used in this study. Before proceeding for the CFD simulations for SCWR where supercritical water flows through fuel rods, the validation of CFD model is important. However, in the literature, no experimental results are available for the supercritical fluid flow in rod bundles. Therefore, the current CFD model is validated for the flow in circular tubes for which there are numerous experimental results. Next, the supercritical water flow through reactor core is approximated to the fluid flow in circular tubes by keeping the heat flux to mass flux ratio same and using the equivalent hydraulic diameter. The methodology used for designing a control system based on CFD simulations is shown in Fig. 1.5.

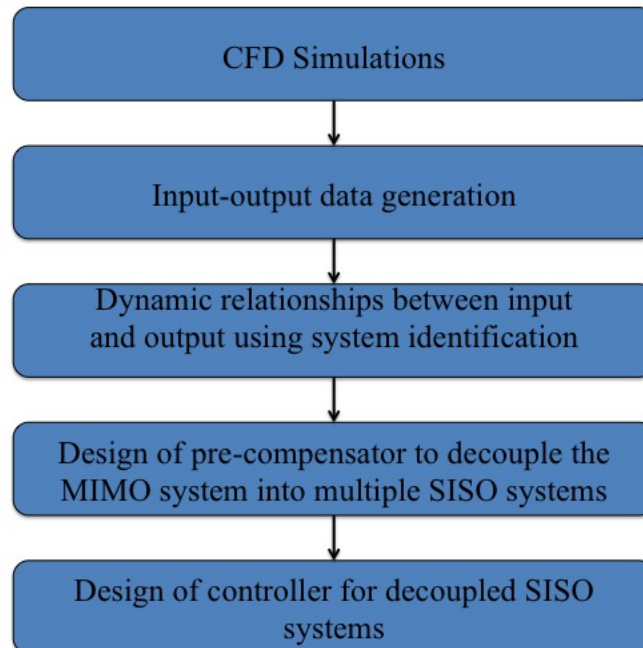


Figure 1.5: Methodology for control system design of SCWR

1.5 Outline of the thesis

The remaining thesis material is organized as follows :

In Chapter 2, a literature review of the thermal-hydraulic analysis and control system studies of supercritical fluid flow is presented. Chapter 3 consists of the comparison of steady state numerical results with the experimental data and the extension of the presented numerical models to simulate transient thermal-hydraulic behaviour for supercritical fluid flows. In Chapter 4, the detailed analysis of different modes for the heat transfer in supercritical fluids is performed by analysing the turbulence kinetic energy and velocity profiles, and various dimensionless parameters under broad range of operating conditions. Chapter 5 presents the methodology of control system design for supercritical water cooled reactor (SCWR) based on CFD results. The conclusion from the study are drawn in Chapter 6.

References

- [1] US DOE, NERAC, and GIF. A Technology Roadmap for Generation IV Nuclear Energy Systems. Technical report, 2002.
- [2] IL Piro, HF Khartabil, and RB Duffey. Heat transfer to supercritical fluids flowing in channels, empirical correlations (survey). *Nuclear Engineering and Design*, 230(1-3):69–91, 2004.
- [3] JY Yoo. The Turbulent Flows of Supercritical Fluids with Heat Transfer. *Annual Review of Fluid Mechanics*, 45:495–525, January 2013.
- [4] X Cheng and T Schulenberg. Heat Transfer at Supercritical Pressures: Literature Review and Application to an HPLWR. *Scientific report FZKA6609, Forschungszentrum Karlsruhe*, 2001.
- [5] S Mokry, I Piro, A Farah, K King, S Gupta, Wa Peiman, and P Kirillov. Development of supercritical water heat-transfer correlation for vertical bare tubes. *Nuclear Engineering and Design*, 241(4):1126–1136, 2011.

Chapter 2

Literature Review

2.1 Flow Dynamics and Heat transfer studies of supercritical fluid flow

The detailed literature review of heat transfer and fluid flow mechanism at supercritical condition is presented in this section. The study of heat transfer for supercritical fluids needs the in depth understanding of flow characteristics near supercritical condition. Thus, this section will consist of discussions on fluid flow structures in order to explain the heat transfer phenomenon.

2.1.1 Theoretical Background

It is indeed very important to discuss the two major effects differentiating fluids at the supercritical condition from the subcritical condition. These two effects besides property variation are the enhanced buoyancy effect and acceleration effect. The enhanced buoyancy effects are the result of the decrease in the density near the PCP whereas acceleration effect results from the increase in the thermal expansion coefficient. The acceleration effect can also be explained using mass conservation principle. When a constant heat is provided to a fluid, density of the fluid decreases near the PCP and to conserve the mass, the decreased density will cause an increase in the velocity, accelerating the flow. The buoyancy effect acts always in the direction of gravitational force, irrespective of the flow direction whereas acceleration effect always acts in

the direction of a flow irrespective of the gravitational force. Although these two effects are result of large property variation, researchers investigated these effects extensively because large changes in the density and thermal expansion coefficient affect the heat transfer phenomenon more than other properties do.

As discussed in the previous chapter, supercritical water shows abrupt changes in the thermophysical properties near the PCP. The peak in C_p near the PCP is one of the main reasons for the selection of supercritical water as a coolant in Gen IV nuclear reactor. Moreover, there is no boiling crisis in supercritical water which avoids severe deterioration in heat transfer (DHT) due to dryout. However, supercritical water shows sharp decrease in density near PCP causing DHT.

Hall et al.¹ explained the dominant cause of DHT as the modification of shear-stress distribution in the flow domain which in turn affects the turbulence production. In the similar direction, Tanaka et al.² developed an approximate analytical equations to predict the velocity and temperature profiles when both the acceleration and buoyancy effects are predominant. It was found that for low mass flux conditions when certain heat flux conditions are satisfied, the shear stress continues to decrease in the near wall region and achieves a negative value. As the consequence of the change in shear stress distribution, the velocity profile changes to "M-shaped" velocity profile indicating peaks in velocity in the near wall region.

2.1.2 Experimental Studies

The two major objectives for the experimental studies in supercritical fluids are, (1) to study the fluid flow and heat transfer mechanism and (2) to develop heat transfer correlations at supercritical conditions.

Although boiling crisis is avoided in supercritical water, strong variation in thermo-physical properties can cause flow instabilities near the PCP. The oscillations in pressure when temper-

ature approached the PCP was first observed by Bishop et al.³ and similar observations were also made by others.⁴⁻⁶ One of the possible reasons for this behaviour was given as unstable characteristics of the thin boundary layer formed because of abrupt thermophysical property changes. The alternate reason for this behaviour was suggested as the pseudoboiling which is similar to boiling in subcritical fluids. However, Shiralkar et al.⁷ and Swenson et al.⁸ commented that pseudoboiling theory does not hold for the supercritical fluids. Moreover, Hall et al.⁹ also concluded that the bubble formation might have caused due to the impurities and not the pseudoboiling. The common consensus among researchers on the satisfactory reason for the instability at supercritical pressures is still not achieved and this subject needs further investigation.¹⁰

The theoretical assumption of the effect of the buoyancy on the heat transfer mechanism in the supercritical fluids became more acceptable when the results for the upward and downward flows were compared.^{1,2} While the deteriorated heat transfer was major concern in the supercritical fluids, Yamagata et al.¹¹ found that in low heat flux conditions, the heat transfer coefficient increases significantly near the PCP. However, the peak in the heat transfer coefficient was found to decrease with the increase in the heat flux.¹² It was also reported that in upward flows, buoyancy effect can cause deterioration or enhancement in the heat transfer but in the downward flows only heat transfer enhancement is observed. However, the deterioration due to the acceleration effect can be observed in upward flows as well as downward flows.¹³ The fundamental reason for the buoyancy effect was given as the density variation in the radial direction whereas for the acceleration effect, it is the axial variation in density.¹⁰

The experiments are also carried out since 1970s to generate the wall temperature data for the validation of numerical models.^{11, 14-16} The validation of numerical models requires the experimental data in broad range of operating conditions of pressure, temperature, heat flux and mass flux. Hence, the experiments are still being carried out with the modern experimental equipments and techniques.^{17, 18} There were also a few experiments performed to find the flow structure in supercritical fluids.^{17, 19-22}

Kurganov et al.¹⁹ performed an experiment for the supercritical CO_2 flow in vertical circular tubes to study heat transfer, and velocity and temperature fields in deteriorated heat transfer condition. It was found that the deterioration is observed only in the upward flows and in the deteriorated heat transfer zone, structural changes in velocity (M-shaped profile) and shear stresses (negative values) are observed due to buoyancy and acceleration effects. Hence, these changes contribute to lower values of eddy viscosity (suppression in turbulence) in the fluid layer causing the deterioration in heat transfer.

The first approach to document the mean velocity and temperature profiles for upward turbulent air flow in uniformly heated circular tube was taken by Shehata et al.¹⁷ The experimental results obtained were used later to validate the DNS code by Bae et al.¹² Researchers have also been performing experiments to gather thermal-hydraulic data for supercritical fluids in geometries other than circular tubes. Experiments were performed by Wardana et al.²⁰ for air flow in annulus with strongly heated inner cylinder, Kang et al.²¹ for liquid R-113 flow in vertical annular channel and by Licht et al.²² for water flow in square annular channels.

The researchers have been trying to formulate the heat transfer correlations for supercritical fluids because the well known Dittus-Boelter correlation fails in the PCR. There are umpteen number of correlations in literature, but there are still discrepancies in the results using them for broad range of operating conditions. The single correlation to cover both the normal and deteriorated heat transfer is still awaited.²³ Piro et al.²⁴ and Yoo¹³ did an extensive literature survey on the research work in this direction and presented correlations developed by different researchers. The majority of those correlations are of Dittus-Boelter type which can be expressed by Equation 2.1.

$$Nu = CRe_{\theta}^{n_1} Pr_{\theta}^{n_2} F \quad (2.1)$$

where,

$$F = \overline{Pr}_{\infty}^{n_3} \left(\frac{\rho_w}{\rho_{\infty}} \right)^{n_4} \left(\frac{\mu_w}{\mu_{\infty}} \right)^{n_5} \left(\frac{\lambda_w}{\lambda_{\infty}} \right)^{n_6} \left(\frac{\bar{c}_p}{c_{p\infty}} \right)^{n_7} \phi$$

Researchers have found different values for C , n_1 & n_2 and expression for F . The factor F is based on the ratio of values of different thermophysical properties of bulk fluid and fluid at

wall. The summary of all the heat transfer correlations for supercritical water flow in circular tubes is given in Table 3.1.

Table 2.1: Parameters corresponding to Heat Transfer correlations

	C	θ	n_1	n_2	n_3	n_4	n_5	n_6	n_7	ϕ
Dittus-Boelter ²⁵	0.023	b	0.80	0.40	0.0	0.0	0.0	0.0	0.0	1.0
Swenson et al. ⁸	0.00459	w	0.923	0.0	0.613	0.231	0.0	0.0	0.0	1.0
Yamagata et al. ¹¹	0.0135	b	0.85	0.8	-	-	-	-	-	-
	where $F = 1$ for $E > 1$ $F = 0.67 + Pr_{pc}^{-0.05} (\overline{C}_p / C_{pb})^{n_1}$ for $0 \leq E \leq 1$ $F = (\overline{C}_p / C_{pb})^{n_2}$ for $E < 0$ $n_1 = -0.77(1 + 1/Pr_{pc}) + 1.49,$ $n_2 = 1.44(1 + 1/Pr_{pc}) - 0.53,$									
Jackson et al. ²⁶	0.0183	b	0.82	0.0	0.5	0.3	0.0	0.0	0.0	1.0
Watt et al. ²⁷	0.021	b	0.80	0.0	0.55	0.350	0.0	0.0	0.0	ϕ_w
	where $\phi_w = 1$ for $Bu^* < 10^{-5}$ $\phi_w = [1 - 3000 Bu^*]^{0.295}$ for $10^{-5} < Bu^* < 10^{-4}$ $\phi_w = [7000 Bu^*]^{0.295}$ for $Bu^* > 10^{-4}$ $Bu^* = \frac{\overline{Gr}_\infty}{Re_\infty^{2.7} \overline{Pr}_\infty^{0.50}}$ and $\overline{Gr}_\infty = g \left(1 - \frac{\rho_w}{\rho_\infty}\right) \frac{D^3}{\nu_\infty^2}$									
Gorban et al. ²⁸	0.0059	b	0.9	-0.12	0.0	0.0	0.0	0.0	0.0	1.0
Jackson ²⁹	0.0183	b	0.82	0.50	0.0	0.30	0.0	0.0	n_j	1.0
	where $n_j = 0.4$ for $T_\infty < T_w < T_{pc}$ and $1.2 T_{pc} < T_\infty < T_w$ $n_j = 0.4 + 0.2 \left(\frac{T_w}{T_{pc}} - 1\right)$ for $T_\infty < T_{pc} < T_w$ $n_j = 0.4 + 0.2 \left(\frac{T_w}{T_{pc}} - 1\right) \left[1 - 5 \left(\frac{T_\infty}{T_{pc}} - 1\right)\right]$ for $T_{pc} < T_\infty < 1.2 T_{pc}$ and $T_\infty < T_w$									
Mokry et al. ¹⁸	0.0061	b	0.904	0.0	0.684	0.564	0.0	0.0	0.0	1.0

2.1.3 Computational Studies

As a cost effective approach, computational studies are also performed to investigate the heat transfer and fluid flow mechanism in supercritical fluids. The CFD studies for turbulent flows are generally categorized as: (1) Direct Numerical Simulations (DNS) (2) Large Eddy Simulations (LES) (3) Reynolds Averaged Navier-Stokes (RANS). In DNS, the smallest eddy is fully resolved and no turbulence models are required to model the Reynolds stresses. However, this method is computationally very expensive and it is not possible for industrial applications with high Reynolds number flows due to higher computational time and cost. Whereas in RANS, all the eddies are modelled using turbulence models. RANS method with appropriate turbulence models is widely used for the industrial applications but some of the fundamental information about the flow is lost. The LES method is a mix of DNS and RANS. In LES, larger eddies are fully resolved and smaller eddies are modelled. The filtering functions are used to differentiate between the smaller and larger eddies. This method is computationally expensive than RANS but less expensive than DNS. However, it is still not widely used for industrial applications due to its higher computational resource requirement. In the experimental studies, it is not possible to extract all the important information regarding turbulence. Hence, DNS studies are used as numerical experiments to provide the inputs for designing of new turbulence models.^{12, 30}

The earlier work to simulate the supercritical fluid flow and heat transfer was carried out using Prandtl's mixing length model. Bellmore et al.³¹ implemented the density fluctuations in the turbulent transport equations to simulate the flow of near critical para- H_2 in vertical tubes. With the development of two-equation $k - \epsilon$ model,^{32, 33} improved results were found in the numerical studies.^{6, 34} Bellinghausen et al.³⁴ implemented the low-Reynolds number $k - \epsilon$ model by resolving the near wall region to consider the enhanced gravitational effects and the results were in close agreement with the experimental data. Koshizuka et al.⁶ also carried out numerical simulations using low-Reynolds number $k - \epsilon$ model for the deteriorated heat transfer case and the satisfactory comparison was found with the experimental results of Yamagata et al.¹¹

Another two equation $k - \omega$ model was developed by Wilcox³⁵ in 1990s. The strength

of $k - \omega$ model is in near wall region where no damping functions have to be used as in the low-Reynolds number $k - \epsilon$ model. However, the $k - \omega$ model³⁵ is sensitive to free stream conditions. To combine the strength of $k - \epsilon$ and $k - \omega$ model, Menter³⁶ proposed a method of blending function. This blending function uses the $k - \epsilon$ model in free stream and switches to $k - \omega$ model in the boundary layer region. This model is known as $k - \omega SST$ model. The modification of the original $k - \omega$ model to $k - \omega SST$ model sparked interest in researchers to simulate the supercritical fluids using the $k - \omega SST$ model.³⁷⁻⁴¹

Yang et al.³⁷ performed numerical simulations for the heat transfer in supercritical water flow in circular tubes using $k - \omega$ and $k - \omega SST$ model. It was reported that both the models fail to predict the heat transfer coefficient near the PCR. However, the results were found to be better than the low-Reynolds number $k - \epsilon$ model.

Palko et al.^{38,40} performed the numerical simulations using $k - \omega SST$ model and compared the results with the experiments of Onratskij et al.¹⁶ and Shitsman.¹⁴ The numerical simulations were able to predict the deteriorated heat transfer and the results showed that the buoyancy and variation in thermal conductivity have significant effect on the heat transfer deterioration phenomenon. However, it was also indicated that these are not the only mechanisms governing the heat transfer deterioration phenomenon. The influences of the density variation and acceleration were not studied in their study owing to the limitations of solver, but it was recommended for the further investigation.

Cheng et al.³⁹ performed the numerical simulations using ω type turbulence models and compared the results with the experimental data of Yamagata et al.¹¹ The ω type turbulence models failed completely to predict the heat transfer coefficient, which might be because of not taking variation in the property of fluid into consideration while implementing the ω type turbulence models. Hence, these models with automatic wall treatment were not recommended to be used for further applications of supercritical fluid flows.

The 2-equation turbulence models are based on the assumptions of isotropy of turbulence

where normal stress in each direction is equal. Although the modelling process is simplified due to this assumption, 2-equation turbulence models can not predict anisotropic behaviour of turbulence stresses. Researchers have also explored the use of anisotropic turbulence models for simulating supercritical fluid flow.^{39, 42} Zhang et al.⁴² implemented the Reynolds Stress Model (RSM) in numerical simulations and compared the results with three different sets of experimental results for supercritical water and CO_2 flowing in circular tubes. Along with RSM, five other isotropic turbulence models are also validated in this study and it is found that the RSM performs better than all other turbulence models. Similarly, excellent agreement with the experimental results were found by Cheng et al.³⁹ when variants of RSM by Launder (LRR) and Speziale (SSG) were implemented in their numerical simulations. Considering the physics behind the development of turbulence models, anisotropic turbulence models are expected to perform better than the isotropic turbulence models. However, the anisotropic models have not been validated extensively by researchers. To assess the capability of the turbulence models, validation with the experiments of broad range of operating conditions is important.

2.2 Control System Studies

The several studies have been carried out for the SCWR's thermal-hydraulic analysis, safety analysis, materials study, instability analysis and fuel channel design. However, there are not adequate studies done in the direction of dynamic analysis and control system design of the SCWR. The SCWR is similar to boiling water reactor (BWR) considering the aspect that both are direct cycle reactors. The SCWR also shares the similarity with the pressurized water reactor (PWR) considering the high operating pressure and single phase flow. Although SCWR has similarities of both BWR and PWR, it also has unique feature of high heat flux to mass flux ratio and sharp changes in thermo-physical properties. Owing to these unique features, SCWR has strong cross-coupling and high degree of non-linearity in its transient behaviour.

Earlier study for the control system design for supercritical fast reactor (SCFR) was done by Nakatsuka et al.⁴³ The transient behaviour of the reactor was analyzed using the Dittus-

Boelter correlation in the numerical simulations. Based on the transient simulations, pairing of the input and output was determined. Based on these pairings, the control strategy used for BWR was used for the control system design of the SCFR. The trial and error method was used to tune the controller parameters. The similar approach was also used by Ishiwatari et al.⁴⁴ for high temperature supercritical light water reactor. In the subsequent work by Ishitawari et al.,⁴⁵ the improvements in the feed water controller were proposed for a Fast Reactor. However, all these studies were designed where multiple input and multiple output (MIMO) system was converted to single input and single output (SISO) systems using decentralized structure.⁴⁶ This approach is valid for the weakly coupled systems but the SCWR is highly coupled MIMO system. The very first approach to decouple the CANDU SCWR MIMO system into multiple SISO systems was taken by Sun.⁴⁶

Sun⁴⁶ has used the simple 1-D model to simulate the transient behaviour of the Canadian SCWR. Based on these results, the dynamic relationship was established between the inputs and output using system identification technique. Next, the direct Nyquist array method was implemented to decouple the system and convert to diagonally dominant form using pre-compensator. Based on the pre-compensated plant, loop compensator was designed for the system control and stability. The control methodology used by Sun⁴⁶ is based on the simple 1-D approximation of the reactor. However, more accurate method to simulate the transient thermal-hydraulic behaviour of SCWR is needed.

2.3 Motivation

As discussed before, the researchers have implemented numerous turbulence models to numerically simulate the thermal-hydraulic behaviour of the supercritical fluids. Among all the studies, $k - \omega SST$ model is found to be better than the $k - \epsilon$ models but there is still no consensus among researchers regarding the behaviour $k - \omega SST$ model in the PCR. Moreover, the anisotropic models which are found to be better than the 2-equation models by previous researchers but the extensive validation and analysis for the anisotropic models is still awaited.

Therefore, the extensive validation of a CFD model using RSM and $k - \omega SST$ model is performed in this study.

The DHT is very important phenomenon in the supercritical fluid flow and heat transfer. The most of the numerical models fail to predict the DHT and the corresponding wall temperatures in the DHT zone. Hence, in this study, the DHT phenomenon is analysed using the turbulent kinetic energy (TKE) and velocity distribution and their effect on heat transfer. Moreover, the acceleration and buoyancy parameters, and different types of pressure drop values are used to study the occurrence of DHT in supercritical fluid flows.

Earlier control system studies for SCWR used the simple 1-D model for establishing the relationship between the inputs and outputs. The MIMO SCWR system is approximated by many researchers to multiple SISO systems ignoring the coupling involved. Therefore, in the present study, CFD simulations are performed to find the relationship between input and outputs. Furthermore, the decoupling methodology is used to make the MIMO system diagonally dominant and finally converting it to multiple SISO systems to facilitate the control system design.

References

- [1] WB Hall and JD Jackson. Laminarization of a turbulent pipe flow by buoyancy forces. In *Mechanical Engineering*, volume 91, page 66. ASME-AMER SOC MECHANICAL ENG 345 E 47TH ST, NEW YORK, NY 10017, 1969.
- [2] H Tanaka, A Tsuge, M Hirata, and N Nishiwaki. Effects of buoyancy and of acceleration owing to thermal expansion on forced turbulent convection in vertical circular tubes criteria of the effects, velocity and temperature profiles, and reverse transition from turbulent to laminar flow. *Journal of Heat and Mass transfer*, 16(6):1267–1288, 1973.
- [3] AA Bishop, RO Sandberg, and LS Tong. Forced-convection heat transfer to water at near-critical temperatures and supercritical pressures. Technical report, Westinghouse Electric Corp., Pittsburgh, Pa. Atomic Power Div., 1964.
- [4] JW Ackerman. Pseudoboiling heat transfer to supercritical pressure water in smooth and ribbed tubes. *Journal of Heat transfer*, 92(3):490–497, 1970.
- [5] V Chatoorgoon. Stability of supercritical fluid flow in a single-channel natural-convection loop. *International Journal of Heat and Mass Transfer*, 44:1963–1972, 2001.
- [6] S Koshizuka, N Takano, and Y Oka. Numerical analysis of deterioration phenomena in heat transfer to supercritical water. *International Journal of Heat and Mass Transfer*, 38(16):3077–3084, 1995.
- [7] B Shiralkar and P Griffith. The effect of swirl, inlet conditions, flow direction, and tube diameter on the heat transfer to fluids at supercritical pressure. *Journal of Heat Transfer*, 92(3):465–471, 1970.
- [8] HS Swenson, JR Carver, and CR Kakarala. Heat transfer to supercritical water in smooth-bore tubes. *Journal of Heat Transfer*, 87(4):477–483, 1965.
- [9] WB Hall and JD Jackson. Heat transfer near the critical point. keynote lecture. pages 377–92. 6th Int. Heat Transfer Conf., 1978.

- [10] H Li, H Wang, Y Luo, H Gu, X Shi, T Chen, E Laurien, and Y Zhu. Experimental investigation on heat transfer from a heated rod with a helically wrapped wire inside a square vertical channel to water at supercritical pressures. *Nuclear Engineering and Design*, 239(10):2004–2012, 2009.
- [11] K Yamagata, K Nishikawa, S Hasegawa, T Fuji, and S Yoshida. Forced convective heat transfer to supercritical water flowing in tubes. *Journal of Heat and Mass transfer*, 15(12):2575–2593, 1972.
- [12] JH Bae, JY Yoo, and H Choi. Direct numerical simulation of turbulent supercritical flows with heat transfer. *Physics of Fluids*, 17(10):105104, 2005.
- [13] JY Yoo. The Turbulent Flows of Supercritical Fluids with Heat Transfer. *Annual Review of Fluid Mechanics*, 45:495–525, January 2013.
- [14] ME Shitsman. Impairment of the heat transmission at supercritical pressures(heat transfer process examined during forced motion of water at supercritical pressures). *High Temperature*, 1:237–244, 1963.
- [15] LF Glushchenko, SI Kalachev, and OF Gandzyuk. Determining the conditions of existence of deteriorated heat-transfer at supercritical pressure of medium. *Thermal Engineering*, 19(2):107–111, 1972.
- [16] AP Ornatskij, LF Glushchenko, and SI Kalachev. Heat transfer with rising and falling flows of water in tubes of small diameter at supercritical pressures. *Thermal Engineering*, 18(5):137–141, 1971.
- [17] AM Shehata and DM McEligot. Mean structure in the viscous layer of strongly-heated internal gas flows measurements. *International Journal of Heat and Mass Transfer*, 41(24):4297–4313, 1998.
- [18] S Mokry, I Pioro, A Farah, K King, S Gupta, W Peiman, and P Kirillov. Development of supercritical water heat-transfer correlation for vertical bare tubes. *Nuclear Engineering and Design*, 241(4):1126–1136, 2011.

- [19] VA Kurganov and AG Kaptil'ny. Velocity and enthalpy fields and eddy diffusivities in a heated supercritical fluid flow. *Experimental Thermal and Fluid Science*, 5(4):465–478, 1992.
- [20] I Wardana, T Ueda, S Kurihara, and M Mizomoto. Turbulence structure in an annuli with strongly heated inner cylinder. *Experiments in Fluids*, 27(2):137–144, 1999.
- [21] S Kang, B Patil, JA Zarate, and RP Roy. Isothermal and heated turbulent upflow in a vertical annular channel—part i. experimental measurements. *International Journal of Heat and Mass Transfer*, 44(6):1171–1184, 2001.
- [22] J Licht, M Anderson, and M Corradini. Heat transfer and fluid flow characteristics in supercritical pressure water. *Journal of Heat Transfer*, 131(7):072502, 2009.
- [23] YY Bae and HY Kim. Convective heat transfer to co2 at a supercritical pressure flowing vertically upward in tubes and an annular channel. *Experimental Thermal and Fluid Science*, 33(2):329–339, 2009.
- [24] IL Piore, HF Khartabil, and RB Duffey. Heat transfer to supercritical fluids flowing in channels, empirical correlations (survey). *Nuclear Engineering and Design*, 230(1-3):69–91, 2004.
- [25] FP Incropera. *Introduction to heat transfer*. John Wiley & Sons, 2011.
- [26] JD Jackson and J Fewster. Forced convection data for supercritical pressure fluids. *Heat Transfer Fluid Flow Science 21540*, Harwell, UK, 1975.
- [27] MJ Watts and CT Chou. Mixed convection heat transfer to supercritical pressure water. In *Proceedings of the 7th International Heat Transfer Conference. Vol 3*, pages 495–500, 1982.
- [28] LM Gorban, RS Pomet'ko, and OA Khryashev. Modeling of water heat transfer with freon of supercritical pressure. *Institute of Physics and Power Engineering, Obninsk*, 1990.

- [29] JD Jackson. Consideration of the heat transfer properties of supercritical pressure water in connection with the cooling of advanced nuclear reactors. In *Proc. 13th Pacific basin Nuclear Conference, Shenzhen City, China*, pages 21–25, 2002.
- [30] JH Bae, JY Yoo, and DM McEligot. Direct numerical simulation of heated co₂ flows at supercritical pressure in a vertical annulus at re= 8900. *Physics of Fluids (1994-present)*, 20(5):055108, 2008.
- [31] CP Bellmore and RL Reid. Numerical prediction of wall temperatures for near-critical para-hydrogen in turbulent upflow inside vertical tubes. *Journal of Heat Transfer*, 105(3):536–541, 1983.
- [32] WP Jones and BE Launder. The prediction of laminarization with a two-equation model of turbulence. *International Journal of Heat and Mass Transfer*, 15(2):301–314, 1972.
- [33] BE Launder and BI Sharma. Application of the energy-dissipation model of turbulence to the calculation of flow near a spinning disc. *Letters in heat and mass transfer*, 1(2):131–137, 1974.
- [34] R Bellinghausen and U Renz. Pseudocritical heat transfer inside vertical tubes. *Chemical Engineering and Processing: Process Intensification*, 28(3):183–186, 1990.
- [35] DC Wilcox. Reassessment of the scale-determining equation for advanced turbulence models. *AIAA journal*, 26(11):1299–1310, 1988.
- [36] FR Menter. Zonal two equation k-turbulence models for aerodynamic flows. *AIAA paper*, 2906:1993, 1993.
- [37] J Yang, Y Oka, Y Ishiwatari, J Liu, and J Yoo. Numerical investigation of heat transfer in upward flows of supercritical water in circular tubes and tight fuel rod bundles. *Nuclear Engineering and Design*, 237(4):420–430, February 2007.
- [38] D Palko and H Anglart. Theoretical and numerical study of heat transfer deterioration in HPLWR. In *Nuclear Energy for Europe*, pages 1–8, 2007.

- [39] X Cheng, B Kuang, and YH Yang. Numerical analysis of heat transfer in supercritical water cooled flow channels. *Nuclear Engineering and Design*, 237(3):240–252, February 2007.
- [40] D Palko and H Anglart. Deteriorated heat transfer at low coolant flow rates. In *International Students Workshop on HPLWR*, pages 1–4, 2008.
- [41] QL Wen and HY Gu. Numerical investigation of acceleration effect on heat transfer deterioration phenomenon in supercritical water. *Progress in Nuclear Energy*, 53(5):480–486, 2011.
- [42] Y Zhang, C Zhang, and J Jiang. Numerical simulation of heat transfer of supercritical fluids in circular tubes using different turbulence models. *Journal of Nuclear Science and Technology*, 48(3):366–373, 2011.
- [43] T Nakatsuka, Y Oka, and S Koshizuka. Control of a fast reactor cooled by supercritical light water. *Nuclear technology*, 121(1):81–92, 1998.
- [44] Y Ishiwatari, Y Oka, and S Koshizuka. Control of a high temperature supercritical pressure light water cooled and moderated reactor with water rods. *Journal of Nuclear Science and Technology*, 40(5):298–306, 2003.
- [45] Y Ishiwatari, C Peng, S Ikejiri, and Y Oka. Improvements of feedwater controller for the super fast reactor. *Journal of Nuclear Science and Technology*, 47(12):1155–1164, 2010.
- [46] P Sun. *Dynamic Model Construction and Control System Design for Canadian Supercritical Water-cooled Reactors*. PhD thesis, The University of Western Ontario, 2012.

Chapter 3

Numerical Models to Predict Steady and Unsteady Thermal-hydraulic Behaviour of Supercritical Water Flow in Circular Tubes

Abstract

The present paper is aimed at the development of numerical models to predict steady and unsteady thermal-hydraulic behavior of supercritical water flow at various operating conditions. A simple one-dimensional numerical thermal-hydraulic model based on a finite-difference scheme has been developed. A detailed computational fluid dynamic (CFD) analysis based on two turbulence models, Reynolds Stress Model and $k - \omega SST$ model, has also been presented in this paper. Seven experimental cases of steady state and vertically up flowing supercritical water in circular tubes operated at various working regimes, such as normal and deteriorated heat transfer regions, are used to validate the numerical models. Comparisons for steady state flow show good agreement between the numerical and experimental results for all normal heat transfer cases and most of the deteriorated heat transfer cases.

Next, the numerical models are used for transient simulations. Three case studies are undertaken with a purpose to quantify the time dependent responses from both the 1-D model and CFD model. The comparisons carried out for both the normal and deteriorated heat transfer conditions show good agreement between the two numerical models.

Keywords: supercritical water, numerical models, deteriorated heat transfer, steady state, transient analysis

Nomenclature

a	Acoustic speed, m/s
A	Area, m^2
c_p	Specific heat capacity at constant pressure, $J/kg K$
\bar{c}_p	$(h_w - h_b)/(T_w - T_b)$, $J/kg K$
D	Diameter of a tube, m
e	Specific internal energy, J/kg
g	Gravitational acceleration, m/s^2
G	Mass flux, $kg/m^2 s$
h	Specific enthalpy, J/kg
h_∞	Heat transfer coefficient, $W/m^2 ^\circ C$
k	Turbulence kinetic energy, m^2/s^2
L	Length, m
L_h	Heated length, m
p	Pressure, Pa
P_w	Wetted perimeter, m
q_w	Wall heat flux, W/m^2
q'_w	Wall heat per unit length, W/m
r	Distance from the centre of the tube, m
r^*	Non-dimensional radial location
t	Time, s
T	Temperature, $^\circ C$
u	Velocity, m/s
W	Mass flow rate, kg/s
y	Distance from the wall, m
y^+	Non-dimensional distance from the wall, $u_\tau y/\nu$, m
z	Axial location, m
z^*	Non-dimensional axial location

Greek Letters

α	Thermal expansion coefficient, $1/K$
ϵ	Energy dissipation per unit mass, m^2/s^3
λ	Thermal conductivity, W/mK
μ	Dynamic viscosity, $Pa\ s$
ν	Kinematic viscosity, m^2/s
ρ	Density of a fluid, kg/m^3
τ	Shear stress ; τ_w , wall shear stress, N/m^2
ω	Specific dissipation rate, $1/s$

Subscripts

cr	Value at critical point
dht	Deteriorated heat transfer
ex	Exit
exp	Experimental data
f	Values at film, reference values between $y=0$ and $y=y$
in	Inlet
m	Mean
num	Numerical
pc	Pseudo-critical
q	Based on local heat flux value
t	Turbulent
w	Wall
∞	Bulk

Dimensionless Numbers

Bu^*	Buoyancy Parameter, $\overline{Gr}_b/Re_b^{2.7}\overline{Pr}_b^{0.50}$
\overline{Gr}_b	$g(1 - \rho_w/\rho_b)D^3/\nu_b^2$
Nu	Nusselt Number
Pr	Prandtl Number, $\mu c_p/k$
\overline{Pr}	$\mu\overline{c}_p/k$
Re	Reynolds Number, $\rho u D/\mu$

Acronyms

AECL	Atomic Energy of Canada Limited
BC	Boundary Condition
BWR	Boiling Water Reactor
CFD	Computational Fluid Dynamics
DHT	Deteriorated Heat Transfer
HTC	Heat Transfer Coefficient
HTCD	Heat Transfer Coefficient by Dittus - Boelter
HTCJ	Heat Transfer Coefficient by Jackson et al.
HTCM	Heat Transfer Coefficient by Mokry et al.
HTCS	Heat Transfer Coefficient by Swenson et al.
HTCW	Heat Transfer Coefficient by Watts et al.
MAE	Mean Absolute Error
NHT	Normal Heat Transfer
PCR	Pseudo Critical Region
RSM	Reynold Stress Model
SCR	Supercritical Reactor
SCW	Supercritical Water
SCWR	Supercritical Water Cooled Reactor
SD	Standard Deviation
SST	Shear Stress Transport
TH	Thermal-Hydraulic
THRUST	Thermal-Hydraulic solveR Undertaking Supercritical waTer
TKE	Turbulence Kinetic Energy

3.1 Introduction

The supercritical water cooled reactor (SCWR) has been identified as one of the six proposed technologies for the Generation IV nuclear reactors¹ because of its advantage of high thermal efficiency, compact plant system, avoidance from boiling crisis and close proximity to the proven technology of supercritical fossil power plants. Therefore, SCWR has received attention among the researchers of various disciplines at present. The fluid flow and heat transfer characteristics and the thermo-physical properties of various substances, such as water and CO₂, at supercritical conditions have been studied extensively since 1950s, such as the experimental research works carried out by Yamagata et al.,² Swenson et al.,³ Jackson⁴ and many more as mentioned in the review papers by Duffey and Pioro,⁵ Pioro et al.⁶ and Jager et al.⁷ However, there are still issues need to be addressed in order to meet the present demand of making the SCWR technologically viable and economically feasible with adequate safety margin and to predict its behavior accurately at normal and anticipated accidental operating situations.

In addition to the numerous experimental studies, economically attractive alternatives, the numerical approaches have been used extensively in recent years to get detailed insight into the heat transfer mechanism in supercritical fluids. In numerical studies, two approaches can be used - (i) CFD models and (ii) one-dimensional thermal-hydraulic (TH) models. The former approach is computationally expensive and its main challenge is to implement the accurate turbulence models for supercritical fluids. However, it can provide detailed information on the flow and heat transfer in all the directions. While the latter approach, which takes into account the axial variation of flow and thermodynamic properties, and averages the quantities along radial and azimuthal directions, is computationally efficient, flexible and may have the required accuracy if the empirical heat transfer correlation (HTC) are implemented properly.

Earlier numerical studies for supercritical flows using CFD models were done by Deissler et al.⁸ and Shiralkar et al.⁹ using the turbulence models based on eddy diffusivity assumption. With the development of two equation turbulence models, $k - \epsilon$ and $k - \omega$ type turbulence models have been validated for the fluid flow and heat transfer investigation for supercritical

fluids. Later, the $k-\omega SST$ model developed by Menter¹⁰ which combines the strength of $k-\epsilon$ model in free stream region and strength of $k-\omega$ in recirculating regions is used by various researchers, such as Cheng et al.¹¹ and Palko et al.^{12, 13} However, there is no common consensus among researchers regarding the capability of $k-\omega SST$ model for studying the heat transfer phenomenon in supercritical fluid flows. Therefore, in the current study, $k-\omega SST$ model will be used to assess its capability in predicting supercritical fluid flows under various operating conditions. It is important to note that the two-equation turbulence models are developed with the isotropic assumption. The researchers have also used anisotropic turbulence models such as the Reynolds Stress Model for supercritical water flow in various geometries.^{11, 14} It was concluded from these studies that anisotropic turbulence models give better agreement with experimental results than other two-equation models with isotropic assumption for chosen experimental conditions. As the turbulence models are sensitive to operating conditions, in the current study, the turbulence model RSM is also evaluated against experimental data to assess its capability under different operating conditions. The CFD simulations are carried out using the commercial software Ansys FLUENT 14.5.

There are several 1-D TH models, such as those developed by Chatoorgoon et al.,¹⁵⁻¹⁷ Ambrosini et al.,¹⁸ Gomez et al.¹⁹ and Jain and Rizwan-uddin.²⁰ But those models were mainly used to predict the static and dynamic instabilities of supercritical reactors (SCRs) without giving much attention to evaluate their capability in predicting the wall temperature. The predicted wall temperature using the 1-D model depends on the empirical HTC's used in the model. Moreover, there are umpteen number of HTC's available in the literature which are experiment specific and thus, need validation before using them with TH model.

The reviews conducted by several authors^{6, 21, 22} showed that the numerically predicted wall temperature is in good agreement with the experimental data mainly for the normal heat transfer (NHT) cases. However, for the deteriorated heat transfer (DHT) cases which are characterised by a sharp increase in the wall temperature, the numerical predictions are found to be challenging. Therefore, the numerical models presented in this study will be validated for both NHT and DHT cases.

The in-house 1-D Thermal-Hydraulic solveR Undertaking Supercritical waTer (THRUST), which is an extension of an earlier model used for simulating boiling water reactor (BWR),²³ is used for SCWR in the present work. It is based on mass, momentum and energy conservation equations and includes the thermodynamic equation of state to take care of pressure and temperature dependent property variations.

In this study, the THRUST and CFD models are evaluated by comparing the simulation results with the experimental data under various operating conditions. Further, both the numerical models are extended to simulate the transient response. Subsequently, the step change and periodic variation of various physical variables are introduced with a purpose to assess the capability of the numerical models to predict the heat transfer phenomenon during the transient process.

3.2 Mathematical details of the numerical models

The mathematical details of the THRUST and CFD models are presented in this section. The present analysis is carried out under both steady state and transient conditions.

3.2.1 Mathematical formulations of the 1-D TH model

In the 1-D THRUST, it is assumed that the thermo-physical flow properties vary along the axial direction only and the heat flux at the periphery of the circular tube is constant. The general fundamental one-dimensional governing equations for fluid flow and heat transfer are as follows:

Mass conservation equation:

$$\frac{\partial}{\partial t} (\rho A) + \frac{\partial}{\partial z} (\rho A u) = 0 \quad (3.1)$$

Momentum conservation equation in the axial direction:

$$\frac{\partial}{\partial t} (\rho A u) + \frac{\partial}{\partial z} (\rho A u^2) = -A \frac{\partial p}{\partial z} - \tau_w P_w - \rho A g \frac{dH}{dz} \quad (3.2)$$

Energy conservation equation:

$$\frac{\partial}{\partial t} (\rho A e) + \frac{\partial}{\partial z} (\rho A u e_f) = q_w P_H \quad (3.3)$$

where $e = e_f - \frac{p}{\rho}$ and $e_f = h + \frac{u^2}{2} + gH$.

These equations can be written in a compact form as follows:

$$\frac{\partial}{\partial t} [\underline{\mathbf{R}}] + \frac{\partial}{\partial z} [\underline{\mathbf{S}}] = [\underline{\mathbf{T}}] \quad (3.4)$$

where

$$\underline{\mathbf{R}} = \begin{bmatrix} \rho A \\ \rho A u \\ \rho A e \end{bmatrix}, \quad \underline{\mathbf{S}} = \begin{bmatrix} \rho A u \\ A(\rho u^2 + p) \\ \rho A u e_f \end{bmatrix}, \quad \underline{\mathbf{T}} = \begin{bmatrix} 0 \\ p \frac{dA}{dz} - \tau_w P_w - \rho A g \frac{dH}{dz} \\ q_w P_H \end{bmatrix}$$

These governing equations in a conservative form are first converted into the following primitive form:

$$\frac{\partial}{\partial t} [\underline{\mathbf{U}}] + \underline{\mathbf{A}}(\underline{\mathbf{U}}) \frac{\partial}{\partial z} [\underline{\mathbf{U}}] = [\underline{\mathbf{D}}(\underline{\mathbf{U}})] \quad (3.5)$$

where $\underline{\mathbf{U}}$ is a vector of unknown dependent variables $[W, h, p]^T$, $\underline{\mathbf{A}}$ is a square matrix of coefficients which are functions of $\underline{\mathbf{U}}$, and $\underline{\mathbf{D}}$ is a vector containing allowances for mass, momentum, and energy to transfer across the system boundaries.

Equation of state, $\rho = \rho(p, h)$, is used and it is noted that all the thermodynamic properties in the present model are subjected to change depending on the pressure and enthalpy along the axial direction of the channel.

The eigenvalues of matrix $\underline{\mathbf{A}}$ determine the mathematical class of Eq. (3.5) and it is found that all eigenvalues of $\underline{\mathbf{A}}$ are real ($u, u + a, u - a$); and hence the governing equations are hyperbolic ones. Next, the set of Eq. (3.5) are transformed into a characteristic form and it can be written as the following:

$$\underline{\underline{\mathbf{B}}} \frac{\partial}{\partial t} [\underline{\mathbf{U}}] + \underline{\underline{\mathbf{A}}} \underline{\underline{\mathbf{B}}} \frac{\partial}{\partial z} [\underline{\mathbf{U}}] = [\underline{\mathbf{C}}] \quad (3.6)$$

where $\underline{\underline{\mathbf{A}}}$ is a diagonal matrix of eigenvalues of $\underline{\underline{\mathbf{A}}}$.

After coefficient and source term linearization, Eq. (3.6) is discretized with a characteristics-dependent implicit finite-difference scheme where the spatial derivative terms are approximated by backward or forward difference depending on the sign of the characteristics. For the present case of subsonic flow ($u < a$), the spatial derivatives for the first two governing equations, which are characterized by $\Lambda_{11} = u + a > 0$ and $\Lambda_{22} = u > 0$, respectively, are approximated by backward difference equations and the third governing equation, which is characterized by $\Lambda_{33} = u - a < 0$, is approximated by forward difference equation. The resultant discretized equations are then combined together and used for numerical solution depending on the boundary conditions for the particular problem.

Steady state solution methodology

The resultant discretized equations for Eqs.(3.1)-(3.3) for steady state flows are as follows:

$$\rho_{i+1} A_{i+1} u_{i+1} = \rho_i A_i u_i \quad (3.7a)$$

$$p_i - p_{i+1} = \frac{1}{2} \left(\frac{1}{A_i} + \frac{1}{A_{i+1}} \right) [(\rho A u^2)_{i+1} - (\rho A u^2)_i] \\ + \frac{1}{2} \left[\{\rho (F + g)\}_i + \{\rho (F + g)\}_{i+1} \right] (z_{i+1} - z_i) \quad (3.7b)$$

$$(e_f)_{i+1} - (e_f)_i = \frac{1}{2} \left[\left(\frac{q'_w}{\rho A u} \right)_i + \left(\frac{q'_w}{\rho A u} \right)_{i+1} \right] (z_{i+1} - z_i) \quad (3.7c)$$

The above set of equations, in addition to the thermodynamic equation of state, are solved numerically by using a forward marching scheme when all the inlet primary variables, i.e., inlet velocity, enthalpy and pressure are specified, otherwise a shooting method along with the forward marching scheme is employed to treat different set of specified boundary conditions.

Heat transfer coefficient and friction factor

The accuracy of such a 1-D TH model largely depends on appropriate selection of friction factor and HTC. In spite of extensive experimental investigations for last several decades, a

common consensus in standardizing the use of general purpose HTC for various geometry and operating conditions at supercritical region is still not available. The commonly used HTCs by Dittus - Boelter²⁴ (HTCD), Swenson et al.³ (HTCS), Watts et al.²⁵ (HTCW), Jackson⁴ (HTCJ) and Mokry et al.²⁶ (HTCM) based on experimental data may be limited to specific conditions.

The simulations in this study are carried out by using Filonenko correlation²⁷ for the friction factor and 5 different HTCs mentioned above. The numerical results using different HTCs will be compared with the available experimental data to verify their suitability and limitations. The study on the effect of the friction factor is not done in the present study because of lack of availability of relevant experimental results on pressure drop and its spatial distribution along the channel.

The 5 HTCs used in this study have the following form:

$$Nu_{\theta} = C \times Re_{\theta}^{n_1} Pr_{\theta}^{n_2} \overline{Pr}_{\infty}^{n_3} \left(\frac{\rho_w}{\rho_{\infty}} \right)^{n_4} \left(\frac{\mu_w}{\mu_{\infty}} \right)^{n_5} \left(\frac{\lambda_w}{\lambda_{\infty}} \right)^{n_6} \left(\frac{\bar{c}_p}{c_{p\infty}} \right)^{n_7} \phi \quad (3.8)$$

where $\phi \equiv \phi \{z, T_{\infty}, T_w, \dots\}$ and the subscript θ represents ∞ , w or f depending on whether the bulk temperature, T_{∞} , wall temperature, T_w or mean film temperature, $T_f = \frac{1}{2}(T_{\infty} + T_w)$, is used to determine the thermodynamic properties in the corresponding correlation. The parametric details of the 5 HTCs used in the 1-D model are listed in the Table 3.1.

Methodology to determine the local wall temperature

The present study deals with the predefined heat flux at the circumference of the circular tubes. Therefore, all the thermodynamic variables representing the bulk properties of the SCW are obtained first by simultaneously solving the nonlinearly coupled steady state governing equations, i.e., Eqs. (3.7a)-(3.7c) and the thermodynamic equation of state. The calculation of Nu_{θ} using the Eq. (3.8) depends on the wall temperature which is assumed first to start the calculation. Next, the heat transfer coefficient, h_{∞} , and wall temperature, T_w , are determined by the

Table 3.1: Parameters corresponding to HTC correlations

	C	θ	n_1	n_2	n_3	n_4	n_5	n_6	n_7	ϕ
HTCD ²⁴	0.023	b	0.80	0.40	0.0	0.0	0.0	0.0	0.0	1.0
HTCJ ⁴	0.0183	b	0.82	0.50	0.0	0.30	0.0	0.0	n_j	1.0
where										
	$n_j = 0.4$	for $T_\infty < T_w < T_{pc}$ and $1.2 T_{pc} < T_\infty < T_w$								
	$n_j = 0.4 + 0.2 \left(\frac{T_w}{T_{pc}} - 1 \right)$	for $T_\infty < T_{pc} < T_w$								
	$n_j = 0.4 + 0.2 \left(\frac{T_w}{T_{pc}} - 1 \right) \left[1 - 5 \left(\frac{T_\infty}{T_{pc}} - 1 \right) \right]$	for $T_{pc} < T_\infty < 1.2 T_{pc}$ and $T_\infty < T_w$								
HTCM ²⁶	0.0061	b	0.904	0.0	0.684	0.564	0.0	0.0	0.0	1.0
HTCS ³	0.00459	w	0.923	0.0	0.613	0.231	0.0	0.0	0.0	1.0
HTCW ²⁵	0.021	b	0.80	0.0	0.55	0.350	0.0	0.0	0.0	ϕ_w
where										
	$\phi_w = 1$	for $Bu^* < 10^{-5}$								
	$\phi_w = [1 - 3000 Bu^*]^{0.295}$	for $10^{-5} < Bu^* < 10^{-4}$								
	$\phi_w = [7000 Bu^*]^{0.295}$	for $Bu^* > 10^{-4}$								
	$Bu^* = \frac{\overline{Gr}_\infty}{Re_\infty^{2.7} \overline{Pr}_\infty^{0.50}}$									
	and $\overline{Gr}_\infty = g \left(1 - \frac{\rho_w}{\rho_\infty} \right) \frac{D^3}{\nu_\infty^2}$									

following equations sequentially:

$$h_\infty = \frac{Nu_\theta \lambda_\theta}{D} \quad (3.9)$$

$$T_w = T_\infty + \frac{q_w}{h_\infty} \quad (3.10)$$

Then, Eqs. (3.8)-(3.10) are solved iteratively until the convergence of the wall temperature is achieved.

Determination of critical heat flux for DHT

The empirical correlation proposed by Mokry et al.²⁶ to predict the value of the minimum heat flux (q_{dht}) for given mass flux at which DHT occurs is as follows:

$$q_{dht} = -58.97 + 0.745G \quad (3.11)$$

It means that NHT occurs when $q_w < q_{dht}$ and DHT occurs when $q_w > q_{dht}$.

3.2.2 Mathematical formulation of the CFD model

In the current CFD simulations, the axisymmetric assumption is used for the simulation of the fluid flow and heat transfer in circular tubes. The governing equations used for the supercritical water flow in uniformly heated vertical circular tubes are the conservation of mass, momentum and energy. The Reynolds averaged form of these governing equations can be expressed in a tensor form as follows:

$$\frac{\partial \rho}{\partial t} + \frac{\partial}{\partial x_i}(\rho \bar{u}_i) = 0; \quad (3.12)$$

$$\frac{\partial}{\partial t}(\rho \bar{u}_i) + \frac{\partial}{\partial x_j}(\rho \bar{u}_i \bar{u}_j) = -\frac{\partial \bar{p}}{\partial x_i} + \frac{\partial}{\partial x_j} \left(\mu \frac{\partial \bar{u}_i}{\partial x_j} - \overline{\rho u'_i u'_j} \right) \quad (3.13)$$

$$\frac{\partial}{\partial t}(\rho C_p T) + \frac{\partial}{\partial x_i}(\bar{u}_i \rho C_p T) = \frac{\partial}{\partial x_i} \left[\left(k + \frac{C_p \mu_t}{Pr_t} \right) \frac{\partial T}{\partial x_i} \right] + \phi \quad (3.14)$$

To solve for the Reynolds stress term $\overline{\rho u'_i u'_j}$, two turbulence models are selected in the current study, RSM and $k - \omega SST$ model. The equation for the transport of the Reynolds stresses in RSM is presented below.²⁸

$$\begin{aligned}
\underbrace{\frac{\partial}{\partial t} (\rho \overline{u'_i u'_j})}_{\text{Local Time Derivative}} + \underbrace{\frac{\partial}{\partial x_k} (\rho u'_k \overline{u'_i u'_j})}_{C_{ij} \equiv \text{Convection}} = & \underbrace{-\frac{\partial}{\partial x_k} \left[\rho \overline{u'_i u'_j u'_k} + p' (\delta_{kj} u'_i + \delta_{ik} u'_j) \right]}_{D_{r,ij} \equiv \text{Turbulent Diffusion}} \\
+ \underbrace{\frac{\partial}{\partial x_k} \left[\mu \frac{\partial}{\partial x_k} (\overline{u'_i u'_j}) \right]}_{D_{L,ij} \equiv \text{Molucular Diffusion}} - \underbrace{\rho \left(\overline{u'_i u'_k} \frac{\partial u'_j}{\partial x_k} + \overline{u'_j u'_k} \frac{\partial u'_i}{\partial x_k} \right)}_{P_{ij} \equiv \text{Stress Production}} - \underbrace{\rho \beta (\overline{g_i u'_j \theta} + \overline{g_j u'_i \theta})}_{G_{ij} \equiv \text{Buoyancy Production}} \\
+ \underbrace{p' \left(\frac{\partial u'_i}{\partial x_j} + \frac{\partial u'_j}{\partial x_i} \right)}_{\phi_{ij} \equiv \text{Pressure Strain}} - \underbrace{2\mu \frac{\partial u'_i}{\partial x_k} \frac{\partial u'_j}{\partial x_k}}_{\epsilon_{ij} \equiv \text{Dissipation}} + \underbrace{S_{user}}_{\text{User Defined Source Term}} \quad (3.15)
\end{aligned}$$

The $k-\omega SST$ model has different form than RSM where transport equations for turbulence kinetic energy (k) and specific dissipation (ω) as opposed to Reynolds stresses. The transport equations for turbulence kinetic energy (k) and specific dissipation rate (ω) are as follows,²⁸

$$\frac{\partial}{\partial t} (\rho k) + \frac{\partial}{\partial x_i} (\rho k u_i) = \frac{\partial}{\partial x_j} \left[\left(\mu + \frac{\mu_t}{Pr_k} \right) \frac{\partial k}{\partial x_j} \right] + \tilde{G}_k - Y_k \quad (3.16)$$

$$\frac{\partial}{\partial t} (\rho \omega) + \frac{\partial}{\partial x_i} (\rho \omega u_i) = \frac{\partial}{\partial x_j} \left[\left(\mu + \frac{\mu_t}{Pr_\omega} \right) \frac{\partial \omega}{\partial x_j} \right] + \tilde{G}_\omega - Y_\omega + D_\omega \quad (3.17)$$

where,

\tilde{G}_k : generation of turbulence kinetic energy; \tilde{G}_ω : Generation of ω ;

Y_k : dissipation of turbulence kinetic energy ; Y_ω : dissipation of ω ; D_ω : cross-diffusion term;

The detailed mathematical modeling of the above mentioned terms can be found in.²⁸

The enhanced wall treatment is used for both turbulence models. The mesh structure near the wall is generated such that non-dimensional wall distance $y^+ < 1$ in the entire computational domain ($y^+ = \frac{u_\tau y}{\nu}$). The SIMPLEC solution scheme is used and QUICK is used as an interpolation scheme. The grid independence tests are carried out for all the cases to ensure the accuracy of results obtained by CFD simulations.

3.3 Results and Discussions

For the purpose of validation of the proposed numerical models and to carry out the intended analysis, 7 different steady state experimental cases are selected. The details of the experimental parameters are presented in Table 3.2. q_{dht} listed in Table 3.2 is calculated from Eq. (3.11). The experiments under consideration dealt with supercritical water flowing vertically upwards in bare circular tubes subjected to constant and uniform heat flux in the periphery. The selected experimental data sets have broad range of operating conditions in terms of mass flux, heat flux, inlet temperature and operating pressure. Cases 1 – 3 represent the situation where no DHT was observed experimentally anywhere in the flow region ($q_w < q_{dht}$). Cases 4 – 7 represent the situation where DHT was observed experimentally ($q_w < q_{dht}$) under low mass flux (Cases 4 – 6) and high mass flux (Case 7) conditions.

Table 3.2: Geometrical and operating parameters of the experiments under consideration

Case #	D (mm)	L (m)	p (MPa)	T_{in} ($^{\circ}C$)	G (kg/m^2s)	q_w (kW/m^2)	q_{dht} (kW/m^2)	Re_{in} ($X 10^4$)
1 ²⁶	10	4	24.1	350	1503	590	1061	20.8
2 ²⁹	10	4	24.0	352	1500	884	1059	21.0
3 ²⁶	10	4	23.9	350	1000	681	688	13.9
4 ²⁶	10	4	24.1	350	203	129	93	2.8
5 ²⁶	8	4	24.5	210	595	570	384	3.6
6 ²⁹	25.4	2.79*	25	200	380	400	224	6.9
7 ³⁰	3	1	25.5	120	1500	1810	1058	1.9

* unheated bottom length: 0.63 m, heated intermediate length: 2 m, unheated top length: 0.16

m

3.3.1 Validation of the numerical models at steady state condition

The numerical simulations are carried out using both THRUST and CFD models. The comparison of the local heat transfer coefficients predicted by THRUST using 5 different HTC models with the experimental data for Case 1 is shown in the Fig.3.1. It is observed that the HTCD and HTCJ overpredict the heat transfer coefficient drastically in comparison to the experimental

results for the 2nd half of the tube. Similar trend is observed for other cases also (not shown in the figure). Thus, those two HTCs are not used in the further study.

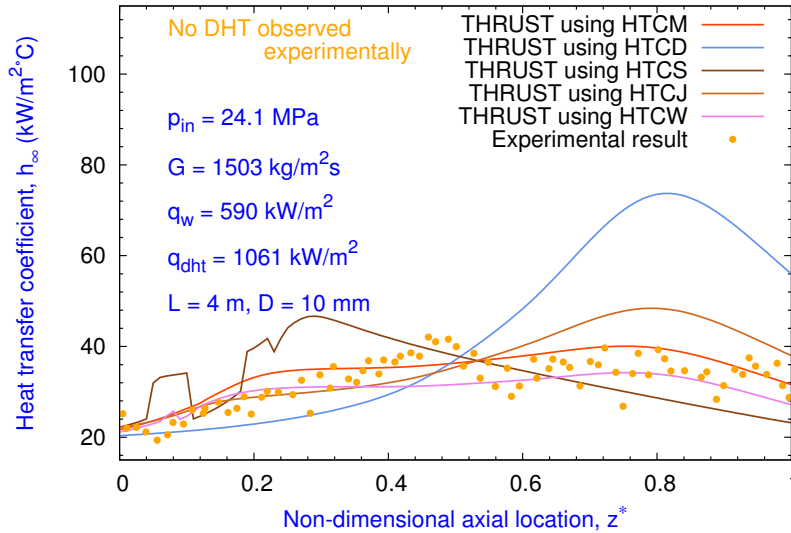


Figure 3.1: Comparison of the heat transfer coefficient by THRUST with the experimental data²⁶ for Case 1

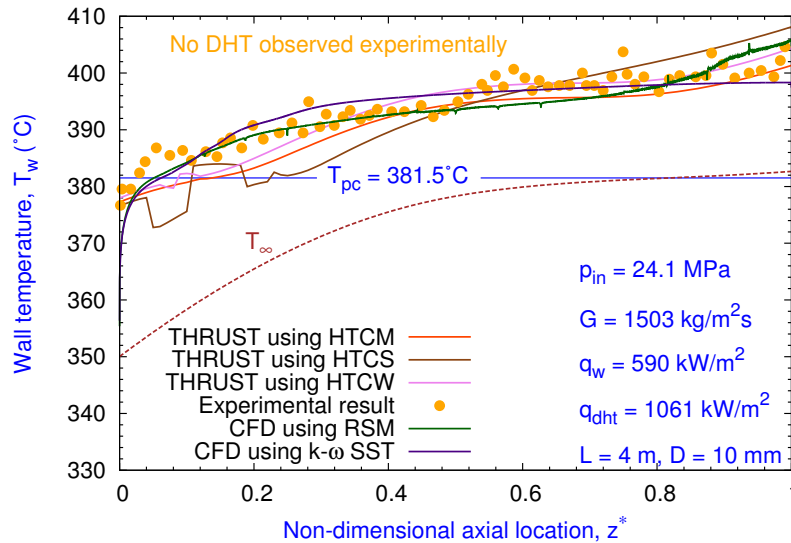


Figure 3.2: Comparison of the wall temperatures with the experimental data²⁶ for Case 1

The HTCM, HTCS and HTCW are found to be comparable with the experimental results in most of the cases. Thus, they are used in the rest of this study. The wall temperatures

of the SCW predicted by the THRUST using 3 different HTC's (HTCM, HTCS and HTCW) and CFD using two different turbulence models (RSM and $k - \omega SST$) are compared with the experimental data for Cases 1 – 7, as shown in Figs. 2 – 8, respectively.

The wall temperatures predicted by THRUST using HTCM and HTCW and CFD using RSM and $k - \omega SST$ are shown in Fig. 3.2 in comparison with the experimental data for Case 1 where no DHT is observed experimentally. The wall temperature predicted by THRUST using HTCS shows fluctuating behaviour when the wall temperature initiates to exceed the pseudo-critical temperature (T_{pc}). Later on, not much deviation from experimental results is observed.

The comparison of the numerical results and experimental data for Cases 2 and 3 are shown in Figs. 3.3 and 3.4, respectively. In both cases where no DHT occurs, very good agreement is observed for all the numerical results compared with the experimental data.

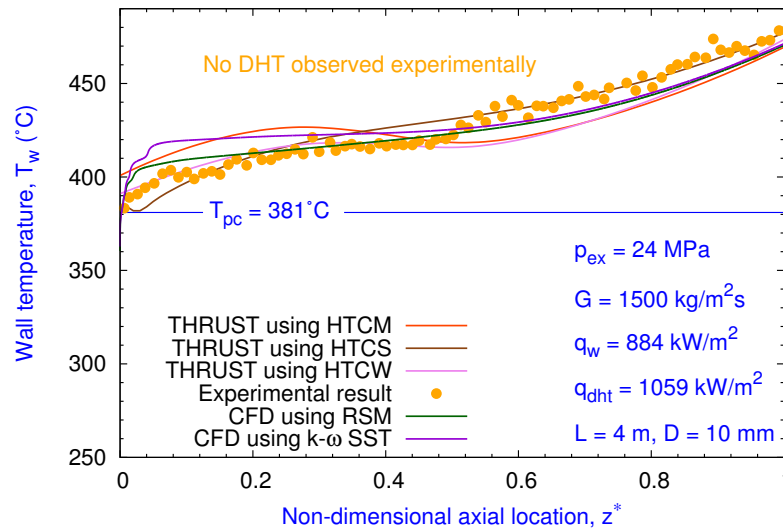


Figure 3.3: Comparison of the wall temperatures with the experimental data²⁹ for Case 2

The comparison of the numerical results with the experimental data for Case 4 in which DHT occurs is shown Fig. 3.5. Two DHT zones are observed in the experiment as shown in Fig. 3.5, one is in the entrance region whereas another one is near $z^* = 0.56$. The CFD models with RSM and $k - \omega SST$ are able to predict the first DHT qualitatively, but they fail to capture the second DHT where the bulk temperature (T_{∞}) is close to T_{pc} . It can be observed

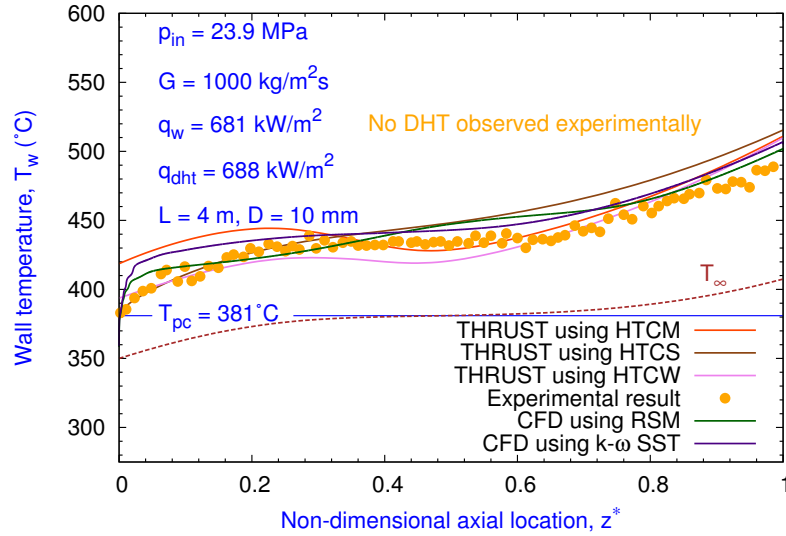


Figure 3.4: Comparison of the wall temperatures with the experimental data²⁶ for Case 3

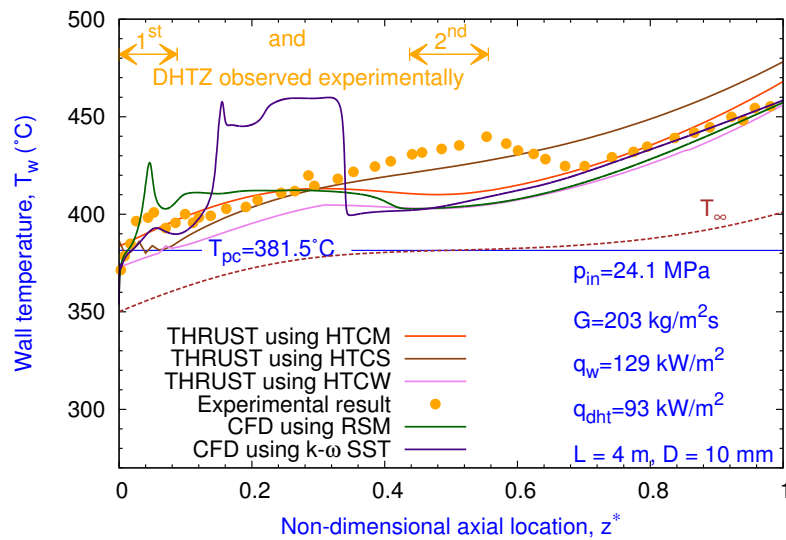


Figure 3.5: Comparison of the wall temperatures with the experimental data²⁶ for Case 4

that the RSM overpredicts and $k-\omega$ SST model underpredicts the wall temperature in the first DHT zone. Moreover, the $k-\omega$ SST model gives much higher wall temperature in the axial region $z^* = 0.125 - 0.375$, failing to regain wall temperature quickly after the sharp increase at $z^* = 0.125$. All the results by THRUST show a very good agreement with the experimental data for Case 4 as shown in Fig. 3.5, except at the second DHT zone, where the bulk temperature

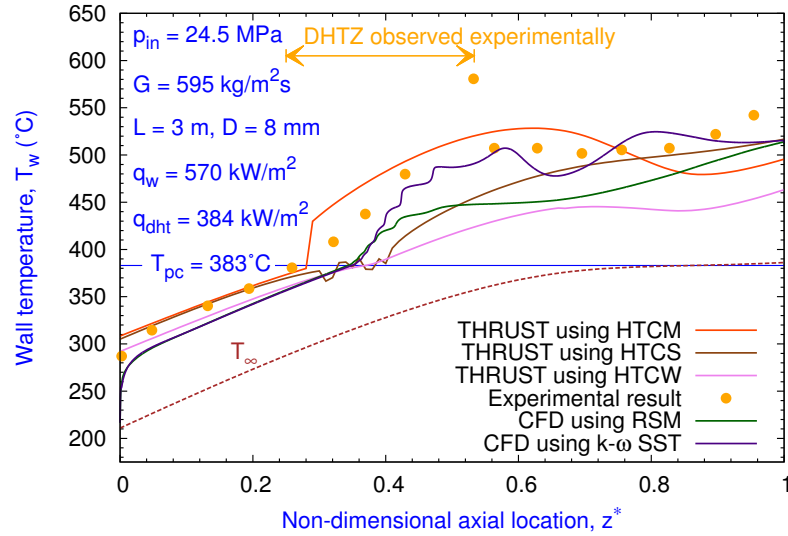


Figure 3.6: Comparison of the wall temperatures with the experimental data²⁶ for Case 5

of SCW is near T_{pc} . None of the models succeed in predicting the sharp increase and decrease in the wall temperature at the second DHT zone. But all models of both THRUST and CFD predict the wall temperature very well after the second DHT zone except for the THRUST using HTCS.

For Case 5, the wall temperature from THRUST based on HTCM is close to the experimental one even in the DHT zone except near the outlet, as shown in Fig. 3.6. THRUST result based on HTCS also has trend in-line with the experimental data. But, the wall temperature predicted by HTCS fluctuates when it is near T_{pc} . The $k - \omega$ SST model gives close agreement with the experimental data, however, the fluctuation in the wall temperature occurs when the wall temperature is higher than T_{pc} and is propagated till the exit of the tube. The RSM gives more smooth wall temperature compared to the $k - \omega$ SST model.

The results for Case 6, where DHT was observed experimentally, are shown in Fig. 3.7. The $k - \omega$ SST model captures the DHT phenomenon, but it is offset by around 0.4 m in the axial direction. The magnitude of the wall temperature in the DHT region is also underpredicted by $k - \omega$ SST. The RSM is not able to capture the DHT phenomenon, but it gives a better agreement outside of the DHT region. All the numerical results by THRUST show a good agreement with the experimental data outside the DHT region.

In Case 7, where DHT was observed experimentally at a high mass flux condition, there is a sharp increase in the wall temperature predicted by THRUST using HTCM as shown in Fig. 3.8. The predicted DHT by THRUST with HTCM occurs earlier in the channel than the experiment and the predicted wall temperature is much higher than the experimental data at the beginning of DHT region. However, HTCM is able to capture the DHT qualitatively whereas, both HTCS and HTCW based THRUST simulations cannot predict the sudden rise in the wall temperature in the DHT region. The numerical results obtained from the CFD model using the $k-\omega$ SST model follows the experimental data accurately till the axial location where the peak wall temperature occurs. It fails to regain the wall temperature after it reaches the maximum, similar to that in Case 4. The RSM shows the excellent agreement with the experimental data when the wall temperature is lower than T_{pc} and underpredicts the wall temperature when it is higher than T_{pc} . However, near the exit of the tube, RSM overpredicts the wall temperature. It is also found that there are sharp step changes in wall temperature for $k-\omega$ SST model whereas RSM provides more smooth profile for the wall temperature.

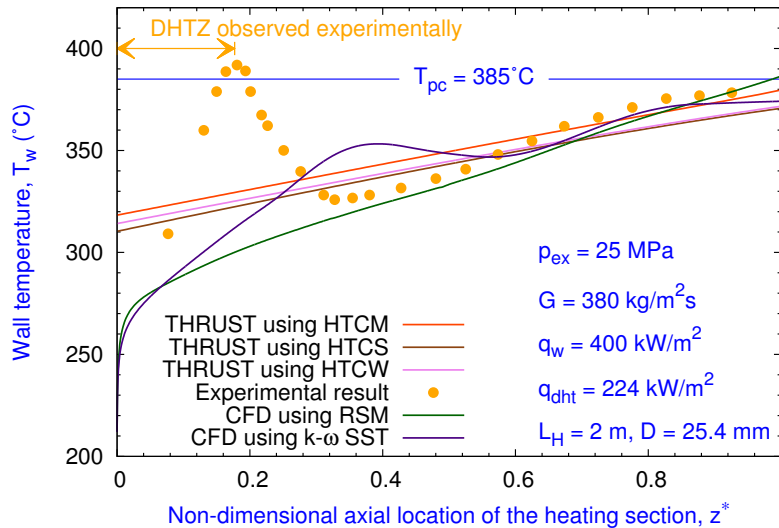


Figure 3.7: Comparison of the wall temperatures with the experimental data²⁹ for Case 6

The errors between the numerical and experimental values for the wall temperature are given in the Table 3.3. It shows that the errors are very small for the cases without DHT for all the numerical results. For the cases with DHT, the errors are higher, but of acceptable range

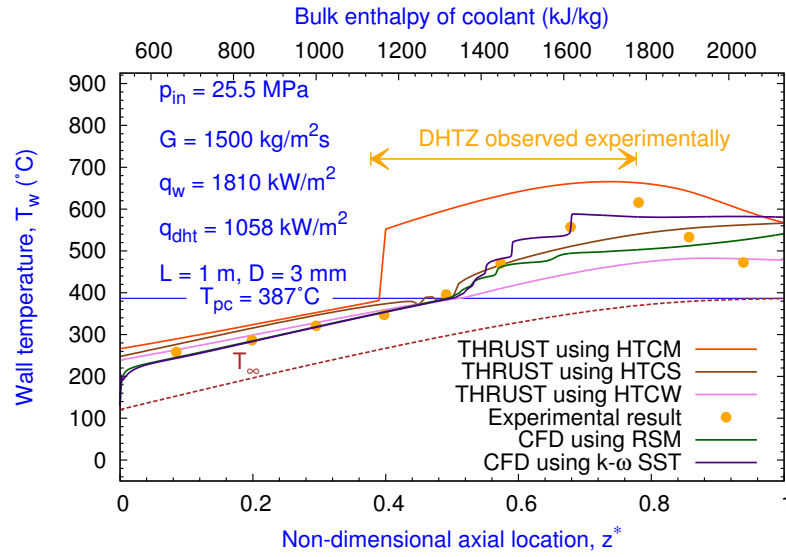


Figure 3.8: Comparison of the wall temperatures with the experimental data²⁶ for Case 7

Table 3.3: Relative errors between the numerical and experimental results for the wall temperature

Case #	Relative errors in the wall temperature, $\left[\frac{T_{w num} - T_{w exp}}{T_{w exp}} \right] (\%)$											
	RSM		k- ω SST		HTCM		HTCW		HTCS		Avg	
	MAE	SD	MAE	SD	MAE	SD	MAE	SD	MAE	SD	MAE	SD
1 ²⁶	0.35	0.40	0.34	0.44	0.46	0.32	0.30	0.37	0.62	0.72	0.41	0.45
2 ²⁹	0.91	1.03	1.29	1.45	1.67	1.80	1.06	1.14	0.65	0.81	1.12	1.25
3 ²⁶	1.22	1.06	1.56	0.75	1.66	1.56	1.18	1.32	1.80	1.39	1.48	1.22
4 ²⁶	1.70	2.04	2.39	3.32	1.14	1.44	2.12	1.21	1.33	1.54	1.73	1.91
5 ²⁶	5.40	2.98	3.40	2.85	3.03	3.75	7.09	4.68	3.90	4.30	4.57	3.71
6 ²⁹	4.68	4.97	4.21	5.19	3.45	4.49	3.62	4.44	3.69	4.46	3.93	4.71
7 ³⁰	3.51	4.96	3.52	5.14	14.90	8.72	5.40	6.49	4.86	5.55	6.44	6.17
Avg	2.54	2.49	2.39	2.73	3.76	3.16	2.97	2.81	2.41	2.68	2.81	2.77

MAE (Mean of Absolute Error), SD (Standard Deviation)

except for Case 7 when HTCM is used in THRUST. From Table 3.3, it can be seen that the highest average error using different models occurs in Case 7. This might be due to the fact that

Case 7 is the only case with DHT at high mass flux, and it is the only DHT case at high mass flux available from the literature. The errors obtained by the CFD results confine to 5.40 % and 5.19 % for RSM and $k - \omega$ SST model, respectively, for all the cases. Except for Case 7, the maximum errors are 4.49 %, 7.09 % and 4.46 % when HTC_M, HTC_W and HTC_S are used in THRUST, respectively.

In summary, the numerical results by THRUST and CFD, provide good agreement for the variation of the wall temperature values for Cases 1 – 3 and 5 whereas none of the numerical models can capture the sharp increase in the wall temperature where DHT appeared for Cases 4 and 6, but provides good match in the rest of the channel. The highest average error in the numerical results occurs in Case 7, which is 6.44%. For all the NHT cases (Cases 1-3) and DHT cases (Cases 4-6) at low mass flux, THRUST based on HTC_M provides the lowest average error (1.9%) among all the numerical results obtained at present, whereas the errors for DHT case at high mass flux (Case 7) is observed to be lowest with HTC_S results. In case of CFD simulations, both the turbulence models, RSM and $k - \omega$ SST model, are found to comparable to each other for all the cases. Therefore, it can be concluded that a good agreement between the numerical results and the experimental data, in general, is obtained; however, the local discrepancies do exist, but generally are confined to a narrow region inside the channel where DHT takes place.

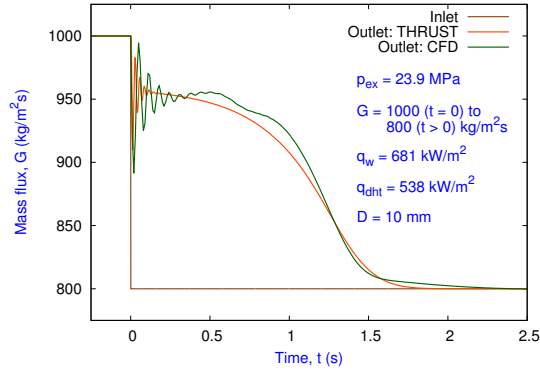
3.3.2 Comparison of the numerical models at transient condition

The in-depth knowledge of dynamic response is vital for safe and smooth operation of nuclear reactors. The SCWR uses single phase supercritical water as a coolant which has different dynamic response than the BWR due to the difference in their TH behaviour. As an initial step for studying dynamic response, the unsteady heat transfer and flow analysis of supercritical water is investigated in vertical circular tubes. For this purpose, two critical input parameters - mass flow rate and heat flux, are varied with time. In response to those changes, the temporal variation of the outlet mass flow rate, outlet bulk temperature and axial wall temperature are obtained using both THRUST and CFD models. As previously discussed, the heat transfer deterioration phenomenon is critical to SCWR and hence the DHT needs to be studied under

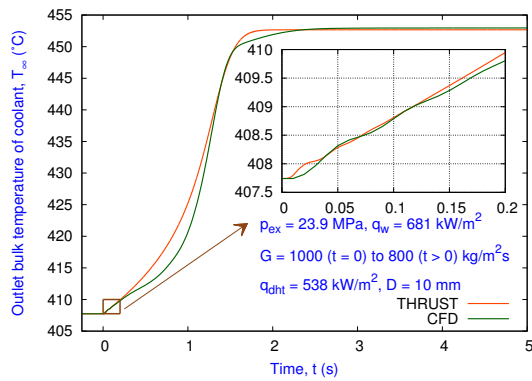
transient conditions. DHT might occur when the mass flow rate decreases while keeping heat flux constant or heat flux increases while keeping the mass flow rate constant. In the present study, the transient simulation is first started with an initial equilibrium condition where DHT was narrowly missed, but likely to occur during the transient process. Three transient conditions are considered, 2 of them with the step change in the input mass flow rate and wall heat flux, respectively and 1 with a periodic change in the input mass flow rate.

Case 3 is selected for the initial condition of the transient study. It represents a situation where DHT was not observed in the experiment, but is predictably close to the occurrence of DHT phenomenon in the channel as shown in Table 3.2 (i.e., $q_w = 681 \text{ kW/m}^2$ and $q_{dht} = 688 \text{ kW/m}^2$). The transient simulations are carried out by THRUST using HTCM and CFD using $k - \omega SST$ model.

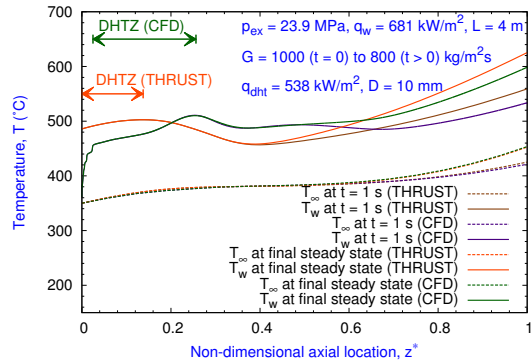
The transient results corresponding to the step change in the inlet mass flow rate are shown in Fig. 3.9. The perturbed value of inlet mass flow rate is chosen such that the DHT phenomenon will occur for the given heat flux. Based on Eq. (3.11), the DHT will occur during this transient process when the mass flux is lower than $993.2 \text{ kg/m}^2\text{s}$ at the given heat flux for Case 3. So, the perturbation in the mass flow rate is from $1000 \text{ kg/m}^2\text{s}$ to $800 \text{ kg/m}^2\text{s}$ (i.e., 20% reduction). The introduction of the perturbation in the input mass flow rate results in initial oscillations of the mass flow rate at the outlet for both the CFD and THRUST simulations as shown in Fig. 3.9a. However, the oscillations die out subsequently. The outlet mass flow rate decreases with time and finally achieves the asymptomatic steady state value which is equal to the perturbed inlet mass flow rate holding the continuity for the newly obtained equilibrium condition. The steady state values obtained using CFD and THRUST are similar. However, the oscillations predicted by THRUST die out sooner than that predicted by the CFD model and it reaches the final steady state about 0.5 seconds earlier than the CFD model. The outlet bulk temperature, as observed in Fig. 3.9b, also shows the oscillating behaviour in the initial transient period, but the amplitude of oscillations is negligible. The DHT can be identified by a sudden increase in the wall temperature as shown in Fig. 3.9c. It can be seen from Fig. 3.9c that the wall temperature at the inlet predicted by the CFD is much lower than that from the THRUST model. But, there is a sudden increase in the wall temperature at the inlet predicted by the CFD. Consequently, there is an increase in the wall temperature and then a



(a) Temporal variation of the mass flow rate



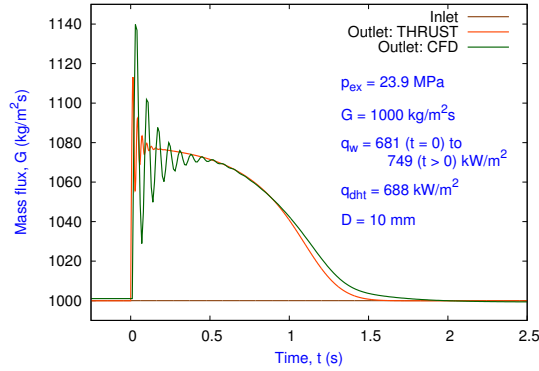
(b) Temporal variation of the bulk temperature of the coolant



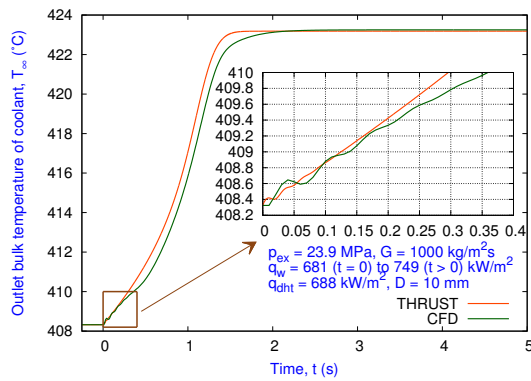
(c) Axial variation of the wall and bulk temperatures at different time

Figure 3.9: Step decrease in the inlet mass flow rate by 20% for Case 3

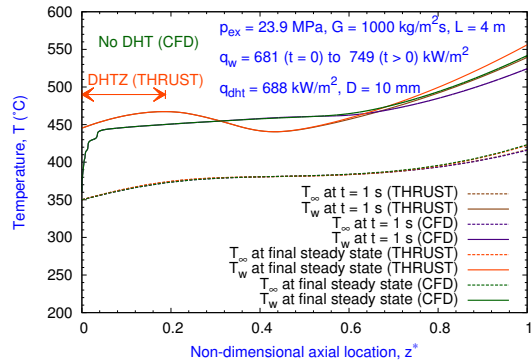
decrease, which corresponds the DHT, as shown in Fig. 3.9c. Both THRUST and the CFD model predicts DHT near the inlet of the channel. But, the DHT zone predicted by THRUST is between $z^* = 0 - 0.125$, whereas the the CFD model predicts it between $z^* = 0.012 - 0.262$.



(a) Temporal variation of the mass flow rate



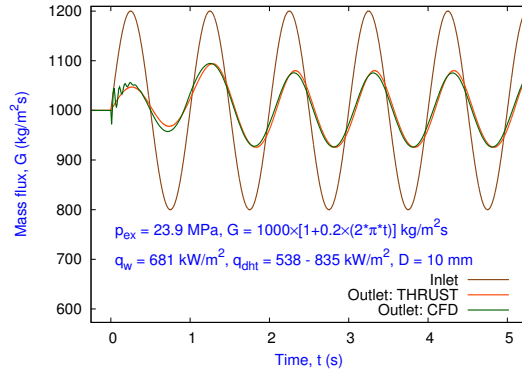
(b) Temporal variation of the bulk temperature of coolant



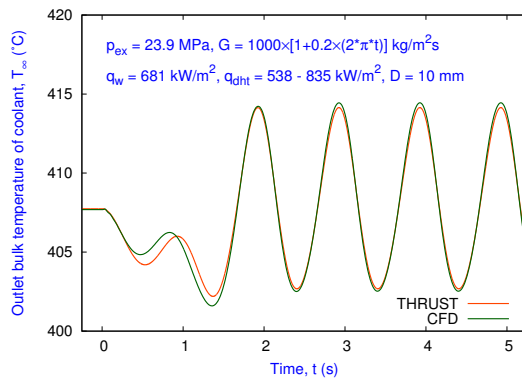
(c) Axial variation of the wall and bulk temperatures at different time

Figure 3.10: Step increase in the wall heat flux by 10% for Case 3

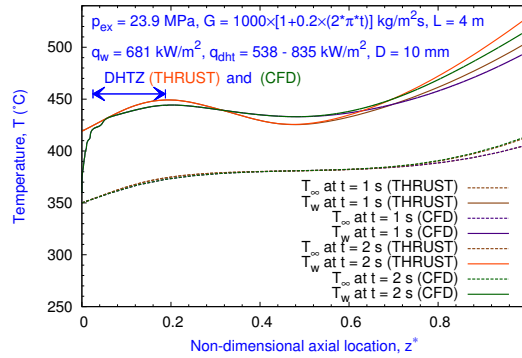
In the exit region, the CFD model and THRUST give similar predictions. The difference in the wall temperatures by the CFD model and THRUST at the exit is lower than the entrance region. The difference in the wall temperature using THRUST and the CFD model is shown in



(a) Temporal variation of the mass flow rate



(b) Temporal variation of the bulk temperature of coolant



(c) Axial variation of the wall and bulk temperatures at different time

Figure 3.11: Sinusoidal variation of the inlet mass flow rate for Case 3

Table 3.4. Contrary to the wall temperature, the bulk temperature shows excellent agreement between the results obtained by the CFD model and THRUST as shown in Figs. 3.9b and 3.9c. The difference in predicted wall temperatures might be due to the empiricisms involved in the

HTC correlation used in THRUST.

Table 3.4: Relative difference obtained by CFD and THRUST for the wall temperature (%)

Case description	Relative difference in the wall temperature			
	Time = 1 s		Final steady state	
	MAE	SD	MAE	SD
Step change in mass flow rate	2.80	3.18	2.67	3.04
Step change in heat flux	1.51	1.73	1.45	1.69
	Time = 1 s		Time = 2 s	
Sinusoidal change in mass flow rate	0.64	0.82	0.64	0.82

The transient results corresponding to the step change in the wall heat flux rate are shown in Fig. 3.10. Based on Eq. (3.11), $q_{dht} = 688 \text{ kW/m}^2$, the step change in the heat flux is from 681 kW/m^2 to 749 kW/m^2 (i.e., 10% increase) to ensure DHT will occur during this transient process. The trend of outlet mass flow rate, as shown in Fig. 3.10a, is similar to the case when the step change occurs in the inlet mass flow rate. The final steady state value of the outlet mass flow rate matches exactly with the inlet mass flow rate for both the CFD model and THRUST. The outlet bulk temperature, as observed in Fig. 3.10b, also has similar qualitative trend as the previous case and the initial oscillations are predicted by both the CFD model and THRUST. The amplitude and time span of oscillations are always higher in CFD results compared to THRUST. The axial variations of the wall temperature and bulk temperature at different time are shown in Fig. 3.10c. The comparison of the bulk temperature using the CFD model and THRUST, as given in Figs. 3.10b and 3.10c, shows an excellent agreement with each other. Fig. 3.10c shows that the wall temperature predicted by the CFD model is also much lower than that by THRUST at the inlet of the channel and there is a sudden increase in the wall temperature predicted by the CFD near the inlet, similar to the previous case shown in Fig. 3.9c. There is monotonic increase in the wall temperature predicted by the CFD model along the axial direction of the channel. One also can observe from Fig. 3.10c that THRUST shows the DHT at $z^* = 0.175$, but the DHT cannot be observed using CFD model for the entire channel. The wall temperature predicted by the CFD model and THRUST are very close at

outlet.

Next, the transient simulations are carried out for the case where inlet mass flux is varied sinusoidally with time. Amplitude of the oscillating inlet mass flux is set to be 20% of the initial value of $1000 \text{ kg/m}^2\text{s}$ to ensure that the mass flux in the channel remains lower than the critical value, $993.2 \text{ kg/m}^2\text{s}$, at the given heat flux condition for a considerable portion of the time period and therefore, the DHT occurs in the channel within that time period. The resultant transient response can be seen in Fig. 3.11. After the initial oscillations, the outlet mass flow rate and bulk temperature, as observed in Figs. 3.11a and 3.11b, respectively, takes about 1.5 seconds to get to the periodic steady state, after which both show periodic trend similar to the inlet mass flow rate. The axial variations of the wall and bulk temperatures at different times are shown in Fig. 3.11c. A very good agreement between the results obtained by THRUST and the CFD model is observed. DHT zone predicted by both models almost coincides to each other. Table 3.4 also confirms the good agreement among the numerical results.

3.4 Conclusions

In this paper, an in-house 1-D numerical code, THRUST and CFD models are validated with the experimental data for SCW flow in circular tubes. Both models are first used to predict the wall temperature at different operating conditions when the channels are subjected to imposed wall heat flux BC. The wall temperatures obtained from both the numerical models are compared with each other and with the experimental data to verify the models and to identify their limitations. The comparative results reveal that the THRUST as well as CFD show the close agreement with the experimental data for the cases of NHT where maximum error is consistently below 2% .

The wall temperature profiles for the cases of DHT show higher error than the NHT cases. For the two turbulence models examined, none of them is found to be unanimously better than the other for all the cases. However, the RSM provides more smooth wall temperature profiles compared to the $k-\omega SST$. The $k-\omega SST$ model fails to retrieve the wall temperature values in some DHT cases that results in conservative estimate in the wall temperature. Similarly, in

THRUST, no single heat transfer correlation is found to be the best for all the cases, however, the HTC_M, HTC_W and HTC_S in general provide satisfactory results. For DHT with low mass flux and high mass flux, the maximum errors associated with both RSM and $k - \omega SST$ model are within 5.4 % and 5.19 %, respectively. For THRUST, the maximum errors associated with the HTC_M, HTC_W and HTC_S are 4.5 %, 7 % and 4.5 %, respectively, for NHT and DHT with low mass flux condition. For DHT with high mass flux condition, THRUST with HTC_M provides maximum error about 15 % whereas HTC_W and HTC_S provide maximum error of 6.5 % and 5.6 %, respectively. It is also found that for DHT with high mass flux case, the $k - \omega SST$ model gives oscillating profiles for wall temperature.

After satisfactory validation of the THRUST and CFD models with 7 different experimental cases of steady state heat transfer, transient simulations under 3 conditions are carried out. Out of these 3 conditions, 2 of them involve the step change in the input mass flow rate and heat flux whereas third one is of sinusoidal variation in the input mass flow rate. The THRUST and CFD models are able predict the temporal and axial variations of the wall and bulk temperatures, and the predictions by THRUST and the CFD models are in good agreement. The temporal variation of the outlet mass flow rate and outlet bulk temperature for all the cases obtained by the THRUST and CFD model show the exact value at the final steady state, but the actual time taken to reach to the final steady state is more in the case of the CFD model than the THRUST. The excellent comparative analysis shows that THRUST and the CFD models are capable to simulate the transient TH behavior for SCW flow and heat transfer phenomena and therefore, both the numerical models can further be extended and used in the future for the analysis of various dynamic case studies.

References

- [1] U S DOE, NERAC, and GIF. A technology roadmap for generation IV nuclear energy systems. Technical report, 2002.
- [2] K Yamagata, K Nishikawa, S Hasegawa, T Fuji, and S Yoshida. Forced convective heat transfer to supercritical water flowing in tubes. *Journal of Heat and Mass transfer*, 15(12):2575–2593, 1972.
- [3] HS Swenson, JR Carver, and CR Kakarala. Heat transfer to supercritical water in smooth-bore tubes. *Journal of Heat Transfer: Transactions of the ASME Series*, c87(4):477–484, 1965.
- [4] JD Jackson. Consideration of the heat transfer properties of supercritical pressure water in connection with the cooling of advanced nuclear reactors. In *Proc. 13th Pacific basin Nuclear Conference, Shenzhen City, China*, pages 21–25, 2002.
- [5] RB Duffey and IL Piro. Experimental heat transfer of supercritical carbon dioxide flowing inside channels (survey). *Nuclear Engineering and Design*, 235(8):913–924, April 2005.
- [6] IL Piro, HF Khartabil, and RB Duffey. Heat transfer to supercritical fluids flowing in channels, empirical correlations (survey). *Nuclear Engineering and Design*, 230(1-3):69–91, May 2004.
- [7] W Jäger, VH Sánchez Espinoza, and A Hurtado. Review and proposal for heat transfer predictions at supercritical water conditions using existing correlations and experiments. *Nuclear Engineering and Design*, 241(6):2184–2203, June 2011.
- [8] RG Desissler. Heat transfer and fluid friction for fully developed turbulent flow of air and supercritical water with variable fluid properties. *Trans. ASME*, 76:73–85, 1954.
- [9] BS Shiralkar and P Griffith. Deterioration in heat transfer to fluids at supercritical pressure and high heat fluxes. *Journal of Heat Transfer*, 91(1):27–36, 1969.

- [10] FR Menter. Zonal two equation k-turbulence models for aerodynamic flows. *AIAA paper*, 2906:1993, 1993.
- [11] X Cheng, B Kuang, and Y H Yang. Numerical analysis of heat transfer in supercritical water cooled flow channels. *Nuclear Engineering and Design*, 237(3):240–252, February 2007.
- [12] D Palko and H Anglart. Theoretical and numerical study of heat transfer deterioration in HPLWR. In *Nuclear Energy for Europe*, pages 1–8, 2007.
- [13] D Palko and H Anglart. Deteriorated heat transfer at low coolant flow rates. In *International Students Workshop on HPLWR*, pages 1–4, 2008.
- [14] Y Zhang, C Zhang, and J Jiang. Numerical Simulation of Heat Transfer of Supercritical Fluids in Circular Tubes Using Different Turbulence Models. *Journal of Nuclear Science and Technology*, 48(3):366–373, March 2011.
- [15] V Chatoorgoon. Stability of supercritical fluid flow in a single-channel natural-convection loop. *International Journal of Heat and Mass Transfer*, 44:1963–1972, 2001.
- [16] V Chatoorgoon, A Voodi, and D Fraser. The stability boundary for supercritical flow in natural convection loops Part I: H₂O studies. *Nuclear Engineering and Design*, 235(24):2570–2580, December 2005.
- [17] V Chatoorgoon, A Voodi, and P Upadhye. The stability boundary for supercritical flow in natural-convection loops Part II: CO₂ and H₂O. *Nuclear Engineering and Design*, 235(24):2581–2593, December 2005.
- [18] W Ambrosini and M Sharabi. Dimensionless parameters in stability analysis of heated channels with fluids at supercritical pressures. *Nuclear Engineering and Design*, 238(8):1917–1929, August 2008.
- [19] TO Gómez, A Class, RT Lahey, and T Schulenberg. Stability analysis of a uniformly heated channel with supercritical water. *Nuclear Engineering and Design*, 238(8):1930–1939, August 2008.

- [20] PK Jain and Rizwan-uddin. Numerical analysis of supercritical flow instabilities in a natural circulation loop. *Nuclear Engineering and Design*, 238(8):1947–1957, August 2008.
- [21] X Cheng and T Schulenberg. Heat transfer at supercritical pressures: literature review and application to an HPLWR, 2001. *Scientific report FZKA6609, Forschungszentrum Karlsruhe*, 2001.
- [22] JY Yoo. The turbulent flows of supercritical fluids with heat transfer. *Annual Review of Fluid Mechanics*, 45:495–525, January 2013.
- [23] G Dutta and JB Doshi. Nonlinear analysis of nuclear coupled density wave instability in time domain for a boiling water reactor core undergoing core-wide and regional modes of oscillations. *Progress in Nuclear Energy*, 51(8):769–787, November 2009.
- [24] FP Incropera. *Introduction to Heat Transfer*. John Wiley & Sons, 2011.
- [25] MJ Watts and CT Chou. Mixed convection heat transfer to supercritical pressure water. In *Proceedings of the 7th International Heat Transfer Conference. Vol 3*, pages 495–500, 1982.
- [26] S Mokry, I Pioro, A Farah, K King, S Gupta, W Peiman, and P Kirillov. Development of supercritical water heat-transfer correlation for vertical bare tubes. *Nuclear Engineering and Design*, 241(4):1126–1136, April 2011.
- [27] MA Kedzierski and MS Kim. Single phase heat transfer and pressure drop characteristics of an integral spine fin within an annulus. Technical report, U.S. Department of Energy, Office of Building Technology, Building Equipment Division, Washington, DC, 1994.
- [28] 14.0 ansys fluent theory guide. *ANSYS inc*, 2011.
- [29] A Churkin, S Bilbao, and K Yamada. Analysis of the IAEA benchmark exercise on steady state flow in a heated pipe with supercritical water. In *Proceedings of ICAPP*, pages 139–145, 2011.

- [30] AP Ornatskij, LF Glushchenko, and SI Kalachev. Heat transfer with rising and falling flows of water in tubes of small diameter at supercritical pressures. *Thermal Engineering*, 18(5):137–141, 1971.

Chapter 4

Numerical Investigation of Deteriorated Heat Transfer Phenomenon for Supercritical Water Flow in Vertical Circular Tubes

Abstract

The present paper is aimed at the in-depth thermal-hydraulic analysis of supercritical water flow at various operating conditions in vertical circular tubes. A one-dimensional thermal-hydraulic solution algorithm and CFD model using two turbulence models, Reynolds Stress Model and $k - \omega SST$ model, have been used for the analysis in this paper. Nine experimental cases are studied thoroughly and out of these, four cases which are operated at various working regimes are chosen and presented for the detailed analysis of deteriorated heat transfer and normal heat transfer cases.

The studies are carried out for the 1) turbulence and velocity profile distributions and their effects on the heat transfer and 2) the distributions of non-dimensional acceleration and buoyancy parameters, and different types of pressure drops along the axial direction and its effect

on the heat transfer. A correlation is reported between the turbulence and velocity profiles and heat transfer phenomenon. Moreover, an attempt is also made to predict the deteriorated heat transfer zone inside the channel using non-dimensional parameters so that one can be aware of the possibility of its occurrence beforehand and take anticipatory measures accordingly.

Keywords:supercritical fluid, deteriorated heat transfer, turbulence kinetic energy, buoyancy, acceleration and pressure drop

Nomenclature

A	Area, m^2
C_p	Specific heat capacity, J/kgK
D	Diameter of a tube, m
e	Specific Internal Energy, J/kg
g	Gravitational Acceleration, m/s^2
G	Mass Flux, $kg/m^2 s$
h	Heat Transfer Coefficient, W/m^2K
k	Turbulence kinetic energy, m^2/s^2
L	Length, m
L_h	Heated length, m
p	Pressure, Pa
P_w	Wetted perimeter, m
q_w	Wall heat flux, W/m^2
q'_w	Wall heat per unit length, W/m
r	distance from centre of the tube, m
r^*	Non-dimensional radial location
t	Time, s
T	Temperature, $^{\circ}C$
u	Velocity, m/s
y	Distance from wall, m
y^+	Non-dimensional distance from wall, $u_{\tau}y/\nu$, m
z	Axial location, m
z^*	Non-dimensional axial location

Greek Letters

α	Thermal expansion coefficient, $1/K$
ϵ	Energy dissipation per unit mass, m^2/s^3
μ	Dynamic viscosity, $Pa\ s$
ν	Kinematic viscosity, m^2/s
β	Isothermal compressibility factor, $1/Pa$
ρ	Density of a fluid, kg/m^3
τ	Shear stress, N/m^2
ω	Specific dissipation rate, $1/s$

Subscripts

avg	Average
cr	Value at critical point
dht	Deteriorated heat transfer
in	Inlet
m	Mean
pc	Pseudo-critical
q	Based on local heat flux value
t	Turbulent
w	Wall
∞	Bulk

Dimensionless Numbers

A^*	Acceleration parameter, $(\nu/u_\infty^2)(du_\infty/dx)$
A_p^*	Compressible acceleration parameter, $-(D/Re)\beta_T(dp/dx)$
A_t^*	Thermal acceleration parameter, $4\alpha_p Dq_w/\mu_b C_p Re^2$
B^*	Buoyancy Parameter, $Gr_b^*/(Re_b^{3.424} Pr_b^{0.80})$
Bu^*	Buoyancy Parameter, $\overline{Gr}_b/Re_b^{2.7} \overline{Pr}_b^{0.50}$
\overline{Gr}_b	$g(1 - \rho_w/\rho_b)D^3/\nu_b^2$
k^*	Buoyancy Parameter, $(1 - \rho_w/\rho_b)\overline{Gr}_b^{2.0}/\nu_b^2$
Nu	Nusselt Number
Pr	Prandtl Number, $\mu c_p/k$
\overline{Pr}	$\mu \overline{c}_p/k$
Re	Reynolds Number, $\rho u D/\mu$

Acronyms

AECL	Atomic Energy of Canada Limited
BC	Boundary Condition
BWR	Boiling Water Reactor
CFD	Computational Fluid Dynamics
DHT	Deteriorated Heat Transfer
DHTZ	Deteriorated HEat Transfer Zone
GIF	Generation IV International Forum
HTC	Heat Transfer Coefficient
HTCM	Heat Transfer Coefficient by Mokry et al.
HTCS	Heat Transfer Coefficient by Swenson et al.
HTCW	Heat Transfer Coefficient by Watts et al.
NHT	Normal Heat Transfer
PCR	Pseudo Critical Region
PWR	Pressurized Water Reactor
RSM	Reynold Stress Model
SCW	Supercritical Water
SCWR	Supercritical Water Cooled Reactor
SST	Shear Stress Transport
TH	Thermal-Hydraulic
THRUST	Thermal-Hydraulic solveR Undertaking Supercritical waTer
TKE	Turbulence Kinetic Energy
TR	Tanaka Ratio

4.1 Introduction

The renewed interest for heat transfer and fluid flow analysis in supercritical fluids is established since the supercritical water cooled reactor (SCWR) has been identified as one of the six Generation IV nuclear reactors by Generation IV International Forum (GIF).¹ The advantage of the SCWR over the Pressurized Water Reactor (PWR) and Boiling Water Reactor (BWR) is the high thermal efficiency, avoidance from the boiling crisis, compact plant system and close proximity to the proven technology for supercritical fossil power plants (SCFPPs). Extensive studies of the heat transfer and fluid flow of water and CO₂ at supercritical conditions have been conducted since 1950s, by several researchers²⁻⁴ and detailed studies are also reported in numerous review papers.⁵⁻⁷

Although the boiling crisis is avoided in SCWRs, there is large variation in thermo-physical properties of supercritical water, especially near pseudo-critical region (PCR) and it is the major cause of deteriorated heat transfer (DHT) which increases the wall temperatures severely. The increase in the wall temperatures is serious concern as the fuel cladding material in fuel rods is designed to sustain a specific temperature and DHT might lead to material failure. Therefore, the detailed knowledge about the DHT is very important for the design of a SCWR. The unusual heat transfer phenomenon in the PCR is also attributed to the enhanced buoyancy and acceleration effects. The enhanced buoyancy effect is a result of a decrease in the density in the PCR whereas the acceleration effect generally results from the increase in the thermal expansion coefficient in this region. The DHT phenomenon is the most challenging issue for supercritical fluid flows and heat transfer. The DHT has been widely investigated by the researchers. Till the date, there is no effective tool to analyze the DHT phenomenon for broad range of operating conditions due to enhanced buoyancy, acceleration effects and abrupt changes in thermo-physical properties.

Several experimental studies have been performed to find the accurate empirical correlation for the heat transfer coefficient in the supercritical region²⁻⁴ which can be implemented in 1-D thermal-hydraulic codes. The detailed reviews of these studies on the heat transfer in supercritical fluids were given by several researchers.^{6, 8, 9} However, there is still not a common

consensus between researchers on heat transfer correlations or a established method to determine the DHT accurately.

The numerical studies using CFD were performed in the past and still being carried out as a cost effective method for the thermal-hydraulic analysis of supercritical fluid flows. The main challenge in using the CFD approach is to implement suitable turbulence models which have the ability to properly incorporate the sharp variation in thermo-physical properties in the PCR. The earlier CFD studies carried out by Deissler et al.¹⁰ and Shiralkar et al.¹¹ used the eddy diffusivity based turbulence models. With the development of two equation turbulence models, $k - \epsilon$ and $k - \omega$ type turbulence models have been used for the heat transfer investigation in supercritical fluid flows. Bellinghausen et al.¹² successfully used the $k - \epsilon$ model including the gravitational effect at supercritical conditions and Koshizuka et al.¹³ validated the numerical results with the experimental data of Yamagata et al.² for supercritical water flows in circular tubes using the $k - \epsilon$ model. Mikielwicz et al.¹⁴ used several turbulence models for the supercritical flow in strongly heated pipe and validated their numerical results with the experimental results of Shehata et al.¹⁵ The $k - \omega SST$ model developed by Menter¹⁶ combines the strength of the $k - \epsilon$ model in free stream region and strength of the $k - \omega$ in recirculating regions. Cheng et al.¹⁷ used this model for supercritical flows and they recommended not to use ω -type turbulence models with the automatic wall treatment for supercritical flows. The same model was also used by Palko et al.^{18, 19} for supercritical water flows and numerical results were compared with the experimental results of Shitsman et al.²⁰ The results showed satisfactory agreement between the numerical results and experimental data. Palko et al.^{18, 19} also presented the analysis for the turbulent kinetic energy (TKE) and velocity profiles and their effects on the heat transfer. Yang et al.²¹ assessed the capability of $k - \omega$ type models including the SST model and concluded that these models fail to predict accurate heat transfer phenomenon in the PCR. However, it was concluded that $k - \omega$ models give better prediction than $k - \epsilon$ models. Therefore, there is no common consensus among researchers regarding the capability of the $k - \omega SST$ model for studying the heat transfer phenomenon in supercritical fluid flows.

The above-mentioned turbulence models are based on the isotropic assumption. The researchers also have implemented anisotropic turbulence models, the Reynolds Stress Models (RSMs) for supercritical water flows in various geometries.^{17, 22} The anisotropic turbulence models were found to give better match with experimental results compared to isotropic models. However, the DHT analysis based on the TKE and velocity profiles using anisotropic turbulence models has not been performed extensively in literature. The high-fidelity simulations like direct numerical simulations (DNS) have also been performed for investigating the fundamental physics in supercritical fluids and detailed analysis of the effects of the TKE and velocity profiles on heat transfer.²³

Buoyancy, flow acceleration and sharp variation of transport properties at the supercritical condition, mainly around the pseudo-critical point, can adversely affect the flow dynamics leading to the suppression of turbulence and thus, cause the significant reduction in the heat transfer locally. The theoretical studies conducted by Mikielewicz et al.¹⁴ and Sharabi and Ambrosini²⁴ confirmed that the buoyancy and sharp variation of transport properties at a low mass flux condition played the major role behind the occurrence of the DHT phenomenon rather than the flow acceleration. Liao and Zhou^{25, 26} experimentally studied the supercritical behavior of CO₂ in mini tubes of different diameters and found that the effect of buoyancy parameters decreases as the size of the tubes decreases. Similar studies conducted by He et al.²⁷ proved the insignificance of buoyancy at low Reynolds numbers for supercritical fluid flows in mini tubes. Jiang et al.^{28, 29} during their studies with mini tubes found that both buoyancy and flow acceleration influence the flow conditions, but the flow acceleration plays the dominant role. Jiang et al.,³⁰ while performing an experimental investigation on supercritical pressure CO₂ in vertical micro tube, quantitatively determined the effects of the thermal (A_t^*) and compressible (A_p^*) acceleration parameters separately and found both are comparable for that specific condition. The effect of the buoyancy parameter was found to have negligible impact for the micro tube and therefore, attributed the cause of reduction in heat transfer to the acceleration parameter. All these studies^{14, 24–30} dealt with the cases where the low mass flux condition was prevalent. The case³¹ where the DHT was observed experimentally at a high mass flux condition was studied through CFD simulations and analytical calculations by Liu et

al.³² which concluded the negligible effect of buoyancy and emphasized the dominant role of acceleration pressure drop causing the DHT phenomenon in that particular situation.

In the present study, the numerical investigation of fluid flow and heat transfer in vertical tubes is performed using both CFD model and 1-D Thermal-Hydraulic solveR Undertaking Supercritical waTer (THRUST) code. For the CFD simulations, two turbulence models, RSM and $k - \omega SST$, which were validated for supercritical fluid flows and heat transfer in previous study,³³ are used in this work. The CFD results are used to analyse the trend of TKE and velocity for different operating conditions, such as NHT, DHT at low mass flux and DHT at high mass flux. The 1-D model, THRUST, is developed in-house. It was earlier used to simulate boiling water reactors (BWR)³⁴ and was extended and validated for SCWRs in the previous study.³³ Several parameters, which were earlier proposed to predict the occurrence of DHT are tested in the present study to verify their applicability in different working regimes and are also used to predict the occurrence of the deteriorated heat transfer zone (DHTZ) inside the channel. Buoyancy and acceleration at low mass flux condition are generally considered to be responsible for DHT and thus, several case studies are carried out for low mass flux flows. One case where DHT was observed experimentally at high mass flux condition is also included for the analysis. Attempts are also made to investigate the effect of pressure drops due to different factors on the occurrence of DHT phenomenon.

4.2 Mathematical details of the numerical models

The mathematical details of the THRUST and the CFD model are presented here. The present analysis is carried out under steady state condition.

4.2.1 Mathematical formulation of CFD model

In the present study, CFD simulations are carried out using commercial software Ansys FLU-ENT for studying thermal-hydraulic behaviour of the supercritical water flow in vertical circular tubes. Axisymmetric assumption is used for the fluid flow and heat transfer analysis. The governing equations for the fluid flow and heat transfer are conservation of mass, momentum

and energy and their Reynolds averaged form is expressed in tensor form as follows:

$$\frac{\partial}{\partial x_i}(\rho \bar{u}_i) = 0; \quad (4.1)$$

$$\frac{\partial}{\partial x_j}(\rho \bar{u}_i \bar{u}_j) = -\frac{\partial \bar{p}}{\partial x_i} + \frac{\partial}{\partial x_j}(\mu \frac{\partial \bar{u}_i}{\partial x_j} - \overline{\rho u'_i u'_j}) \quad (4.2)$$

$$\frac{\partial(\bar{u}_i \rho C_p T)}{\partial x_i} = \frac{\partial}{\partial x_i} \left[\left(k + \frac{C_p \mu_t}{Pr_t} \right) \frac{\partial T}{\partial x_i} \right] + \phi \quad (4.3)$$

The equations for the RSM are presented below.³⁵

$$\begin{aligned} \underbrace{\frac{\partial}{\partial x_k}(\rho u_k \overline{u'_i u'_j})}_{C_{ij} \equiv \text{Convection}} &= - \underbrace{\frac{\partial}{\partial x_k} \left[\overline{\rho u'_i u'_j u'_k} + p' (\delta_{kj} u'_i + \delta_{ik} u'_j) \right]}_{D_{T,ij} \equiv \text{Turbulent Diffusion}} \\ &+ \underbrace{\frac{\partial}{\partial x_k} \left[\mu \frac{\partial}{\partial x_k} (\overline{u'_i u'_j}) \right]}_{D_{L,ij} \equiv \text{Molecular Diffusion}} - \underbrace{\rho \left(\overline{u'_i u'_k} \frac{\partial u_j}{\partial x_k} + \overline{u'_j u'_k} \frac{\partial u_i}{\partial x_k} \right)}_{P_{ij} \equiv \text{Stress Production}} - \underbrace{\rho \beta (g_i \overline{u'_j \theta} + g_j \overline{u'_i \theta})}_{G_{ij} \equiv \text{Buoyancy Production}} \\ &+ \underbrace{p' \left(\frac{\partial u'_i}{\partial x_j} + \frac{\partial u'_j}{\partial x_i} \right)}_{\phi_{ij} \equiv \text{Pressure Strain}} - \underbrace{2\mu \frac{\partial u'_i}{\partial x_k} \frac{\partial u'_j}{\partial x_k}}_{\epsilon_{ij} \equiv \text{Dissipation}} + \underbrace{S_{user}}_{\text{User Defined Source Term}} \end{aligned} \quad (4.4)$$

The $k - \omega SST$ model has similar form as the standard $k - \omega$ model. The transport equations for turbulence kinetic energy(k) and specific dissipation rate(ω) are as follow,³⁵

$$\frac{\partial}{\partial t}(\rho k) + \frac{\partial}{\partial x_i}(\rho k u_i) = \frac{\partial}{\partial x_j} \left[\left(\mu + \frac{\mu_t}{Pr_k} \right) \frac{\partial k}{\partial x_j} \right] + \tilde{G}_k - Y_k \quad (4.5)$$

$$\frac{\partial}{\partial t}(\rho \omega) + \frac{\partial}{\partial x_i}(\rho \omega u_i) = \frac{\partial}{\partial x_j} \left[\left(\mu + \frac{\mu_t}{Pr_\omega} \right) \frac{\partial \omega}{\partial x_j} \right] + \tilde{G}_\omega - Y_\omega + D_\omega \quad (4.6)$$

where,

\tilde{G}_k : generation of turbulence kinetic energy; \tilde{G}_ω : Generation of ω ;

Y_k : dissipation of turbulence kinetic energy ; Y_ω : dissipation of ω ; D_ω : cross-diffusion term;

The detailed mathematical modeling of the above mentioned terms can be found in.³⁵

The enhanced wall treatment is used for the near wall treatment for the RSM. The non-dimensional wall distance, $y^+ \left(= \frac{u_\tau y}{\nu} \right)$ is kept below 1 in the entire computational domain to resolve the boundary layers accurately. The SIMPLEC solution scheme is implemented and second order QUICK method is used as an interpolation scheme. The grid independence tests are carried out for all the cases to ensure the accuracy of results obtained.

4.2.2 Mathematical formulations of the THRUST

In the 1-D TH model, it is assumed that the thermo-physical flow properties vary along the axial direction and the heat flux at the periphery of the circular tube is constant. The conservation equations are solved numerically using a spatially fixed grid structure. The fundamental one-dimensional governing equations for the fluid flow under the steady state condition are as follows:

Mass conservation equation:

$$\frac{\partial}{\partial z} (\rho A u) = 0 \quad (4.7)$$

Momentum conservation equation in the axial direction:

$$\frac{\partial}{\partial z} (\rho A u^2) = -A \frac{\partial p}{\partial z} - \tau_w P_w - \rho A g \frac{dH}{dz} \quad (4.8)$$

Energy conservation equation:

$$\frac{\partial}{\partial z} (\rho A u e_f) = q_w P_H \quad (4.9)$$

where $e = e_f - \frac{p}{\rho}$ and $e_f = h + \frac{u^2}{2} + gH$.

The equation of state, $\rho = \rho(p, h)$, is also used.

Solution methodology

The resultant discretized equations are as follows:

$$\rho_{i+1} A_{i+1} u_{i+1} = \rho_i A_i u_i \quad (4.10a)$$

$$\begin{aligned}
p_i - p_{i+1} &= \frac{1}{2} \left(\frac{1}{A_i} + \frac{1}{A_{i+1}} \right) [(\rho Au^2)_{i+1} - (\rho Au^2)_i] \\
&+ \frac{1}{2} \left[\{\rho (F + g)\}_i + \{\rho (F + g)\}_{i+1} \right] (z_{i+1} - z_i)
\end{aligned} \tag{4.10b}$$

$$(e_f)_{i+1} - (e_f)_i = \frac{1}{2} \left[\left(\frac{q'_w}{\rho Au} \right)_i + \left(\frac{q'_w}{\rho Au} \right)_{i+1} \right] (z_{i+1} - z_i) \tag{4.10c}$$

The above set of equations, in addition to thermodynamic equation of state, are solved numerically by using a forward marching scheme when all the inlet primary variables, i.e., inlet velocity, enthalpy and pressure are specified, otherwise a shooting method along with the forward marching scheme is employed to treat different set of specified conditions.

Heat transfer coefficient and friction factor

The accuracy of 1-D TH models largely depends on the appropriate selection of correlations for friction factor and heat transfer coefficient (HTC). The Filonenko correlation for the friction factor and three HTCs provided by Swenson et al.³ (HTCS), Watts et al.³⁶ (HTCW) and Mokry et al.³⁷ (HTCM) are used in this study. The previous study³³ verified the applicability of the above mentioned HTCs by comparing with the experimental results.

4.2.3 Parameters to analyze DHT

Different parameters used in THRUST, to predict the occurrence of DHT and DHTZ are described below.

Buoyancy parameter, B^* , is defined as follows for the real fluid, which is widely used in the literature to account for the effect of buoyancy at a low mass flux condition.

$$B^* = \frac{Gr_b^*}{Re_b^{3.425} Pr_b^{0.80}} \tag{4.11}$$

where

$$Gr_b^* = \frac{g \alpha_p D^4 q_w}{\nu_b^2 k_b} \tag{4.12}$$

It was suggested that the DHT due to buoyancy is expected to take place when $5.67 \times 10^{-7} < B^* < 8.0 \times 10^{-6}$.¹⁴

Other parameters, Bu^* , k^* and Tanaka ratio, TR , are also used to account for the effect of buoyancy on DHT at a low mass flux condition. The parameters are defined as the following:

$$Bu^* = \frac{\overline{Gr}_b}{Re_b^{2.7} \overline{Pr}_b^{0.50}} \quad (4.13)$$

$$k^* = \left(1 - \frac{\rho_w}{\rho_b}\right) \frac{\overline{Gr}_b^{2.0}}{\nu_b^2} \quad (4.14)$$

$$TR = Re_f / Re_{fc}, \quad (4.15)$$

where

$$\overline{Gr}_b = g \left(1 - \frac{\rho_w}{\rho_b}\right) \frac{D^3}{\nu_b^2}, \quad (4.16)$$

$$Re_{fc} = 50 \times Gr_f^{\frac{8}{21}}, \quad (4.17)$$

$$Gr_f = \frac{g \alpha_p (T_f - T_b) D^3}{\nu_f^2} \quad (4.18)$$

T_f , the mean film temperature, is evaluated at $T_f = \frac{1}{2} (T_w + T_b)$.

The occurrence of buoyancy induced DHT will be observed if $Bu^* > 1.0 \times 10^{-5}$,³⁸ $0.01 < k^* < 0.40$ ⁶ and³⁹ or $TR < 1.05$.⁴⁰

The acceleration parameter, A^* , is considered to be responsible for DHT due to acceleration at a low mass flux condition and was found playing an important role for very small diameter tubes.³⁰ The parameter, A^* , can be formulated as follows:

$$A^* = \left(\frac{\nu}{u_\infty^2}\right) \frac{du_\infty}{dx} = A_p^* + A_t^* \quad (4.19)$$

where the compressible acceleration parameter, A_p^* is defined as

$$A_p^* = -\left(\frac{D}{Re}\right) \beta_T \frac{dp}{dx} \quad (4.20)$$

and the thermal acceleration parameter, A_t^* is defined as

$$A_t^* = \frac{4\alpha_p D q_w}{\mu_b c_p Re^2} \quad (4.21)$$

Mikielewicz et al.¹⁴ suggested that DHT due to acceleration at a low mass flux condition will be observed when $A^* > 3 \times 10^{-6}$. The acceleration parameter, A^* or any one of the buoyancy parameters, B^* , Bu^* , k^* and TR or both of the acceleration and buoyancy parameters can be responsible for the DHT at a low mass flux condition. It is also expected that any one of the above mentioned parameters will not be able to predict the DHT at a high mass flux condition.

The pressure drops due to different factors, which are used during the present study to analyze and differentiate the DHT phenomenon at low and high mass flux conditions, are derived based on Eq.(4.8) under transient conditions as follows:

$$-\frac{\partial p}{\partial z} = \frac{1}{A} \frac{\partial}{\partial z} (\rho A u^2) + \frac{\tau_w P_w}{A} + \rho g \frac{dH}{dz} \quad (4.22)$$

$$-\frac{\partial p}{\partial z} = \left(\frac{\partial p}{\partial z} \right)_{acc} + \left(\frac{\partial p}{\partial z} \right)_{fric} + \left(\frac{\partial p}{\partial z} \right)_{grav} \quad (4.23)$$

4.3 Results and Discussions

Nine different experimental cases are studied thoroughly and out of these cases, four cases are selected for the simulations carried out in this paper. The details of the experimental parameters are presented in Table 4.1. The Case 1 represents the NHT situation whereas Cases 2a and 2b represent DHT at a low mass flux condition and Case 3 shows the DHT at a high mass flux condition. The experiments under consideration dealt with supercritical water flowing vertically upwards in bare circular tubes subjected to constant and uniform heat flux in the periphery. The experimental datasets have broad range of operating conditions in terms of mass flux, heat flux, inlet temperature and operating pressure. The validation of CFD model and THRUST with the above mentioned experimental conditions was carried out by Maitri et al.³³ and a satisfactory match with experimental results was reported.

Table 4.1: Geometrical and operating parameters of experiments

Case #	D (mm)	L (m)	p (MPa)	G (kg/m^2s)	q (kW/m^2)	T_{in} ($^{\circ}C$)	HT
1 ³⁷	10	4	24.1	1503	590	350	NHT
2a ³⁷	10	4	24.1	203	129	350	DHT
2b ⁴¹	25.4	2.79*	25	380	400	200	DHT
3 ³¹	3	1	25.5	1500	1810	120	DHT

* unheated bottom length: 0.63 m, heated intermediate length: 2 m, unheated top length: 0.16

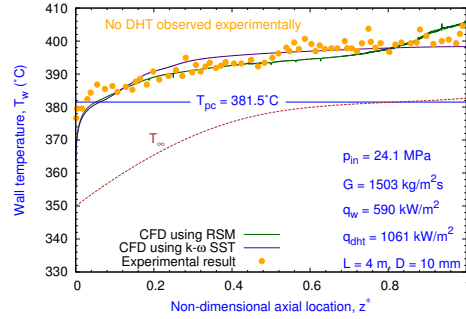
m

4.3.1 Flow structure of supercritical water under various heat transfer conditions using CFD

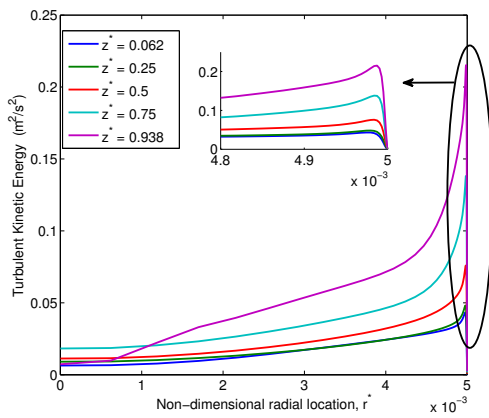
In this section, the flow structure of supercritical water is studied under various heat transfer conditions. The velocity and turbulence kinetic energy (TKE) profiles in the radial direction are presented at various axial locations for Case 1 (NHT), Case 2a (DHT at a low mass flux) and Case 3 (DHT at a high mass flux).

The results of the CFD simulations for Case 1 are shown in Fig. 4.1. The wall temperatures predicted from the RSM and $k - \omega SST$ model are similar except near the tube exit, as shown in Fig. 4.2a. It can be observed from Fig. 4.1b that TKE radial profiles have a similar shapes at different axial locations but its value increases along the axial direction indicating the gradual enhancement in the turbulence. The TKE profile at each axial location has a peak in the near wall region and its value decrease smoothly towards the centre ($r^* = 0$). For this case, it can be noted that the $\frac{TKE_{peak@z^*=0.062}}{TKE_{peak@z^*=1}} \approx 0.2$. The sharp increase in the turbulence near the wall helps to increase the heat transfer from the wall to the free stream, so, avoids the deteriorated heat transfer.

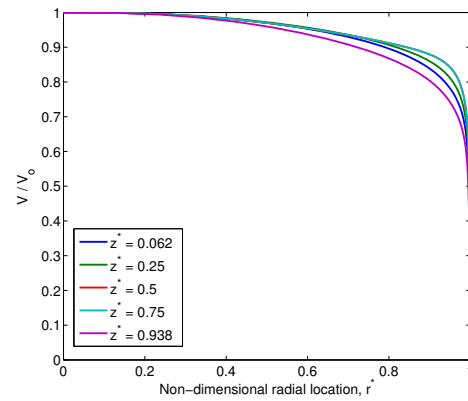
On the other hand, for Case 2a where DHT is observed at a low mass flux in the experiment, the DHT is predicted by both RSM and $k - \omega SST$ model as shown in Figs. 4.2b and 4.2c. The TKE in DHTZ for this case is substantially lower than the zone where no DHT occurs as shown in Figs. 4.2b and 4.2c. Using RSM, the ratio $\frac{TKE_{peak@z^*=0.062}}{TKE_{peak@z^*=1}} \approx 0.04$, which shows that the degree of reduction of the TKE in the near wall region of DHTZ compared to maximum TKE in the



(a) Wall temperature



(b) The radial distribution of turbulence kinetic energy using RSM

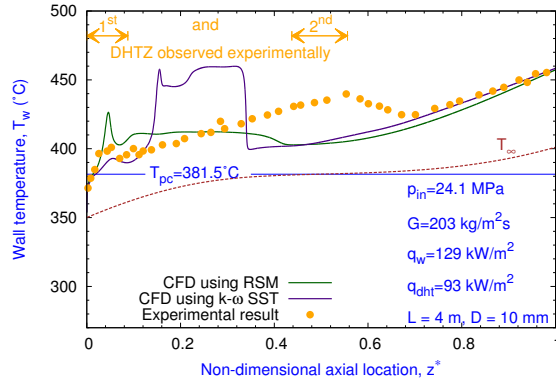


(c) Radial velocity distribution using RSM

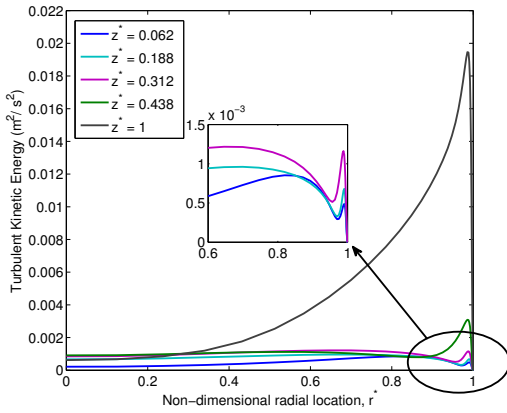
Figure 4.1: Results using CFD for Case 1

flow region, is higher in the DHT case compared to the NHT case. On contrary to the RSM, the peak in the TKE in the near wall region is not observed in DHTZ ($z^* = 0.188$ and 0.312) using $k - \omega SST$ model as shown in Fig. 4.2c, indicating the decrease in the turbulence in the near wall region which results in the sharp increase in the wall temperature that indicating the heat transfer deterioration. The peak in the TKE is observed in the near wall region using RSM, however, the magnitude of the TKE peak in the DHTZ ($z^* = 0.062$) near the wall is negligible compared to a maximum TKE value (at $z^* = 1$) causing the deterioration of heat transfer. It is important to note that at the location where deteriorated heat transfer is observed the TKE shows a minimum value for both RSM and $k - \omega SST$ model.

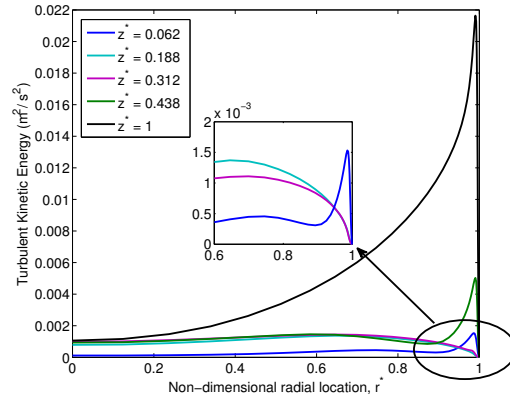
Although TKE value is negligible in the DHTZ ($z^* = 0.062$), it shows two peaks in the



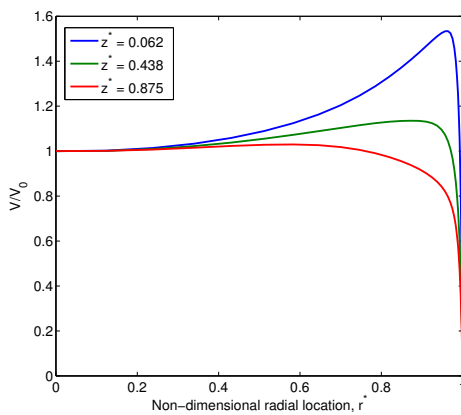
(a) Wall temperature



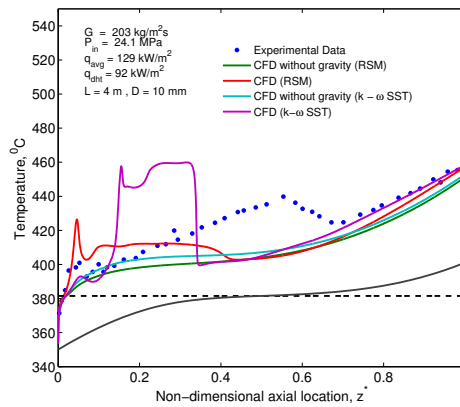
(b) The radial distribution of turbulence kinetic energy using RSM



(c) The radial distribution of turbulence kinetic energy using $k - \omega$ SST



(d) Radial velocity distribution using RSM



(e) Effect of gravity (buoyancy) on CFD simulations

Figure 4.2: Results using CFD for Case 2a

near wall region using RSM. The generation of the TKE is directly proportional to the product of mean strain rate and correlation in velocity fluctuations ($\propto \overline{u'_i u'_j \frac{\partial \bar{u}_i}{\partial x_j}}$). This explains the first peak in the TKE as the mean strain rate, which is proportional to velocity gradient, is the highest in the near wall region. Afterwards, the TKE shows one lower peak and then increases from there showing second peak before it decreases smoothly towards the centre of the tube similar to the observation made in the NHT case. The second peak, in spite of decreased mean strain rate, might have observed due to the increase in the value of $\overline{u'_i u'_j}$. The existence of two peaks was confirmed by the DNS study of Bae et al.²³ Hence, despite the fact that RSM model does not follow the experimental data for wall temperature in the DHTZ, it is able to show the proper TKE distribution in the near wall region whereas $k-\omega SST$ model fails to show the peak in the near wall region ($z^* = 0.188$ and 0.312) and the two peaks in the DHTZ ($z^* = 0.062$) for Case 2a.

Furthermore, it is observed from Fig. 4.2a that the steep change in temperature is observed using the $k-\omega SST$ model at $z^* = 0.125$ and the wall temperature remains almost constant till $z^* = 0.375$ where a sharp decrease in the wall temperature occurs. The unusual behavior of the wall temperature using the $k-\omega SST$ model might be attributed to its inability to incorporate strong buoyancy effect in the turbulence equation near the PCR. To confirm that the unusual behavior is due to buoyancy effect, a simulation is carried out without considering gravity in the equations and the result is shown in Fig. 4.2e. It can be seen that the sharp increase in wall temperature vanishes when the gravity effect is neglected in the simulation using the $k-\omega SST$ model. Similar trend is also observed in the RSM model. Therefore, the HTD in Case 2a is observed due to the strong buoyancy effect.

The TKE analysis is also carried out for Case 3, where DHT is observed at a high mass flux condition and the results are shown in Fig. 4.3. It is found that the TKE radial profiles have similar shape but value keeps increasing along the axial direction, similar to the NHT case. Although DHT was observed in this case, the reduction in TKE in DHTZ is in lesser extent than it is observed the case of DHT with a low mass flux. This behaviour might be observed because the near wall flow structure are convected strongly due to high mass flux. However,

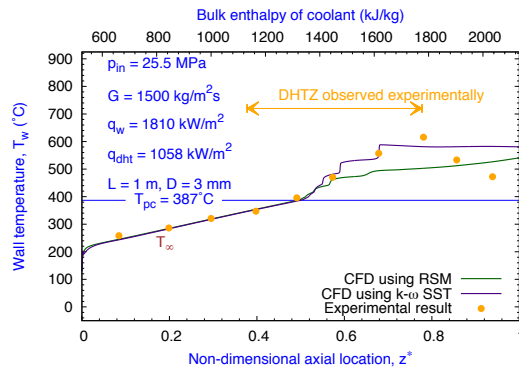
the DNS or LES results are not available to verify the behaviour of turbulence structure at high mass flux conditions.

Furthermore, the radial velocity profiles are also studied for DHT and NHT cases. Owing to changes in thermo-physical properties, the average velocity is different along the axial direction for the given mass flow rate. However, for the presentation purpose, the velocity at every axial location is normalized with the value of velocity at the axis. For Case 1 (NHT), the velocity profiles at different axial locations have similar shapes as shown in Fig. 4.1c whereas for Case 2a, a peak in the velocity in the near wall region is observed in DHTZ ($z^* = 0.062$) as shown in Fig. 4.2d. The peak in velocity magnitude in the near wall region at DHTZ disappears along the axial locations ($z^* = 0.438$ and $z = 0.875$) showing the velocity profile similar to what is observed in the NHT case. The peak in the velocity magnitude near the wall which occurs due to the local acceleration in fluid under strong buoyancy forces in the near wall region, is known as “M-shaped profile” for supercritical fluid flows and its existence was proved analytically by Tanaka et al.⁴⁰ based on the analysis of shear stress distribution in the radial direction. Hence, the CFD with RSM is capable of predicting the M-shaped velocity profile for supercritical water flows in vertical circular tubes in the DHTZ at the low mass flux condition. Similar observations were also made for $k - \omega SST$ model (not shown here). For Case 3 where DHT was observed at a high mass flux, the velocity profile is also found to be similar to that in NHT case. Hence, the local acceleration in fluid in the near wall region does not have a strong influence on the flow structure compared to the bulk fluid motion due to high mass flux condition.

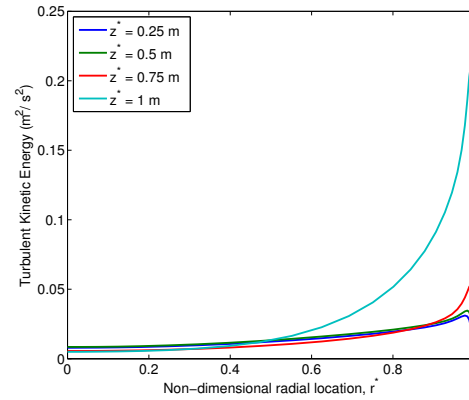
4.3.2 Analysis of DHT based on the acceleration parameters using THRUST

The acceleration parameter, in fact, is found to be of lower value than the required magnitude for DHT to occur in all the four cases considered in the present study as evident in Figs. 4.4b, 4.5b, 4.6b & 4.7b.

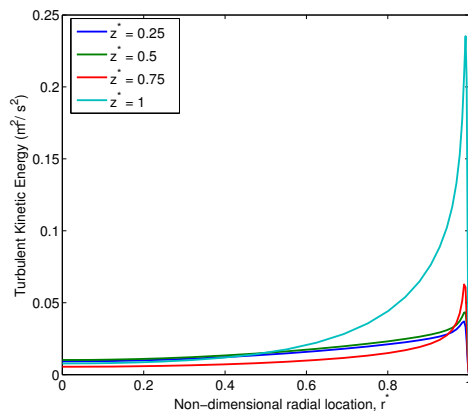
The simulations for all four cases indicate that $O[A_t^*] \sim 10^{-8} - 10^{-9}$, $O[A_p^*] \sim 10^{-11} - 10^{-12}$ and therefore, $A^* \simeq A_t^*$ remains valid for all cases. It is noticed that a low value of the compressible acceleration parameter, A_p^* ($\ll A_t^*$), is obtained even the pressure dependence variation of



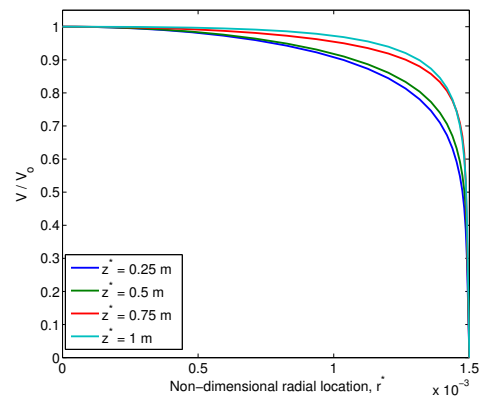
(a) Wall temperature



(b) The radial distribution of turbulence kinetic energy using RSM



(c) The radial distribution of turbulence kinetic energy using $k - \omega$ SST



(d) Radial velocity distribution using RSM

Figure 4.3: Results using CFD for Case 3

thermo-physical properties is considered in THRUST, i.e. the compressibility effect of super-critical water is accounted for. Therefore, the dominance of the thermal acceleration parameter, A_t^* , over the compressible acceleration parameter, A_p^* , is confirmed, leading to $A^* \simeq A_t^*$ for the given conditions. It is also noticed that the dominance of the thermal acceleration parameter over the compressible acceleration parameter may have been established for the present case studies, but more importantly, the effective acceleration parameter remains unable to play a role in influencing the DHT phenomenon as it is negligibly small, $O[A^*] \sim 10^{-8}$ in comparison to its threshold value ($= 3.0 \times 10^{-6}$) for the entire range of operation under consideration.

4.3.3 Prediction of DHT based on the buoyancy parameters and pressure drop components using THRUST

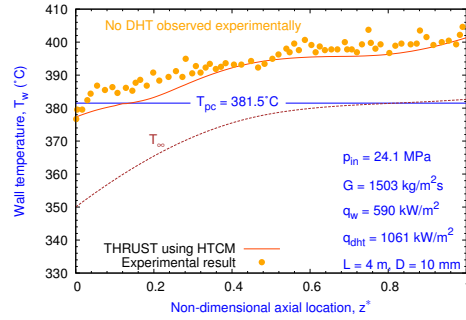
Table 4.2: Prediction of DHT on the basis of buoyancy parameters

Case #	G ($\frac{kg}{m^2 \cdot s}$)	q ($\frac{kW}{m^2}$)	Extremum axial value of relative ratio of buoyancy parameters			
			$\frac{B_{Max}^*}{B_{cr}^*}$	$\frac{Bu_{Max}^*}{Bu_{cr}^*}$	$\frac{k_{Max}^*}{k_{cr}^*}$	$\frac{TR_{min}}{TR_{cr}}$
1	1503	590	0.06	0.07	0.47	2.52
2a	203	129	11.7	24.9	42.6	0.26
2b	380	400	5.94	14.0	19.1	0.69
3	1500	1810	0.08	0.38	0.68	1.18

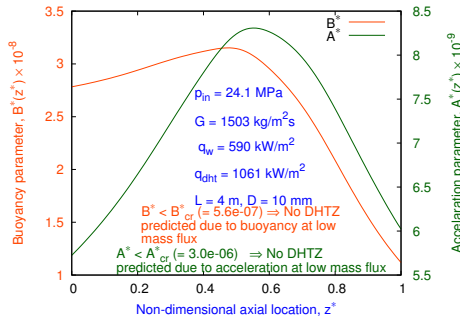
: Case where DHT observed experimentally

number in red : Nonconformity in experimental and numerical results

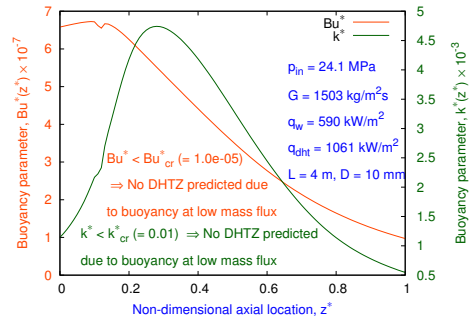
Table 4.2 provides the summary of the calculated values of the buoyancy parameters for all the cases so that one can get a first-hand estimate to evaluate the effect of those parameters on predicting DHT accurately in comparison to the actual observation.



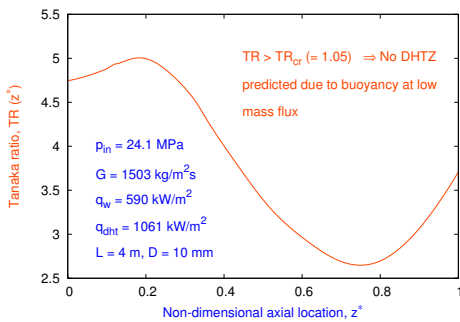
(a) Wall temperature



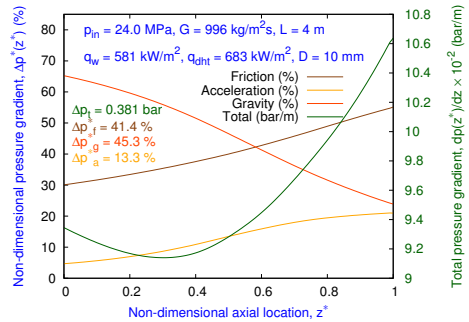
(b) Buoyancy (B^*) and acceleration (A^*) parameters



(c) Buoyancy parameters (Bu^* and k^*)



(d) Buoyancy parameter (TR)



(e) Pressure gradients

Figure 4.4: Results using THRUST for Case 1

No DHT in the experiment

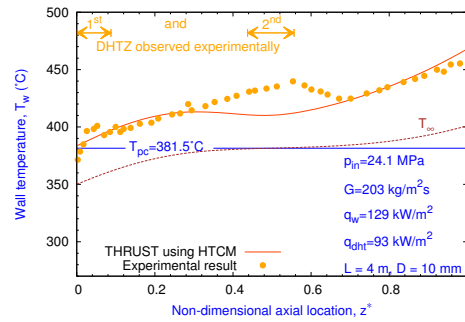
Case 1 where no DHT was observed in the experiment is considered first. Figs. 4.4b-4.4d for the Case 1 show that all the buoyancy parameters, B^* , Bu^* , k^* and TR , evaluated along the axial direction do not meet the respective criteria required for the onset of DHT. Flow acceleration induced DHT is also out of possibility for the given condition as already discussed earlier. Therefore, the numerical predictions indicate the absence of DHT throughout the channel which is the case in reality as observed in Fig. 4.4a. One important observation from Fig. 4.4e is that the gravitational and frictional pressure drops across the channel are of comparable values, though the former is dominant initially and the reverse is the case later on, whereas the acceleration pressure drop across the channel is always less than the other two components.

DHT in the experiment observed at a low mass flux condition

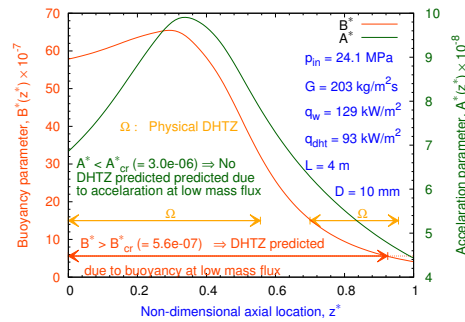
One can observe from Fig. 4.5a, the occurrence of DHT in the experiment for Case 2a in the section close to the channel inlet and the middle section of the channel. In those sections, the buoyancy parameter, B^* , is found to exceed its threshold limit for the DHT as shown in the Fig. 4.5b. The similar trends are also observed by other buoyancy parameters Bu^* , k^* and TR (not shown). However, the predicted DHTZs are longer than the experimental ones. Therefore, it can be concluded that the numerical models are able to provide a conservative estimate of the DHTZ for the particular case. The DHTZ was observed for Case 2b experimentally almost everywhere in the channel except around $z^* = 0.075$ as shown in Fig. 4.6a. However, the DHTZ predicted by A^* and B^* is in the entire channel, as shown in Fig. 4.6b. The strong dominance of the gravitational pressure drop over the others is observed in Fig. 4.6c

DHT in the experiment at a high mass flux condition

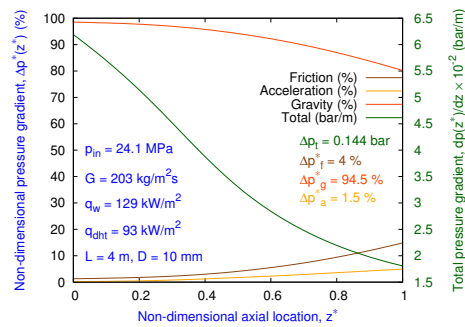
For the Case 3 where the high mass flux condition prevails, it is evident from Table 4.2 and Fig. 4.7b, that none of the buoyancy parameter can predict DHT phenomenon inside the channel, though it was experimentally observed as evident in the Fig. 4.7a. On the other hand it is also observed that the frictional pressure drop is always higher than the gravity and accelerating pressure drops for the Case 3 as shown in Fig. 4.7c and thus, justifies the negligible effect of



(a) Wall temperature

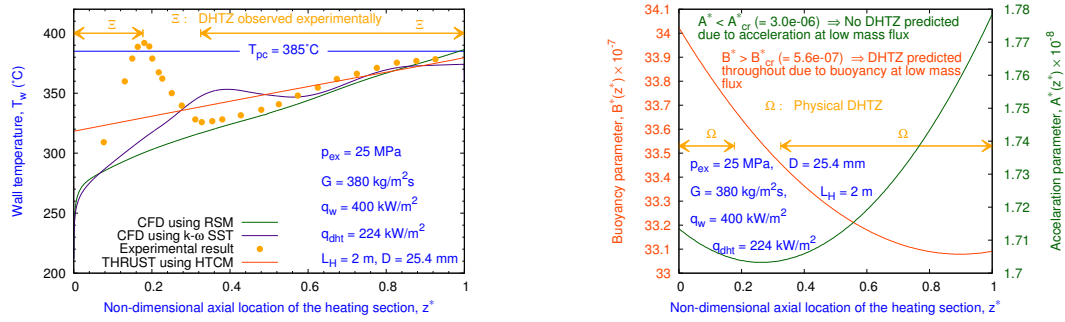


(b) Buoyancy and acceleration parameters



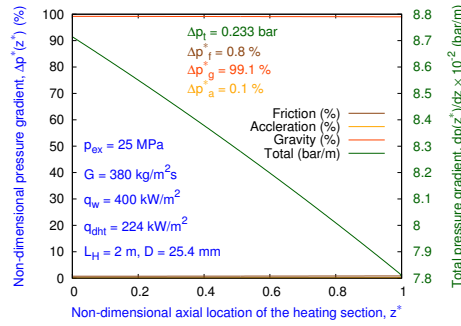
(c) Pressure gradients

Figure 4.5: Results using THRUST for Case 2a



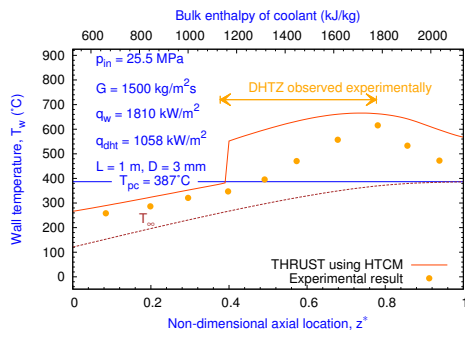
(a) Wall temperature

(b) Buoyancy and acceleration parameters

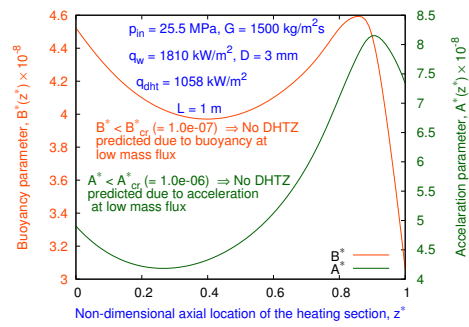


(c) Pressure gradients

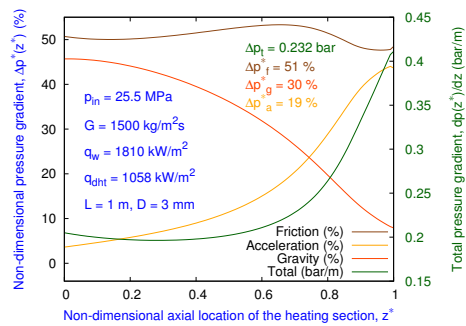
Figure 4.6: Results using THRUST for Case 2b



(a) Wall temperature



(b) Buoyancy and acceleration parameters



(c) Pressure gradients

Figure 4.7: Results using THRUST for Case 3

the buoyancy for the occurrence of DHT at those conditions. Acceleration pressure gradient, which is having minimal effect at the inlet region of the channel and keeps on increasing along the channel as expected because of continuous heating of the fluid, overcomes the gravitational pressure gradient in the middle section of the channel. It is comparable with the gravitational pressure drop in the channel, but more importantly plays a major role at the exit section of the channel where the acceleration pressure gradient takes the lead responsibility for the rapid increase of the total pressure gradient. As a matter of fact, the same exit section corresponds to the physical DHTZ as observed in Fig. 4.7a. It is noticed that the similar case was studied by Liu et al.³² and the importance of acceleration pressure drop was emphasized for the given conditions. However, in comparison to the present study, Liu et al.³² seems to over emphasize the effect of acceleration pressure gradient which was found to be ranging from 64-98% of total pressure gradient depending on its axial location. The acceleration pressure gradient, for the same case study with the present model, THRUST, varies from 4-45% along the axial direction of the channel. Both the studies establish that the friction and acceleration pressure drops play the dominant role in predicting DHTZ at the high mass flux condition rather than the gravitational pressure drop.

4.4 Conclusions

The detailed fluid flow and heat transfer analysis of supercritical water flowing in vertically upward tubes is presented. The analysis is carried out by a CFD model and 1-D model THRUST. Four different cases are chosen for the detailed analysis of the NHT and DHT using CFD and THRUST at both low and high mass flux situations. The analysis is carried out with an in-depth study of the influence of turbulent kinetic energy and velocity profiles on the heat transfer in supercritical fluids whereas in THRUST, the dimensionless acceleration and buoyancy parameters are used for predicting the DHT in the flow regime. Moreover, the influence of a pressure variation on the heat transfer phenomenon is also discussed.

The CFD model using two turbulence models, $k-\omega$ SST model and Reynolds Stress Model, for supercritical fluid flow in uniformly heated circular tube under various heat transfer condi-

tions is used. The analysis of the DHT is performed based on the TKE and velocity profiles in radial directions at different axial locations. It is found that the RSM and $k - \omega SST$ are able to predict the difference in turbulence distribution between the DHT and NHT cases. The turbulence is found to be suppressed severely for the DHT case and is one of the reasons for the deterioration in heat transfer. Although the suppression is predicted by both the turbulence models, RSM shows two peaks in the TKE profile which is in line with previous DNS studies, but $k - \omega SST$ model predicts only one peak or no peak in the whole flow region. Hence, $k - \omega SST$ fails to predict the proper TKE profile in the near wall region. The turbulence models are able to predict the well known "M-shaped" velocity profile for the supercritical fluid flow for the case of the DHT at the low mass flux. However, the "M-shaped" velocity profile is not found for the case of the DHT at the high mass flux and NHT. The influence of the gravity on the wall temperature is also studied by running the simulations with and without the gravity and it is found that the sharp increase in the wall temperature vanishes if the gravity is neglected. Hence, it can be concluded that buoyancy plays a dominant role in deteriorating the heat transfer for the cases of a low mass flux condition.

To quantify the localized effects of turbulent convection, flow acceleration and drastic change of thermo-physical properties of SCW, a study based on various non-dimensional numbers is carried out using THRUST. An attempt is made to formulate a strategy, not only to predict the occurrence of the DHT for the particular case, but also to estimate the DHTZ inside the channel based on the axial distributions of the buoyancy and acceleration parameters and various pressure gradient components along the channel. The notable findings of the related studies are as follows:

- For the case without the DHT, all the buoyancy parameters, B^* , Bu^* , k^* and TR , can correctly predict that there is no DHT. Also, for the present case, the gravitational and frictional pressure drops across the channel are comparable.
- For the cases with the DHT is observed at a low mass flux, the predicted DHTZs by the buoyancy parameters, B^* , match well with the experimental results. The strong dominance of gravitational pressure drop over the frictional and acceleration pressure drops

is observed, which confirms that the DHT is induced by the buoyancy.

- For the case with DHT at a high mass flux condition, none of the buoyancy parameters can predict the occurrence of the DHT because the effect of the gravity becomes secondary in comparison to the pressure drop due to friction. Moreover, the acceleration pressure gradient turns out to be having higher influence than the gravitational pressure drop at the exit section of the channel and contributes dominantly for the rapid rise of total pressure gradient in that portion. The existence of the DHTZ for this case is in the latter half of the channel where acceleration pressure gradient is more or less comparable or higher than the gravitational pressure gradient.
- Flow acceleration due to both pressure drop and thermal expansion is negligible for all of the cases under consideration.

References

- [1] U S DOE, NERAC, and GIF. A technology roadmap for generation IV nuclear energy systems. Technical report, 2002.
- [2] K Yamagata, K Nishikawa, S Hasegawa, T Fuji, and S Yoshida. Forced convective heat transfer to supercritical water flowing in tubes. *Journal of Heat and Mass transfer*, 15(12):2575–2593, 1972.
- [3] HS Swenson, JR Carver, and CR Kakarala. Heat transfer to supercritical water in smooth-bore tubes. *Journal of Heat Transfer: Transactions of the ASME Series*, c87(4):477–484, 1965.
- [4] JD Jackson. Consideration of the heat transfer properties of supercritical pressure water in connection with the cooling of advanced nuclear reactors. In *Proc. 13th Pacific basin Nuclear Conference, Shenzhen City, China*, pages 21–25, 2002.
- [5] RB Duffey and IL Piro. Experimental heat transfer of supercritical carbon dioxide flowing inside channels (survey). *Nuclear Engineering and Design*, 235(8):913–924, April 2005.
- [6] IL Piro, HF Khartabil, and RB Duffey. Heat transfer to supercritical fluids flowing in channels, empirical correlations (survey). *Nuclear Engineering and Design*, 230(1-3):69–91, May 2004.
- [7] W Jäger, VH Sánchez Espinoza, and A Hurtado. Review and proposal for heat transfer predictions at supercritical water conditions using existing correlations and experiments. *Nuclear Engineering and Design*, 241(6):2184–2203, June 2011.
- [8] X Cheng and T Schulenberg. Heat transfer at supercritical pressures: literature review and application to an HPLWR. *Scientific report FZKA6609, Forschungszentrum Karlsruhe*, 2001.
- [9] JY Yoo. The turbulent flows of supercritical fluids with heat transfer. *Annual Review of Fluid Mechanics*, 45:495–525, January 2013.

- [10] RG Desissler. Heat transfer and fluid friction for fully developed turbulent flow of air and supercritical water with variable fluid properties. *Trans. ASME*, 76:73–85, 1954.
- [11] B Shiralkar and P Griffith. Deterioration in heat transfer to fluids at supercritical pressure and high heat fluxes. *Cambridge, Mass.: MIT Engineering Projects Laboratory*, 1968.
- [12] R Bellinghausen and U Renz. Heat transfer inside vertical tubes. *Chemical Engineering and Processing*, 28(3):183–186, 1990.
- [13] S Koshizuka, N Takano, and Y Oka. Numerical analysis of deterioration phenomena in heat transfer to supercritical water. *International Journal of Heat and Mass Transfer*, 38(16):3077–3084, 1995.
- [14] DP Mikielewicz, AM Shehata, JD Jackson, and DM McEligot. Temperature , velocity and mean turbulence structure in strongly heated internal gas flows Comparison of numerical predictions with data. *International Journal of Heat and Mass Transfer*, 45:4333–4352, 2002.
- [15] AM Shehata and DM McEligot. Mean structure in the viscous layer of strongly-heated internal gas flows measurements. *International Journal of Heat and Mass Transfer*, 41(24):4297–4313, 1998.
- [16] FR Menter. Zonal two equation k-turbulence models for aerodynamic flows. *AIAA paper*, 2906:1993, 1993.
- [17] X Cheng, B Kuang, and YH Yang. Numerical analysis of heat transfer in supercritical water cooled flow channels. *Nuclear Engineering and Design*, 237(3):240–252, February 2007.
- [18] D Palko and H Anglart. Theoretical and numerical study of heat transfer deterioration in HPLWR. In *Nuclear Energy for Europe*, pages 1–8, 2007.
- [19] D Palko and H Anglart. Deteriorated heat transfer at low coolant flow rates. In *International Students Workshop on HPLWR*, pages 1–4, 2008.

- [20] ME Shitsman. Impairment of the heat transmission at supercritical pressures. *High Temperature*, (1):237–244, 1963.
- [21] J Yang, Y Oka, Y Ishiwatari, J Liu, and J Yoo. Numerical investigation of heat transfer in upward flows of supercritical water in circular tubes and tight fuel rod bundles. *Nuclear Engineering and Design*, 237(4):420–430, February 2007.
- [22] Y Zhang, C Zhang, and J Jiang. Numerical Simulation of Heat Transfer of Supercritical Fluids in Circular Tubes Using Different Turbulence Models. *Journal of Nuclear Science and Technology*, 48(3):366–373, March 2011.
- [23] JH Bae, JY Yoo, and H Choi. Direct numerical simulation of turbulent supercritical flows with heat transfer. *Physics of Fluids*, 17(10):105104, 2005.
- [24] M Sharabi and W Ambrosini. Discussion of heat transfer phenomena in fluids at supercritical pressure with the aid of CFD models. *Annals of Nuclear Energy*, 36(1):60–71, January 2009.
- [25] SM Liao and TS Zhao. Measurements of Heat Transfer Coefficients From Supercritical Carbon Dioxide Flowing in Horizontal Mini/Micro Channels. *Journal of Heat Transfer*, 124(3):413, 2002.
- [26] SM Liao and TS Zhao. An experimental investigation of convection heat transfer to supercritical carbon dioxide in miniature tubes. *International Journal of Heat and Mass Transfer*, 45(25):5025–5034, December 2002.
- [27] S He, PX Jiang, YJ Xu, RF Shi, WS Kim, and JD Jackson. A computational study of convection heat transfer to CO₂ at supercritical pressures in a vertical mini tube. *International Journal of Thermal Sciences*, 44(6):521–530, June 2005.
- [28] PX Jiang, Y Zhang, YJ Xu, and RF Shi. Experimental and numerical investigation of convection heat transfer of CO₂ at supercritical pressures in a vertical tube at low Reynolds numbers. *International Journal of Thermal Sciences*, 47(8):998–1011, August 2008.

- [29] PX Jiang, Y Zhang, CR Zhao, and RF Shi. Convection heat transfer of CO₂ at supercritical pressures in a vertical mini tube at relatively low reynolds numbers. *Experimental Thermal and Fluid Science*, 32(8):1628–1637, September 2008.
- [30] PX Jiang, B Liu, CR Zhao, and F Luo. Convection heat transfer of supercritical pressure carbon dioxide in a vertical micro tube from transition to turbulent flow regime. *International Journal of Heat and Mass Transfer*, 56(1-2):741–749, January 2013.
- [31] AP Ornatskij, LF Glushchenko, and SI Kalachev. Heat transfer with rising and falling flows of water in tubes of small diameter at supercritical pressures. *Thermal Engineering*, 18(5):137–141, 1971.
- [32] L Liu, Z Xiao, X Yan, X Zeng, and Y Huang. Heat transfer deterioration to supercritical water in circular tube and annular channel. *Nuclear Engineering and Design*, 255:97–104, February 2013.
- [33] RV Maitri, G Dutta, C Zhang, and J Jiang. Numerical models to predict teady and unsteady themal-hydraulic behaviour of supercritical water flow in circular tubes. (*Submitted*).
- [34] G Dutta and JB Doshi. Nonlinear analysis of nuclear coupled density wave instability in time domain for a boiling water reactor core undergoing core-wide and regional modes of oscillations. *Progress in Nuclear Energy*, 51(8):769–787, 2009.
- [35] 14.0 ansys fluent theory guide. *ANSYS inc*, 2011.
- [36] MJ Watts and CT Chou. Mixed convection heat transfer to supercritical pressure water. In *Proceedings of the 7th International Heat Transfer Conference. Vol 3*, pages 495–500, 1982.
- [37] S Mokry, I Pioro, A Farah, K King, S Gupta, W Peiman, and P Kirillov. Development of supercritical water heat-transfer correlation for vertical bare tubes. *Nuclear Engineering and Design*, 241(4):1126–1136, April 2011.

- [38] QT Zhou. Influences of buoyancy on heat transfer to supercritical pressure water in vertical tubes. *Journal of Engineering Thermophysics*, 4(May (2)):165–172, 1983.
- [39] AF Polyakov. Heat Transfer under Supercritical Pressures. *Advances in Heat Transfer*, 21:1–53, 1991.
- [40] H Tanaka, A Tsuge, M Hirata, and N Nishiwaki. Effects of buoyancy and of acceleration owing to thermal expansion on forced turbulent convection in vertical circular tubes criteria of the effects, velocity and temperature profiles, and reverse transition from turbulent to laminar flow. *Journal of Heat and Mass transfer*, 16(6):1267–1288, 1973.
- [41] A Churkin, S Bilbao, and K Yamada. Analysis of the IAEA benchmark exercise on steady state flow in a heated pipe with supercritical water. In *Proceedings of ICAPP*, pages 139–145, 2011.

Chapter 5

A CFD Assisted Control System Design Using System Identification Technique for CANDU SCWR

Abstract

The supercritical water cooled reactor (SCWR) is one of the six reactor concepts of Generation IV nuclear reactors. A new control system design method for the Canadian SCWR is developed in this paper. The CANDU SCWR is a multiple input and multiple output (MIMO) system with highly non-linear governing equations. The non-linear governing equations for the SCWR are solved using computational fluid dynamics (CFD). It is difficult to convert the existing non-linear equations for the SCWR to linear dynamic models to facilitate the control system design. Therefore, a new approach is taken to use the CFD simulations to derive the linear dynamic models around the given operating point based on the system identification technique for the CANDU SCWR. The proposed linear dynamic models are validated with the non-linear dynamic model data.

In this paper, the cross-coupling between the inputs and outputs of SCWR is taken into consideration and the pre-compensator is constructed to decouple the given MIMO system into

several single input and single output systems (SISO). The loop compensator is also developed to control the decoupled SCWR plant around a reference point.

Keywords: CANDU SCWR, CFD, control system, system identification, pre-compensator, decoupling, loop compensator

5.1 Introduction

The supercritical water cooled reactor (SCWR) has been identified as one of the six proposed technologies for the Generation IV nuclear reactors.¹ The SCWR is the only Generation IV reactor concept where water will be used as the coolant. The SCWR has advantage over boiling water reactor (BWR) and pressurized water reactors (PWR) in terms of thermal efficiency, compactness of a power plant and avoidance of boiling crisis. Based on the design of the reactor and arrangement of fuel rods, SCWRs are divided into two type: pressure-tube type reactors and pressure vessel type reactors. Moreover, SCWRs are also divided as fast reactors and thermal reactors depending on whether moderator is used or not. Among the various concepts put forward for the SCWR, CANDU SCWR is one of the potential candidates which use pressure-tube type thermal reactor.

The supercritical water has higher specific heat capacity near the pseudo-critical point and therefore, the SCWR has high heat flux to mass flux ratio compared to BWR and PWR. The intense heating and lower mass flow rate increases the cross-coupling among the input and outputs of the SCWR.² It is important to deal with the cross-coupling for the design of a control system for the SCWR. The control studies were carried out by Nakatsuka et al.³ and Ishiwatari et al.⁴ for supercritical fast reactor and high-temperature supercritical light water reactor, respectively. However, in these studies, the cross-coupling is totally ignored and the reactors are treated as several SISO system without decoupling the original MIMO system. Even though the design improvements were made in subsequent work,⁵ the unavailability of dynamic relationship between inputs and outputs still poses the challenge for the design of a control system. Sun² has done work in this direction for establishing the dynamic relationship between inputs and outputs for the Canadian SCWR using system identification method and reported a good agreement between the linear dynamic model and non-linear dynamic model. However, a simple 1-D model was used by Sun² to model the thermal-hydraulic behaviour of the SCWR.

In this work, the CFD model with Reynolds Strees Model (RSM) is used for simulating the transient thermal-hydraulic behaviour of the CANDU SCWR. Furthermore, the strongly

coupled MIMO system is decoupled first before modeling the SCWR as several SISO systems. To achieve this, the pseudodiagonalization method is used to make the SCWR plant diagonally dominant using pre-compensator. Finally, based on the pre-compensated and decoupled SCWR plant, the loop compensator is designed for the control and stability of the reactor.

The remaining paper is organised as following : in Section 5.2, the method for the simulations of the CFD studies in CANDU SCWR is presented. In Section 5.3, the construction and validation of linear dynamic models based on CFD simulations is carried out. Section 5.4 is divided into two parts. In the first part, the decoupling of the CANDU SCWR MIMO system into several SISO systems using pre-compensator is discussed and in the second part, the design of a loop compensator is performed to control the given CANDU SCWR system. The conclusions from the study are drawn in the Section 5.5.

5.2 CFD method for CANDU SCWR simulations

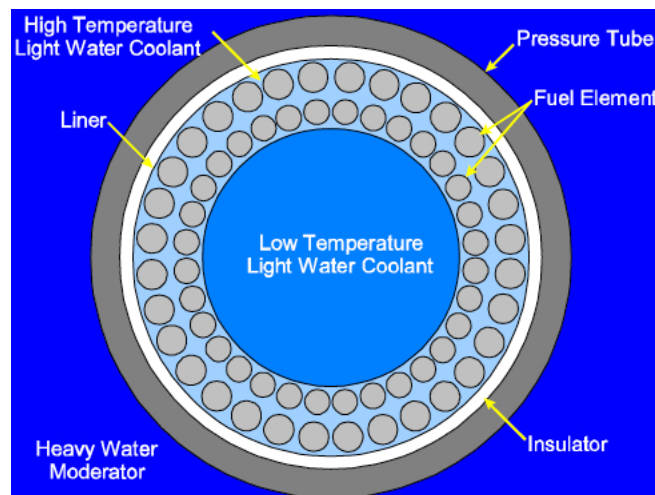
In the present work, the CFD simulations for the CANDU SCWR are performed using the axisymmetric assumption in commercial software FLUENT. The specifications of CANDU SCWR are shown in Table 5.1. As the development of CANDU SCWR is in research phase, the rod bundle configuration is not yet finalized. However, the cross-section of the most recent fuel channel design is shown Fig. 5.1.

The rod bundle design consists of 32 fuel rods of 9.5 mm diameter and 32 fuel rods of 10.5 mm diameter as shown in Fig. 5.1. The fuel channel is vertical and the supercritical water flows vertical upward. These fuel rods are symmetrically distributed in the circumferential direction as shown in Fig. 5.1. Hence, for the thermal-hydraulic analysis, a flow channel consisting of 1 fuel rod of 9.5 mm and 1 fuel rod of 10.5 mm diameter is used.

The governing equations used for the supercritical water flow and heat transfer are the conservation of mass, momentum and energy. The Reynolds averaged form of these governing equations can be expressed in a tensor form is as follows:⁸

Table 5.1: Specifications of the CANDU-SCWR^{6,7}

Spectrum	Thermal
Moderator	Heavy Water (D ₂ O)
Coolant	Light Water (H ₂ O)
Thermal power	2540 MW
Flow Rate	1320 kg/s
Number of Channels	336
Electric Power	1200 MW
Efficiency	48 %
Fuel	UO ₂ /Th
Enrichment	4%
Inlet Temperature	350°C
Outlet Temperature	625°C
Cladding Temperature	< 850°C
Heated Length	5 m
Operating Pressure	25 MPa
Calandria Diameter	4 m

Figure 5.1: CANDU SCWR Fuel⁷ channel

$$\frac{\partial \rho}{\partial t} + \frac{\partial}{\partial x_i}(\rho \bar{u}_i) = 0; \quad (5.1)$$

$$\frac{\partial}{\partial t}(\rho \bar{u}_i) + \frac{\partial}{\partial x_j}(\rho \bar{u}_i \bar{u}_j) = -\frac{\partial \bar{p}}{\partial x_i} + \frac{\partial}{\partial x_j} \left(\mu \frac{\partial \bar{u}_i}{\partial x_j} - \overline{\rho u'_i u'_j} \right) \quad (5.2)$$

$$\frac{\partial}{\partial t}(\rho C_p T) + \frac{\partial}{\partial x_i}(\bar{u}_i \rho C_p T) = \frac{\partial}{\partial x_i} \left[\left(k + \frac{C_p \mu_t}{Pr_t} \right) \frac{\partial T}{\partial x_i} \right] + \phi \quad (5.3)$$

To solve for the Reynolds stress term $(\overline{\rho u'_i u'_j})$, the Reynolds Stress Model (RSM) is selected in the current study and the expression for the corresponding transport term is as follows :

$$\begin{aligned} & \underbrace{\frac{\partial}{\partial t}(\overline{\rho u'_i u'_j})}_{\text{Local Time Derivative}} + \underbrace{\frac{\partial}{\partial x_k}(\rho u_k \overline{u'_i u'_j})}_{C_{ij} \equiv \text{Convection}} = -\underbrace{\frac{\partial}{\partial x_k} \left[\overline{\rho u'_i u'_j u'_k} + p'(\delta_{kj} u'_i + \delta_{ik} u'_j) \right]}_{D_{T,ij} \equiv \text{Turbulent Diffusion}} \\ & + \underbrace{\frac{\partial}{\partial x_k} \left[\mu \frac{\partial}{\partial x_k}(\overline{u'_i u'_j}) \right]}_{D_{L,ij} \equiv \text{Molecular Diffusion}} - \underbrace{\rho \left(\overline{u'_i u'_k} \frac{\partial u_j}{\partial x_k} + \overline{u'_j u'_k} \frac{\partial u_i}{\partial x_k} \right)}_{P_{ij} \equiv \text{Stress Production}} - \underbrace{\rho \beta (g_i \overline{u'_j \theta} + g_j \overline{u'_i \theta})}_{G_{ij} \equiv \text{Buoyancy Production}} \\ & + \underbrace{p' \left(\frac{\partial u'_i}{\partial x_j} + \frac{\partial u'_j}{\partial x_i} \right)}_{\phi_{ij} \equiv \text{Pressure Strain}} - \underbrace{2\mu \frac{\partial u'_i}{\partial x_k} \frac{\partial u'_j}{\partial x_k}}_{\epsilon_{ij} \equiv \text{Dissipation}} + \underbrace{S_{user}}_{\text{User Defined Source Term}} \end{aligned} \quad (5.4)$$

The CFD model using RSM was validated for the steady state fluid flow and heat transfer in supercritical water.⁹ The transient CFD simulations studies are carried out to generate the input-output data which will be used for constructing the linear dynamic models for the control of the CANDU SCWR.

5.3 Development of a linear dynamic model

The CFD model can be used to simulate the transient behaviour of CANDU SCWR. However, this model is highly non-linear and cannot be directly implemented for the designing of a control system. Therefore, linear dynamic models are needed for the design of a control system for the CANDU SCWR. The direct conversion of the non-linear governing equations to linear



Figure 5.2: Dynamic model for the CANDU SCWR

dynamic models is difficult. Hence, the CFD data generated by non-linear governing equations can be used to construct the linear dynamic models.

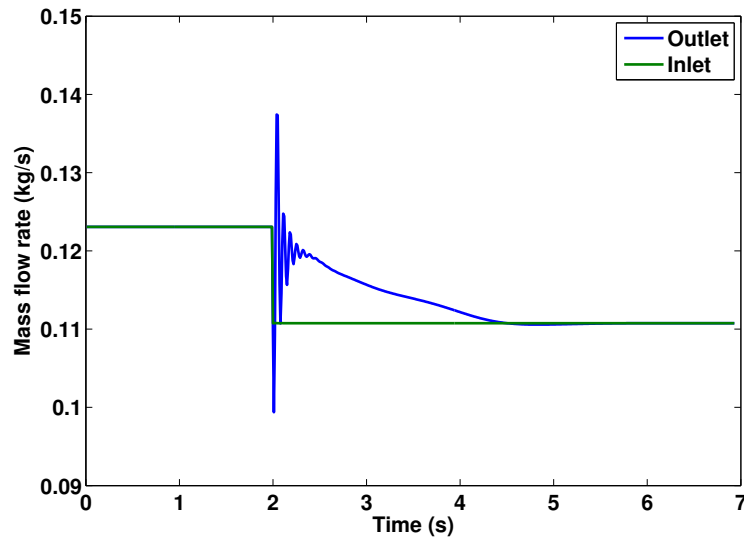
The dynamic model for the CANDU SCWR consists of two inputs, the inlet mass flow rate and heat flux, and two outputs, the outlet mass flow rate and outlet temperature as shown in Fig. 5.2. The step changes in both inputs are introduced at time, $t = 2$ s and the transient responses of the outputs of the SCWR are shown in Figs. 5.3 and 5.4. Only one input is perturbed at one time and the effect of the perturbation on both outputs is captured. Hence, total 4 input-output datasets are generated as shown in Figs. 5.3a and 5.4a, and Figs. 5.3b and 5.4b, respectively. Based on these datasets, system identification technique¹⁰ is used to establish the linearised dynamic models in the form of transfer functions. The expressions for the transfer function of the linear dynamic models are :

$$G_{11} = \frac{352.4 (s + 0.3055) (s^2 + 11.9145s + 738.14) (s^2 + 2.4124s + 15.4238) (s^2 + 1.2360s + 4.8218)}{(s + 59.7329)(s + 3.2868) (s^2 + 34.9066s + 8348.8)(s^2 + 0.2392s + 9.6757)(s^2 + 1.0344s + 0.4117)} \quad (5.5)$$

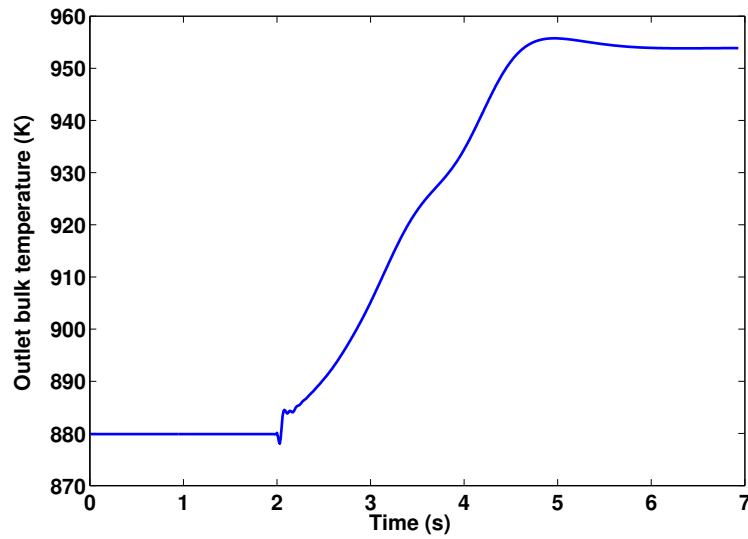
$$G_{12} = 1.587 \frac{(s + 258.47) (s^2 + 0.2019s + 0.0838)}{(s^2 + 31.2531s + 7498.9) (s^2 + 0.7169 + 0.6785)} \quad (5.6)$$

$$G_{21} = -0.2419 \frac{(s + 1.8185)}{(s^2 + 0.5157s + 0.6283)} \quad (5.7)$$

$$G_{22} = 1.1939 \frac{(s + 2.217)}{(s^2 + 0.4678s + 0.7237)} \quad (5.8)$$



(a) Temporal variation of the mass flow rate



(b) Temporal variation of the outlet bulk temperature of the coolant

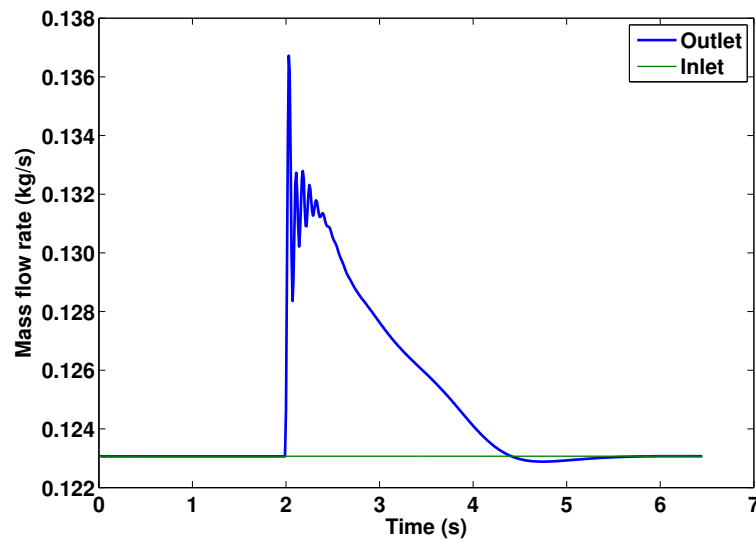
Figure 5.3: Transient response to the step decrease in the inlet mass flow rate by 10%

where, G_{11} : The dynamic model for inlet mass flow rate & outlet mass flow rate

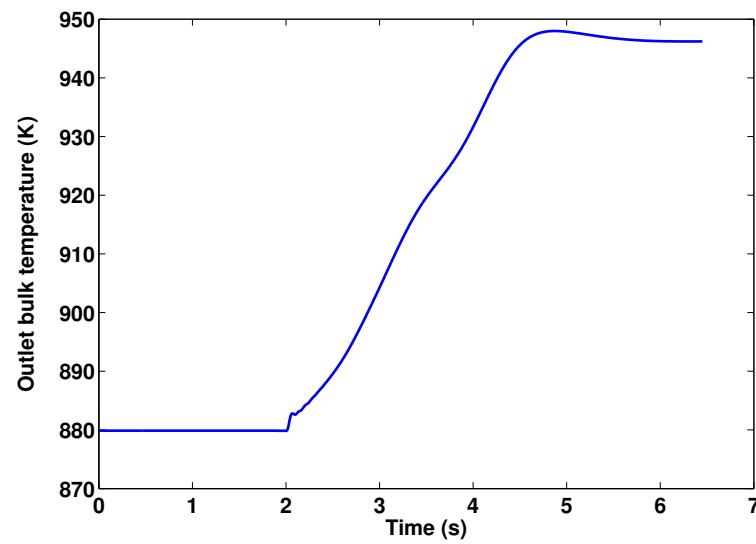
G_{12} : The dynamic model for inlet mass flow rate & outlet bulk temperature

G_{21} : The dynamic model for input heat flux & outlet mass flow rate

G_{22} : The dynamic model for input heat flux & outlet bulk temperature

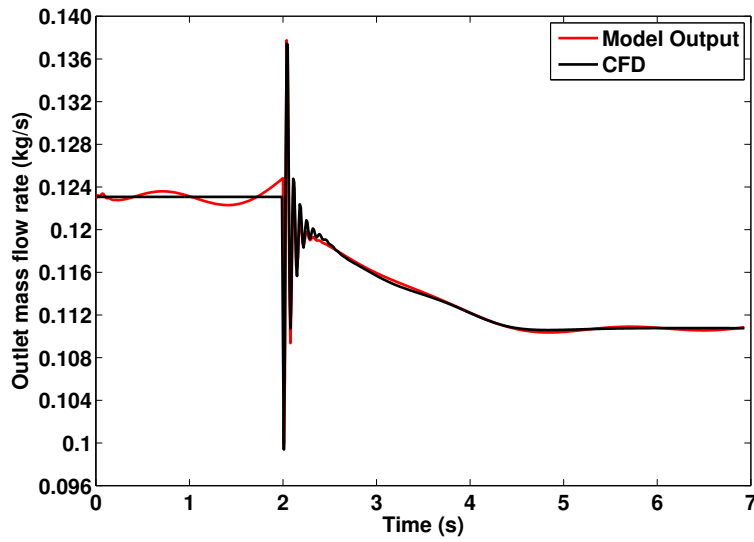


(a) Temporal variation of the mass flow rate

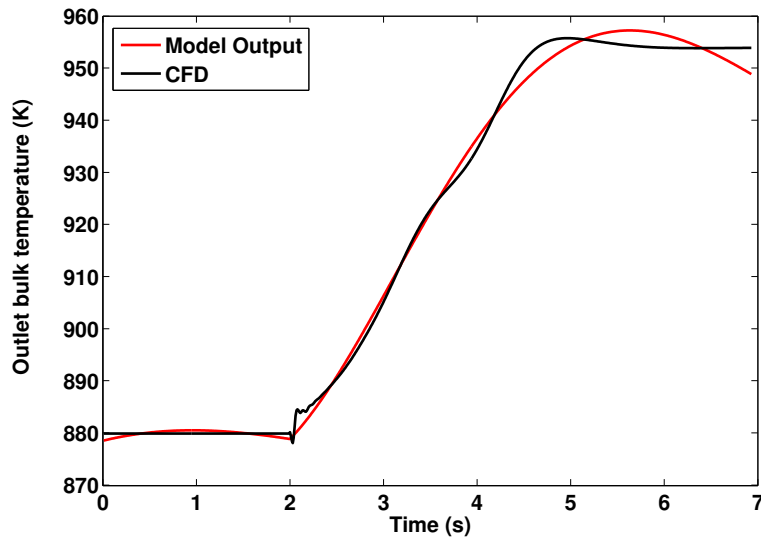


(b) Temporal variation of the outlet bulk temperature of the coolant

Figure 5.4: Transient response to the step increase in the heat flux rate by 10%



(a) Outlet mass flow rate

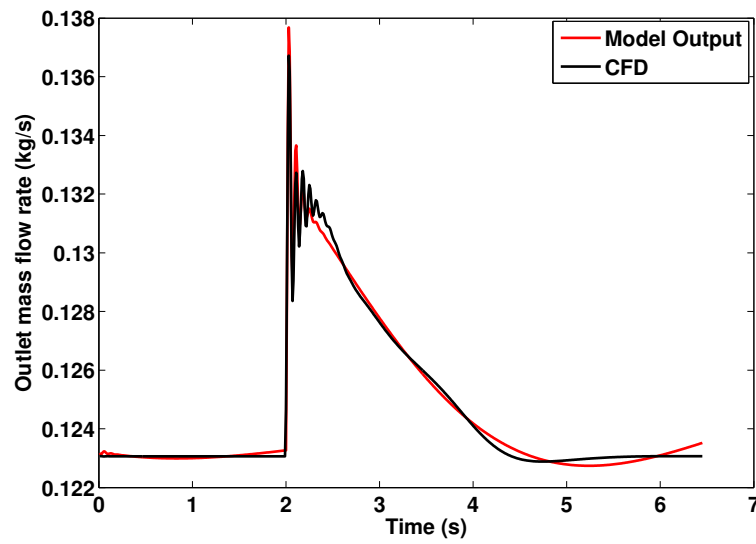


(b) Outlet bulk temperature

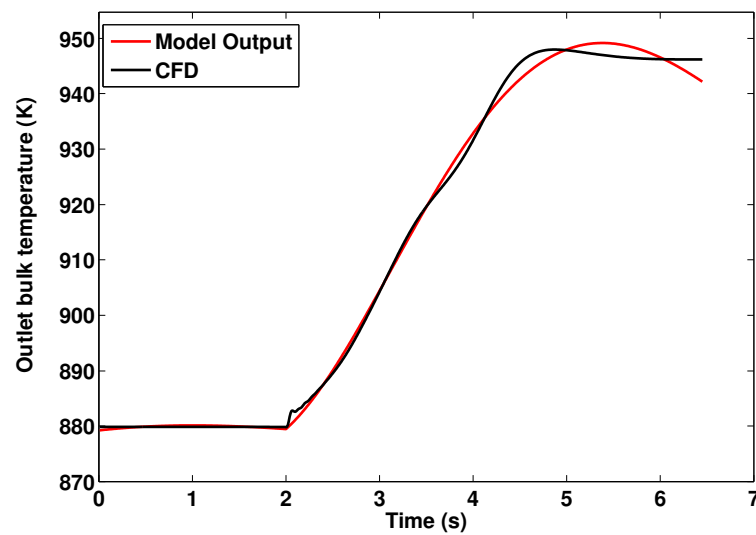
Figure 5.5: Linear dynamic model validation with the CFD results with the step change in the inlet mass flow rate

5.4 Designing of a control system

The CANDU SCWR is a MIMO system. The two inputs, inlet mass flow rate and heat flux, are used to control the system whereas the two outputs, outlet mass flow rate and outlet tempera-



(a) Outlet mass flow rate



(b) Outlet bulk temperature

Figure 5.6: Linear dynamic model validation with the CFD results with the step change in the input heat flux

ture are used as the feedback signals for the controller which will control the input variables. The design of a control system for coupled MIMO system can be complicated. Hence, to simplify the control system design process, the coupled MIMO system has to be converted into

multiple SISO systems. This conversion requires the decoupling of the MIMO system through a pre-compensation.



Figure 5.7: Block diagram of the control system for the CANDU SCWR

Before proceeding to the designing of the pre-compensator matrix, the cross-coupling analysis has to be done. The perturbation in one input causes the change in both outputs. However, the percentage variation in different output is different for the same perturbation in the input. The output which is relatively influenced more than the other output by the given input perturbation, is cross-coupled with the perturbed input. Based on the cross-coupling analysis, it is established that the outlet mass flow rate should mainly be regulated by inlet mass flow rate and outlet temperature should mainly be regulated by the input heat flux. Once the pairing is established, the input-output system can be represented in terms of the transfer functions as follows:

$$Y(s) = \begin{bmatrix} Y_1(s) \\ Y_2(s) \end{bmatrix} = G(s)U(s) = \begin{bmatrix} G_{11}(s) & G_{12}(s) \\ G_{21}(s) & G_{22}(s) \end{bmatrix} \begin{bmatrix} U_1(s) \\ U_2(s) \end{bmatrix} \quad (5.9)$$

The parameters $Y_1(s)$ and $Y_2(s)$ are the Laplace transforms of the outputs, the outlet mass flow rate and outlet temperature, respectively, whereas $U_1(s)$ and $U_2(s)$ are the Laplace transform of the inputs, the inlet mass flow rate and input heat flux, respectively.

The feedback control system for the Canadian SCWR is shown in Fig. 5.7. In this system, $G(s)$ is the plant, $K(s)$ is the decoupling pre-compensator matrix and $C(s)$ is the controller matrix. The pre-compensator is used to decouple the system into multiple SISO systems. Hence, the controller matrix has only diagonal elements. The transfer function matrix for $K(s)$

and $C(s)$ is given as :

$$K(s) = \begin{bmatrix} K_{11}(s) & K_{12}(s) \\ K_{21}(s) & K_{22}(s) \end{bmatrix} \quad (5.10)$$

$$C(s) = \begin{bmatrix} C_{11}(s) & 0 \\ 0 & C_{22}(s) \end{bmatrix} \quad (5.11)$$

The pre-compensated plant, $P(s)$, will be used for the design of the controller. The matrix for $P(s)$ is given as:

$$P(s) = G(s)K(s) = \begin{bmatrix} P_{11}(s) & P_{12}(s) \\ P_{21}(s) & P_{22}(s) \end{bmatrix} \quad (5.12)$$

As shown in the Fig. 5.7, the $R(s)$, $E(s)$ are the reference signal and error signal, respectively. The loop transfer function matrix $Q(s)$ is defined as (Fig. 5.7),

$$Q(s) = G(s)K(s)C(s) = \begin{bmatrix} Q_{11}(s) & Q_{12}(s) \\ Q_{21}(s) & Q_{22}(s) \end{bmatrix} \quad (5.13)$$

The design of a control system using DNA method as explained by Sun² has two steps - (1) The pre-compensator is used to decouple the system and establish the diagonal dominance of $P(s)$ and (2) The loop compensator $C(s)$ is designed once the diagonal dominance is achieved.

The pre-compensator can be designed based on the steady state decoupling or the dynamic decoupling. However, the steady state decoupling is used to establish the column dominance only at lower frequencies and system might not be decoupled for higher frequencies during transient conditions. Hence, dynamic decoupling is chosen in this study for the frequency range 0.001 - 10 rad/s based on the previous work.²

5.4.1 Design of a pre-compensator

The need for a pre-compensator is assessed based on the dominance of diagonal element in a column. The diagonal dominance in column can be measured using the following function:¹¹

$$d_j(\omega) = \frac{\sum_{i=1, i \neq j}^3 |G_{ij}(j\omega)|}{|G_{jj}(j\omega)|} \quad (5.14)$$

The above expression is measure of the effect of the perturbation in one input on off-diagonal elements to the diagonal element. The system is said to be diagonal dominant when the $d_j(\omega) \ll 1$ for selected frequency range. The plot of $d_j(\omega)$ for the column 1 and column 2 is shown Fig. 5.8. It is observed that the column 2 is already diagonal dominant for all the frequency values whereas for the column 1, $d_j(\omega) \ll 1$ for all the frequencies except around $\omega \approx 1$, where the diagonal and non-diagonal elements become comparable.

For the design of pre-compensator $K(s)$ to decouple $G(s)$, pseudodiagonalization method is used. For more complex systems where there are larger number of input and outputs, the ALIGN algorithm is used to increase the diagonal dominance as described in.¹¹ However, for the present study, only one value K_{21} has to be found out as the diagonal dominance of column 2 has already been established. The trial and error method is used for finalizing the expression for K_{21} . The final pre-compensator matrix $K(s)$ is given as:

$$K(s) = \begin{bmatrix} 1 & 0 \\ \frac{1}{s^2+7s+12} & 1 \end{bmatrix} \quad (5.15)$$

The diagonal dominance of the pre-compensated plant columns is shown in Fig. 5.8 in comparison with the original plant columns. It is observed that the diagonal dominance for both columns is established for the chosen frequency range.

5.4.2 Design of a loop compensator

Having decoupled the MIMO system with the pre-compensator, the given system can be treated as multiple SISO systems. Therefore, the control techniques for SISO systems are used for CANDU SCWR. The the controller is designed based on the following design requirements :

1. The maximum overshoot $< 10\%$

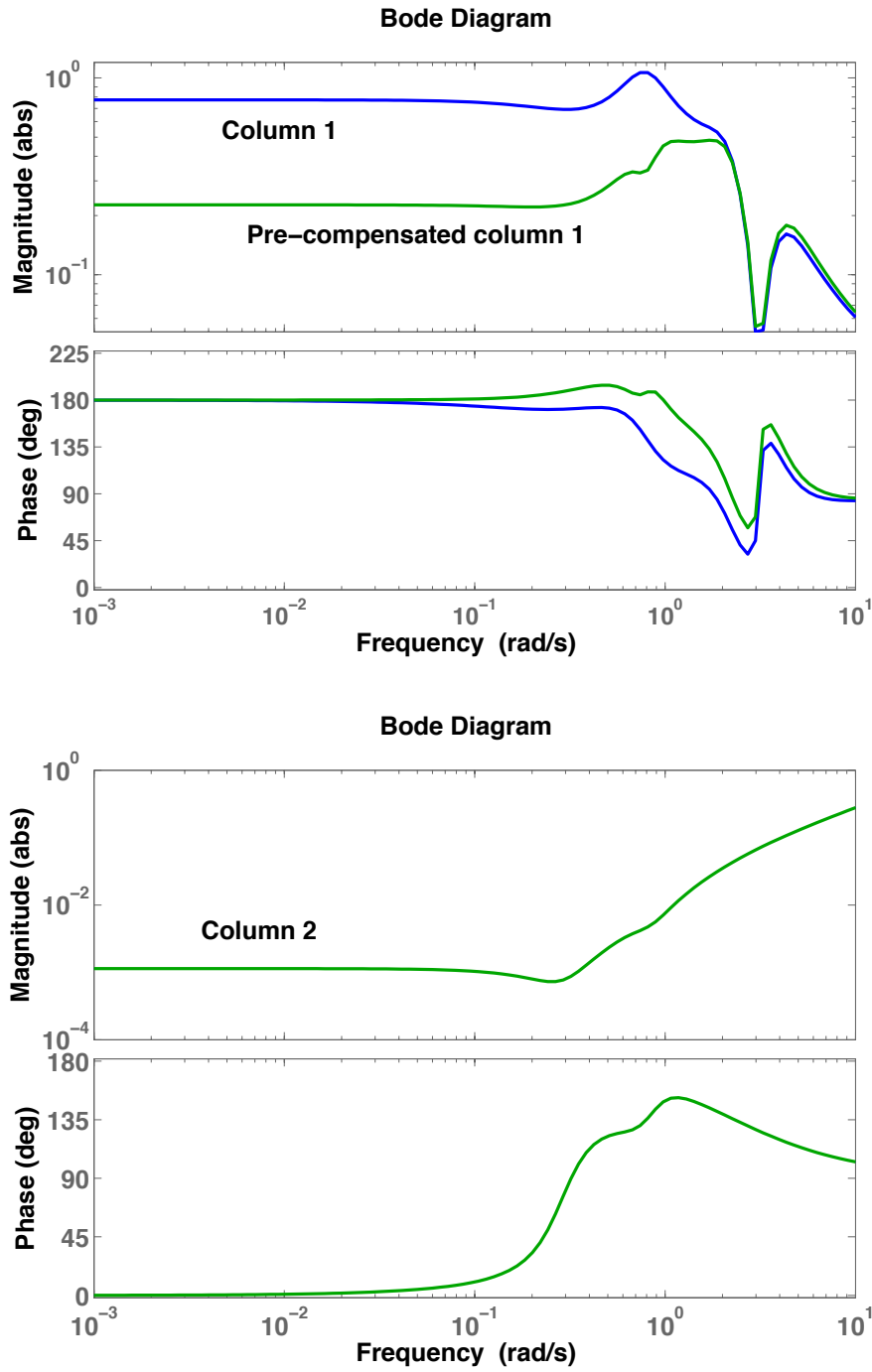


Figure 5.8: The distribution of $d_j(\omega)$ for different columns of original and pre-compensated plant

2. Rise time < 1 s

3. settling time < 5 s
4. No unstable poles for the loop transfer function

Outlet Mass Flow Rate Control

The outlet mass flow rate is regulated by the inlet mass flow rate. The PI controller is selected to have a zero steady-state error when a step input is applied. The expression for the transfer function of the designed PI controller (C_{11}) is :

$$C_{11} = 21.22 \frac{s + 1190}{s} \quad (5.16)$$

Outlet Temperature Control

The outlet temperature is regulated by the heat flux input. Similar to the previous case C_{11} , PI controller is chosen for this case as well to achieve zero steady-state error and fulfil the design requirements of maximum overshoot, rise time and settling time. The final expression for C_{22} is :

$$C_{22} = 6.15 \frac{s + 0.28}{s} \quad (5.17)$$

The loop compensator transfer function matrix is :

$$C(s) = \begin{bmatrix} \frac{21.22(s+1190)}{s} & 0 \\ 0 & \frac{6.15(s+0.28)}{s} \end{bmatrix} \quad (5.18)$$

The $C(s)$ is the loop compensator for plant $P(s)$ but the $P(s)$ is pre-compensated plant and not an original plant of SCWR. Hence, taking into consideration the original plant $G(s)$, $K(s)C(s)$ becomes the actual loop compensator for the CANDU SCWR. The transfer function matrix for the $K(s)C(s)$ is :

$$K(s)C(s) = \begin{bmatrix} \frac{21.22(s+1190)}{s} & 0 \\ \frac{21.22(s+1190)}{s^3+7s^2+12s} & \frac{6.15(s+0.28)}{s} \end{bmatrix} \quad (5.19)$$

5.5 Conclusions

The methodology to design a control system for CANDU SCWR based on the CFD model is developed in this paper. It is found that the CFD simulations can be successfully used for the development of linear dynamic models for CANDU SCWR. The numerical results show that the designed linear dynamic models agree well with the non-linear dynamic models.

An attempt to convert the coupled MIMO system to multiple SISO systems is undertaken. The pre-compensator is used for this purpose and it is found that the pre-compensator can satisfactorily decouple the given cross-coupled plant into diagonally dominant system allowing to treat the CANDU SCWR as multiple SISO systems. Finally, based on the decoupled system, loop compensator is designed to control and ensure the stability of a CANDU SCWR.

References

- [1] US DOE, NERAC, and GIF. A Technology Roadmap for Generation IV Nuclear Energy Systems. Technical report, 2002.
- [2] P Sun. *Dynamic Model Construction and Control System Design for Canadian Supercritical Water-cooled Reactors*. PhD thesis, The University of Western Ontario, 2012.
- [3] T Nakatsuka, Y Oka, and S Koshizuka. Control of a fast reactor cooled by supercritical light water. *Nuclear technology*, 121(1):81–92, 1998.
- [4] Y Ishiwatari, Y Oka, and S Koshizuka. Control of a high temperature supercritical pressure light water cooled and moderated reactor with water rods. *Journal of Nuclear Science and Technology*, 40(5):298–306, 2003.
- [5] Y Ishiwatari, C Peng, S Ikejiri, and Y Oka. Improvements of feedwater controller for the super fast reactor. *Journal of Nuclear Science and Technology*, 47(12):1155–1164, 2010.
- [6] CK Chow and HF Khartabil. Conceptual fuel channel designs for candu-scwr. *Nuclear Engineering and Technology*, 40(2):139, 2008.
- [7] L Leung. Overview of SCWR Concepts. In *IAEA-SJTU Course on Science and Technology of SCWRs*, Shanghai, China, 2013.
- [8] 14.0 ansys fluent theory guide. *ANSYS inc*, 2011.
- [9] RV Maitri, G Dutta, C Zhang, and J Jiang. Numerical models to predict teady and unsteady themal-hydraulic behaviour of supercritical water flow in circular tubes. (*Submitted*).
- [10] L Ljung. *System identification toolbox: User’s Guide*. 2013.
- [11] JM Maciejowski. Multivariable feedback design. *Electronic Systems Engineering Series*, Wokingham, England: Addison-Wesley, 1989.

Chapter 6

Conclusions and Future Work

In this study, the computational fluid dynamics (CFD) assisted control system methodology is developed for the Canadian supercritical water cooled reactor (SCWR). Firstly, the CFD model with Reynolds Stress Model (RSM) and $k - \omega SST$ model, and 1-D numerical code, THRUST are validated with the experimental data for the supercritical water flow in circular tubes. The distribution of wall temperatures is used for the comparison of numerical model and experimental data. After the validation of numerical models at steady state, transient simulations are carried out for 3 different conditions and the results obtained using CFD and THRUST are compared with each other. As a next step, the detailed fluid flow and heat transfer analysis for supercritical water flow in vertically upward tubes is carried out using the turbulent kinetic energy (TKE) and velocity profiles, and buoyancy and acceleration parameters. Four different cases are chosen for the detailed analysis of the NHT and DHT using CFD and THRUST at both low and high mass flux conditions. The CFD model is implemented using two turbulence models, $k - \omega SST$ model and Reynolds Stress Model. The analysis of NHT and DHT is performed with TKE and velocity profiles in radial directions at various axial locations. A detailed investigation using buoyancy and acceleration parameters is also carried out next in order to be aware of the possibility of the occurrence of DHT while using such numerical predictions. An attempt is made to formulate a strategy, not only to predict the occurrence of DHT for the particular case, but also to estimate the DHTZ inside the channel based on the axial distributions of the buoyancy and acceleration parameters and various pressure gradient components along the channel. Finally, the methodology to design a control system based on CFD simula-

tions is developed in this study. The conclusions and possible future work based on the current research work and obtained results is discussed below.

6.1 Conclusions

1) The comparative results for validation cases reveal that the numerical models (CFD and THRUST) predict the wall temperature for normal heat transfer (NHT) cases with maximum error being consistently below 2%. The wall temperature profiles for the deteriorated heat transfer (DHT) cases have higher error than the NHT cases. The maximum errors associated with the RSM and $k-\omega SST$ model are 5.4% and 5.19%, respectively. The analysis for seven experimental cases concluded that among RSM and $k-\omega SST$, no one model is found to be unanimously better for all the cases. However, using RSM, more stable wall temperature profile is observed compared to the $k-\omega SST$ model. The $k-\omega SST$ model also fails to retrieve the wall temperature values in some DHT cases which results in conservative estimate in the wall temperature. It is also found that for the DHT with high mass flux case, the $k-\omega SST$ model gives oscillating profile. Similar to the conclusion from comparison of the turbulence models, no single heat transfer correlation (HTC) is found to be best in terms of the lowest errors for all the cases when THRUST is used. For the DHT with low mass flux condition, the maximum errors associated with the HTC by Mokry, Watt and Swenson are 4.5%, 7% and 4.5%, respectively whereas for the DHT with high mass flux case, these error values are 15%, 6.5% and 5.6%, respectively.

In transient simulations, the THRUST and CFD models are able predict the temporal and axial variations of the wall and bulk temperatures, and the predictions by THRUST and the CFD models are in good agreement. The temporal variation of the outlet mass flow rate and outlet bulk temperature for all the cases obtained by the THRUST and CFD model show the exact value at the final steady state, but the actual time taken to reach to the final steady state is more in the case of the CFD model than the THRUST. The excellent comparative analysis shows that THRUST and the CFD models are capable to simulate the transient TH behavior for SCW flow and heat transfer phenomena and therefore, both the numerical models can further be extended and used in the future for the analysis of various dynamic case studies.

2) In the analysis of different modes of heat transfer, it is observed that the RSM and $k - \omega SST$ are able to predict the difference in turbulence distribution in the DHT and NHT cases. The turbulence is found to be suppressed in the DHT zone for the DHT with low mass flux case and is one of the reasons for the deterioration in heat transfer. Although the suppression is predicted by both the turbulence models, RSM shows two peaks in TKE profile which is in line with previous DNS studies, but $k - \omega SST$ model predicts only one peak or no peak in the whole flow region. Hence, $k - \omega SST$ fails to predict the proper TKE profile in the near wall region. The turbulence models are able to predict the well known "M-shaped" velocity profile in supercritical fluid flow for the case of DHT at the low mass flux. However, the "M-shaped" velocity profile is not found for the case of DHT at the high mass flux and NHT. The influence of the gravity on the wall temperature is also studied by running the simulations with and without the gravity and it is found that the sharp increase in the wall temperature vanishes if the gravity is neglected. Hence, it can be concluded that buoyancy plays a dominant role in deteriorating the heat transfer for the cases of low mass flux.

The notable findings based on the buoyancy and acceleration parameters of the related studies are as follows:

- For the case without DHT, all the buoyancy parameters, B^* , Bu^* , k^* and TR are correctly predicted. For the present case, the gravitational and frictional pressure drops across the channel are comparable.
- For the cases with DHT is observed at a low mass flux, the predicted DHTZs by the buoyancy parameters, B^* , match well with the experimental results. Strong dominance of gravitational pressure drop over the frictional and acceleration pressure drops are observed confirming the buoyancy induced DHT.
- For the with DHT at a high mass flux condition, none of the buoyancy parameters can predict DHT because the effect of the gravity becomes secondary in comparison to the pressure drop due to friction. Moreover, the acceleration pressure gradient turns out to be having higher impact than the gravitational pressure drop at the exit section of the channel and contributes dominantly for the rapid rise of total pressure gradient in that

portion. The existence of DHTZ for this case is in the latter half of the channel where acceleration pressure gradient is more or less comparable or higher than the gravitational pressure gradient.

- Flow acceleration due to both pressure drop and thermal expansion is negligible for all of the cases under consideration.

3) It is reported that the input-output data generated by governing non-linear equations can be successfully used to develop the linear dynamic models for Canadian SCWR. The validation exercise shows that the designed linear dynamic models agree upto 85-90% accuracy with non-linear dynamic models. Considering that the SCWR is strongly cross-coupled multiple input and multiple output system (MIMO), a pre-compensator is designed to decouple the given MIMO system into multiple SISO systems. Based on the Bode diagram analysis, it is found that the designed pre-compensator can be successfully applied to establish the diagonal dominance among the transfer function matrix. Finally, based on the decoupled systems, loop compensator is designed to control and ensure the stability of Canadian SCWR.

6.2 Future work

Based on the research work carried out in this study, following suggestions are made for future work :

1. Validation of the transient model with the experimental results :

Currently, the experimental data is available for the steady state supercritical fluid flow and heat transfer in the circular channel. However, the transient experimental data is important to validate the numerical models.

2. Proposing the heat transfer correlations for supercritical water flow in deteriorated heat transfer zone :

Till present, the proposed heat transfer correlations are designed based on the empirical data available for the normal or enhanced heat transfer conditions. However, to accurately predict the heat transfer phenomenon in deteriorated heat transfer cases, new correlations are required based on extensive empirical data.

3. Experimental data for the flow structure in deteriorated heat transfer zone :

There are lot experiments which presented the wall temperature data for the supercritical fluid flows but very few have presented the flow structure data like velocity and turbulent kinetic energy (TKE). The flow structures in the supercritical flows have large impact on the heat transfer phenomenon. Hence, for the in-depth analysis of heat transfer phenomenon in supercritical fluids and to assess the capability of numerical models, extensive experimental data is required.

Curriculum Vitae

Name: Rohit Maitri

Post-Secondary Education and Degrees: Bachelor of Technology, Mechanical Engineering

Indian Institute of Technology Jodhpur

Jodhpur, Rajasthan, India

2008-2012

Master of Engineering Science, Mechanical and Materials Engineering

University of Western Ontario

London, Ontario, Canada

2012 - 2014

Honours and Awards: Best Academic Performance in Mechanical Engineering

Indian Institute of Technology Jodhpur, 2012

Western Engineering Scholarship (WES)

University of Western Ontario

Related Work Experience: Teaching Assistant

University of Western Ontario

2012 - 2014

Publications:

1. Rohit V. Maitri, Goutam Dutta, Chao Zhang and Jin Jiang. Numerical Analysis of the Deterioration of Heat Transfer Phenomenon in Supercritical Water Flow in Circular Tubes Using Different Turbulence Models. *22nd Annual Conference of the CFD Society of Canada*, Toronto, Canada, 2014.
2. Goutam Dutta, Rohit V. Maitri, Chao Zhang and Jin Jiang. Numerical Analysis of Heat Transfer for Supercritical Water Flow in Circular Tubes Using a Newly Developed Thermal Hydraulic Model. *Canadian Society for Mechanical Engineering International Congress*, Toronto, Canada, 2014.
3. Rohit V. Maitri, Goutam Dutta, Chao Zhang and Jin Jiang. Numerical Models to Predict Steady and Unsteady Thermal-hydraulic Behaviour of Supercritical Water Flow in Circular Tubes. *(To be submitted)*
4. Rohit V. Maitri, Goutam Dutta, Chao Zhang and Jin Jiang. Numerical Investigation of Deteriorated Heat Transfer Phenomenon for Supercritical Water Flow in Vertical Circular Tubes. *(To be submitted)*
5. Rohit V. Maitri, Chao Zhang and Jin Jiang. A CFD Assisted Control System Design Using System Identification Technique for CANDU SCWR. *(To be submitted)*